Volume 69C
Number 2
April–June 1965

Engineering and Instrumentation

U.S. DEPARTMENT OF COMMERCE

SECTION C

JOURNAL OF RESEARCH

NATIONAL BUREAU OF STANDARDS

Journal of Research
of the
National Bureau of Standards

C. Engineering and Instrumentation

APR.–JUNE • 1965

VOLUME • 69C

NUMBER • 2

Editor: Martin Greenspan

Associate Editors: G. F. Montgomery, R. V. Smith

Publication dates:
Feb. 15, May 15, Aug. 15, Nov. 15, 1965

JOURNAL OF RESEARCH

The National Bureau of Standards Journal of Research reports research and development in the fields of activity shown at right. Also included from time to time are survey articles on topics closely related to the Bureau's scientific and technical program.

The Journal is published in four separate sections as follows:

A. Physics and Chemistry

Contains papers of interest primarily to scientists working in these fields. Issued six times a year. Annual subscription: domestic, $4.00; foreign, $4.75. Single copy, 70¢.

B. Mathematics and Mathematical Physics

Presents studies and compilations designed mainly for the mathematician and the theoretical physicist. Issued quarterly. Annual subscription: domestic, $2.25; foreign, $2.75. Single copy, 75¢.

C. Engineering and Instrumentation

Reports research and development results of interest chiefly to the engineer and the applied scientist. Issued quarterly. Annual subscription: domestic, $2.25; foreign, $2.75. Single copy, 75¢.

D. Radio Science (formerly Radio Propagation)

Published in cooperation with U.S. National Committee of URSI. Presents papers in radio propagation, communications, and radio science generally. Issued monthly. Annual subscription: domestic, $9.00; foreign, $11.50. Single copy, $1.00.

The National Bureau of Standards is a principal focal point in the Federal Government for assuring maximum application of the physical and engineering sciences to the advancement of technology in industry and commerce. Its responsibilities include development and maintenance of the national standards of measurement, and the provisions of means for making measurements consistent with those standards; determination of physical constants and properties of materials; development of methods for testing materials, mechanisms, and structures, and making such tests as may be necessary, particularly for government agencies; cooperation in the establishment of standard practices for incorporation in codes and specifications; advisory service to government agencies on scientific and technical problems; invention and development of devices to serve special needs of the Government; assistance to industry, business, and consumers in the development and acceptance of commercial standards and simplified trade practice recommendations; administration of programs in cooperation with United States business groups and standards organizations for the development of international standards of practice; and maintenance of a clearinghouse for the collection and dissemination of scientific, technical, and engineering information.

Institute for Basic Standards. Electricity. Metrology. Heat. Radiation Physics. Mechanics. Applied Mathematics. Atomic Physics. Physical Chemistry. Laboratory Astrophysics.* Radio Standards Laboratory: Radio Standards Physics; Radio Standards Engineering.** Office of Standard Reference Data.

Institute for Materials Research. Analytical Chemistry. Polymers. Metallurgy. Inorganic Materials. Reactor Radiations. Cryogenics.** Office of Standard Reference Materials.

Central Radio Propagation Laboratory.** Ionosphere Research and Propagation. Troposphere and Space Communications. Radio Systems. Upper Atmosphere and Space Physics.

Institute for Applied Technology. Textiles and Apparel Technology Center. Building Research. Industrial Equipment. Information Technology. Performance Test Development. Instrumentation. Transport Systems. Office of Technical Services. Office of Weights and Measures. Office of Engineering Standards. Office of Industrial Services.

*NBS Group, Joint Institute for Laboratory Astrophysics at the University of Colorado.
**Located at Boulder, Colo.

U.S. DEPARTMENT OF COMMERCE
John T. Connor, Secretary
NATIONAL BUREAU OF STANDARDS
A. V. Astin, Director

Order all publications from the Superintendent of Documents
U.S. Government Printing Office, Washington, D.C., 20402.

Use of funds for printing this publication approved by the Director of the Bureau of the Budget (June 19, 1961).

JOURNAL OF RESEARCH of the National Bureau of Standards—C. Engineering and Instrumentation
Vol. 69C, No. 2, April–June 1965

Temperatures of Thermocouple Reference Junctions in an Ice Bath

Frank R. Caldwell

(January 5, 1965)

Errors obtained when using several sizes of ISA Type K thermocouple wires (14 to 20 AWG) and of copper lead wires (14 to 26 AWG) at different immersions in a properly prepared and maintained ice bath are given. Variables considered include in addition to the wire diameters and materials, depth of immersion (2 to 9 in.), solid cross section of the Pyrex junction tubes, and type of insulation on the copper lead wires. The wires studied represent the maximum (copper) and the minimum (Chromel) thermal conductivities of any of the normally used thermocouple wires. A small amount of data on platinum is included.

Depth of immersion and diameter of the copper wire are extremely important if a high degree of accuracy is to be attained. The solid cross section of the Pyrex junction tubes and type of insulation used are of lesser importance.

1. Introduction

A thermocouple used to measure temperature is, from its nature, a differential sensor which actually measures the thermal emf generated as a result of the difference in temperature between its two junctions. It follows then, that the temperature of one of its junctions must be known if the measured emf is to be related to the temperature being measured. This junction is known variously as the "cold," "ice," or "reference" junction; and the fact that in measurements at low temperatures it may be the warmest part of interest in the measuring circuit seems often to make no difference; this is still the "cold junction" to many, in spite of efforts of purists to have it called the "reference," or when applicable the "ice" junction. The other is the "measuring" junction that often similarly is called the "hot" junction. In the discussions that follow, the "reference" or "ice" junction refers to the electrical connection between the thermocouple and copper wires leading to the measuring instrument. This connection is made by mercury in the bottom of a Pyrex tube immersed in a bath of water-ice slush at, hopefully, 0 °C (32 °F). This is a conventional bath, descriptions of which can be found in the literature [1, 2].[1] A discussion of the makeup of the ice bath including effects on its temperature of using tap or distilled water with tap or distilled water ice is given by McElroy in reference [3]. He warns that the reference junction tubes should be located properly in the slush bath if errors "as serious as 2 to 3 °C" are to be avoided.

The studies reported herein followed discussions in Committee AE–2, Temperature Measurement Sensing, of the Society of Automotive Engineers, that led to the recommended practice of reference [2]. These emphasized the desirability of evaluating the errors resulting from varying geometries of tubes and wires in the ice bath. Conversely, such an evaluation would provide information on the sizes of tubes and wires and depths of immersion that would lead to certain tolerable limits of errors.

The purpose of this paper is, therefore, to point out and give quantitative information on errors that may arise from misuse of thermocouple reference junctions in ice baths, or on the limiting conditions that will cause an error not to exceed the maximum tolerable. Figure 1 is a sketch of an ice bath of the type used in this investigation.

The temptation to cover the entire field of conventional thermocouple wires has been withstood, and as a result, the data obtained are confined almost exclusively to the ISA type K thermocouple wires (Chromel P and Alumel in this case) and copper leads. A few observations were made with platinum wire and copper leads. The data presented thus are applicable to thermocouple elements of the lowest conductivity normally used (type K) and also of the highest (copper).

The assumption is made in presenting this paper that the reader is familiar with the basic principles of thermoelectric thermometry to the extent, at least, that he can intelligently apply them to practice.

[1] Figures in brackets indicate the literature references at the end of this paper.

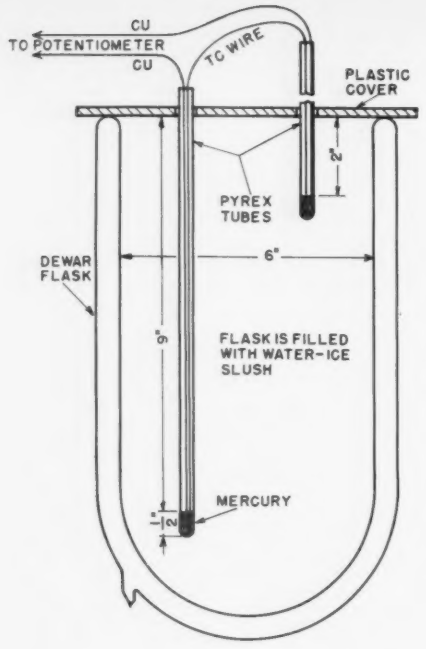

FIGURE 1. *Ice bath and reference junctions.*

2. Practical Considerations

If one end of a wire is immersed deeper and deeper into a bath of uniform temperature, a depth is reached at which greater immersion produces no further measurable or appreciable change in temperature of the immersed end. When the wire is in a glass tube as considered here and illustrated in figure 1, the same condition is reached, but at a somewhat greater depth. In addition to the depth of immersion, the thermal conductivity of the wires and material of the tubes, cross sections of the wires and tubes, depth of, and immersion of wires in the mercury in the tubes, type of insulation on the thermocouple wires or copper lead wires, and contact of the wires with the sides of the tubes all may affect the temperature at the reference junctions. The condition of the ice bath also is important, and it should be renewed or replenished often enough that no measurable gradient exists in either the vertical or horizontal direction in the area of the tubes.

Within limits, then, several choices are available for reducing the temperature of the reference junction in an ice bath and consequently the error introduced by the difference between the temperature of the junction and 0 °C. The choices examined in this work are: cross sections of wires, of both copper and thermocouple materials; type of insulation on the copper wire leads; immersion of junctions in the ice bath; and cross section of the glass tubes.

3. Materials and Procedure

The first thermocouple wires examined were four sizes of Chromel and Alumel (ISA type K): 8-, 14-, 20-, and 26-gage (American Wire Gage). Copper wires used with these were 14-, 20-, and 26-gage. The type K wires were oxidized, and the copper was enamel-insulated. Each increment between these wire sizes starting with the smallest represents an increase of about twice the diameter and four times the cross section. The dimensions of the several gages of wires used are given in table 1.

TABLE 1. *Diameters and cross-sectional areas at 20 °C of the wires used* [a]

American wire gage	Diameter		Cross section	
	in.	*mm*	*in.²*	*mm²*
8	0.1285	3.264	0.01297	8.366
14	.06408	1.628	.003225	2.081
20	.03196	.8118	.0008023	0.5176
26	.01594	.4049	.0001996	.1288

[a] From Smithsonian Physical Tables (Smithsonian Institution, Washington, D.C., 1954) ninth revised edition; W. E. Forsythe, Editor.

Thermal conductivities of Chromel, Alumel, copper, and Pyrex No. 7740 are given in table 2. Here copper is seen to have over 21 times the thermal conductivity of Chromel P, about 13 times that of Alumel, 5.5 times that of platinum, and nearly 350 times the thermal conductivity of Pyrex.

TABLE 2. *Thermal conductivities at 0 °C of copper, Chromel P, Alumel, and Pyrex, and of copper and Pyrex relative to the others*

Material	k	k_{cu}/k	k_{Pyrex}/k
Copper	[a] 0.912	1	0.00286
Chromel P	[b] .0420	21.71	.0621
Alumel	[b] .0679	13.43	.0384
Platinum	[c] .1660	5.49	.0157
Pyrex 7740	[d] .00261	349.4	1
Pyrex 7740	[e] .0027		

[a] C. S. Smith, The Physical Constants of Copper, Metals Handbook p. 1380 (The American Society for Metals, 1939).

[b] Extrapolated from table in Hoskins Manufacturing Company Catalog M-61, C-A, 1961, p. 5, and converted from watts/cm °C. Chromel and Alumel are registered trade-marks of the Hoskins Mfg. Co.

[c] Calculated from equation of Holm and Störmer, Measurement of the thermal conductivity of a platinum specimen in the temperature range 19–1020 °C, Wiss. Veroffentlich. Siemens-Konzerns **9**, part II, 312 (1930).

[d] Private communication from T. W. Watson, Building Research Division, National Bureau of Standards, and converted from milliwatts/cm °C. Pyrex is a registered trade-mark of the Corning Glass Works. This is the value that is compared with those of the alloy and copper wires.

[e] Smithsonian Physical Tables, ninth revised edition; table 555, p. 534.

Note: k is thermal conductivity in cal/cm sec °C.

Thermal conductivities of all of the commonly used thermocouple materials are within the range between copper and Chromel. For wires of a particular diameter therefore, copper, having the highest conductivity, may be expected to cause the greatest error; and use of the low-conductivity Chromel alone, if possible, would result in the smallest. This latter condition is not practical, because copper is used almost universally for the lead from the ice bath regardless of the type of thermocouple used. For practical applications of copper

in conjunction with other thermocouple wires whose combined thermal conduction lies between those of copper and Chromel, the errors also will lie between those resulting from the use of copper and Chromel alone.

The diameters and solid cross sections of the Pyrex tubes used are given in table 3. Sizes of tubes are identified in the table and in the text by the letters of column 1.

TABLE 3. *Diameters and solid cross-sectional areas of the Pyrex tubes used*

Tube	O.D.	I.D.	Solid cross section	
	in.	*in.*	*in.*^{2}	*mm*^{2}
I	0.312	0.230	0.0351	22.6
B	.245	.162	.0265	17.1
[illegible]	.234	.152	.0249	16.1
D	.199	.131	.0176	11.4
E	.154	.079	.0137	8.84
H	.121	.071	.0075	4.84

Thermal electromotive force (emf) was measured with a type K–3 potentiometer and a galvanometer with a sensitivity of about 5 mm/μV.

The ice bath illustrated in figure 1 was made in a large Dewar flask with a clear plastic cover, drilled to receive the Pyrex reference junction tubes. This cover was substituted for the often used cork stopper in order that the depth of immersion of the tubes could be measured more accurately. The intended depth of mercury in the tubes was ½ in. when the wires were immersed in it. Mercury does not, however, normally wet the Chromel and Alumel wires and so the depth of the mercury often was irregular across the tubes, deeper than ½ in. on one side and not so deep on the other. This effect was greater with the larger wires, and undoubtedly in some cases affected the indicated temperature of the junction between the alloy and copper wires. Although only two tubes are shown in the cross-sectional view of figure 1, observations often were taken with several in the ice bath at once.

All of the results presented herein were obtained in ice baths that were made and maintained according to the directions given in references [1] and [2]. Clear shaved ice and tap water were used, and a water-ice slush filled the Dewar flask at all times during observations. This latter precaution is important in the use of an ice bath, because the water at the bottom of a bath in which the ice is merely floating may be as high as 4 °C, the temperature of maximum density of water. This is not just academic; it has been observed in many instances in which long reference junction tubes have been used in an inadequately maintained ice bath. The junctions in these long tubes that extended through the slush into the water below actually have been found to be at temperatures well above 0 °C, and replenishing the ice bath has corrected conditions.

Use of tap water may, as discussed in reference [3], have some effect on the temperature of the ice bath, and this should be considered in cases where extreme accuracy is required. For the purposes of this paper though, this effect is unimportant; because all observations are differential. The chief requirement here has been that the ice bath be at as nearly a uniform temperature as possible throughout.

The procedure used was to immerse a tube containing one junction of, for example, a Chromel versus copper thermocouple so deeply in an ice bath that further immersion caused no detectible change in the thermal emf. This depth was found for the largest wires, both alloy and copper, and the largest glass tubes used, to be 9 in. or less; consequently, the stationary leg of the thermocouple in all cases was immersed to a depth at which the top of the mercury in the reference junction tube was at least 9 in. below the top of the ice bath. The other leg was immersed initially to a depth of 2 in. above the mercury and, with the thermocouple connected to the potentiometer by copper leads, a reading of the thermal emf was taken. The two junctions and the circuitry are shown in figure 1. The immersion was increased by an inch and another reading was taken. This was repeated for immersions up to 9 in., or to depths at which the emf became zero or constant. In the latter case the constant emf, normally a fraction of a microvolt was taken as an indication of inhomogeneity of the wires, and not a true reflection of a temperature difference between the two junctions. In such cases the constant readings were corrected to zero, and the same correction was added to the readings at all depths.

The first observations taken were obtained by repeating the procedures just described for all combinations of gages of Chromel P and copper and of Alumel and copper. At least two sets of data were taken in this phase for each combination, and in one case nine sets were taken. Three sizes of Pyrex tubes were used for the variable-immersion leg; the smallest had a solid cross section of about 71 percent of that of the largest. These are the first three sizes of table 3.

Although the thermal conductivity of the Pyrex reference junction tubes is very low relative to that of Chromel or Alumel, and extremely low relative to copper, separate data were taken to determine the effect, if any, of a change in the solid cross section of the tubes on the temperature of the reference junction.

Another set was taken to find whether or not the type of insulation on the copper lead wires to the reference junction had a measurable effect. In one case the single silk enameled insulation was used with 22-gage Alumel, and in the other the silk was removed, leaving only the enamel. The same leads were used with a platinum wire 0.020 in. in diameter (24-gage), a commonly used size. The Pyrex tube in each case was E with a solid cross section of 0.0137 in.^{2} and 0.079 in. I.D. This size was chosen as a compromise between the fragility of the smaller, thinner-walled tubes and the larger, more durable tubes of higher thermal conductance.

4. Results and Discussion

Data taken to find the effects of changing size and immersion of the type K and copper wires are presented in figures 2 and 3. Plotted in each figure are curves of emf of one type K wire of one gage against copper of three gages versus depth of immersion of the reference junctions in the ice bath. Figure 2 is for Chromel versus copper, and the data for Alumel are given in figure 3.

Chromel is thermoelectrically positive to copper, and Alumel and platinum are negative. This means, for example, that the positive Chromel element of a Chromel versus copper thermocouple must be connected to the plus terminal of a measuring instrument in order to get a positive reading when the measuring junction is at a temperature higher than that of the reference junction. Similarly, in the case of a copper versus Alumel thermocouple, the copper must be connected to the + terminal of the measuring instrument.

In the discussions and figures that follow all thermoelectric data are positive, i.e., the thermocouples considered are Chromel versus copper, copper versus Alumel, and copper versus platinum. The thermoelectric power at 0 °C of Chromel to copper is 19.57 μV/°C (10.87 μV/°F), of copper to Alumel is 19.71 μV/°C (10.95 μV/°F), and of copper to platinum is 6.15 μV/°C (3.42 μV/°F). The following list of abbreviations are those used in figures 2, 3, 4, and 5, and in the tables.

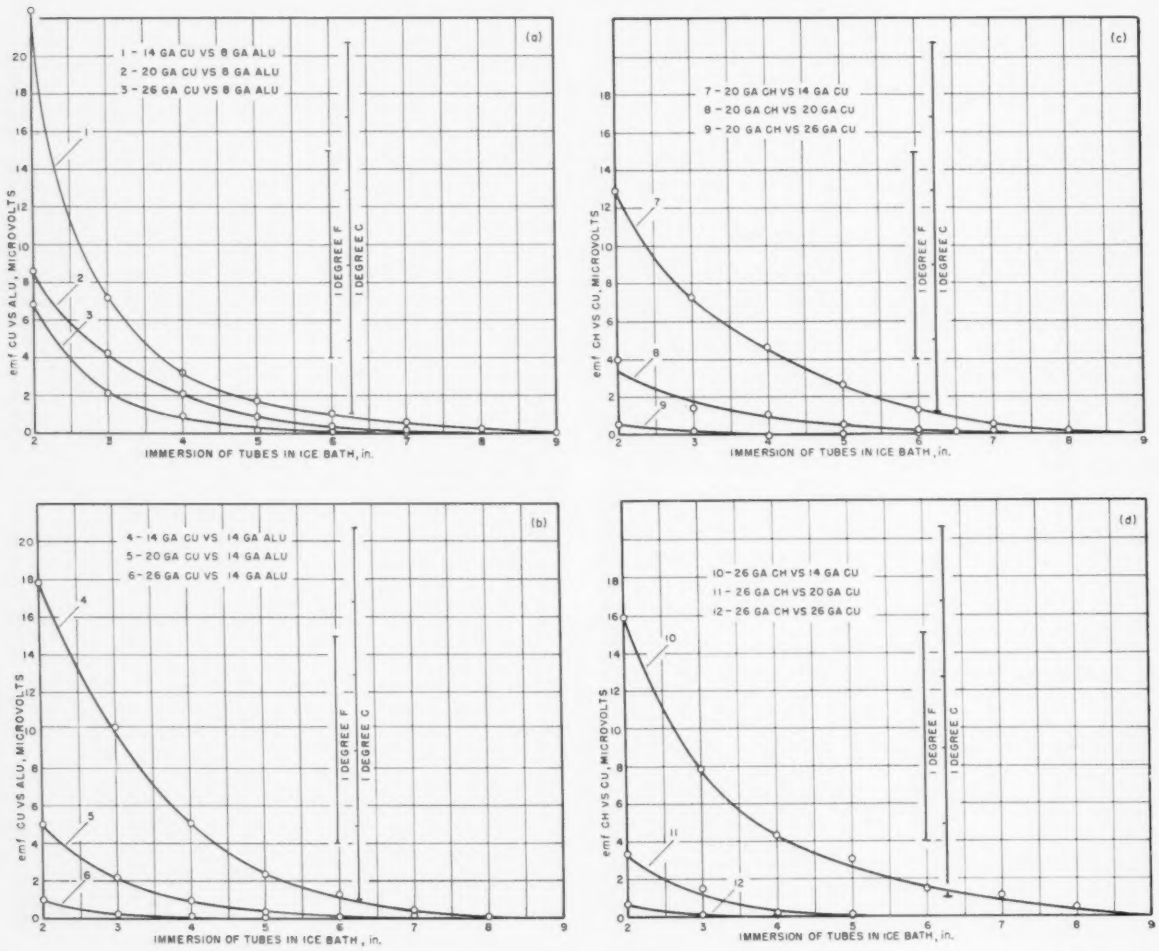
(a)
1 - 14 GA CU VS 8 GA ALU
2 - 20 GA CU VS 8 GA ALU
3 - 26 GA CU VS 8 GA ALU
emf CU VS ALU, MICROVOLTS
1 DEGREE F
1 DEGREE C
IMMERSION OF TUBES IN ICE BATH, in.
(c)
7 - 20 GA CH VS 14 GA CU
8 - 20 GA CH VS 20 GA CU
9 - 20 GA CH VS 26 GA CU
emf CH VS CU, MICROVOLTS
IMMERSION OF TUBES IN ICE BATH, in.
(b)
4 - 14 GA CU VS 14 GA ALU
5 - 20 GA CU VS 14 GA ALU
6 - 26 GA CU VS 14 GA ALU
emf CU VS ALU, MICROVOLTS
IMMERSION OF TUBES IN ICE BATH, in.
(d)
10 - 26 GA CH VS 14 GA CU
11 - 26 GA CH VS 20 GA CU
12 - 26 GA CH VS 26 GA CU
emf CH VS CU, MICROVOLTS
IMMERSION OF TUBES IN ICE BATH, in.

FIGURE 2. *Thermal emf of Chromel versus 14-, 20-, and 26-gage copper at various depths of immersion in an ice bath.*

a. 8-gage Chromel.
b. 14-gage Chromel.
c. 20-gage Chromel.
d. 26-gage Chromel.

ALU = Bare Alumel wire
C = Celsius
CH = Bare Chromel wire
CU = Copper wire
EN = Enamel electric insulation
F = Fahrenheit
GA = American wire gage
ID = Inside diameter
OD = Outside diameter
PT = Platinum wire
SE = Single layer silk + enamel electric insulation
TC = Thermocouple

Although the data are somewhat erratic, especially at the lowest immersions, some facts are immediately apparent. As expected, deeper immersion is seen to result in smaller error, or deviation of the temperature of the junction from 0 °C (32 °F). The error appears generally to be slightly smaller for Chromel than for Alumel, though this is masked in some cases by the lack of precision of the measurements; otherwise the patterns are quite similar.

The most potent variable is seen from the figures to be the size of the copper leads from the ice junctions. The relatively mild changes of solid cross

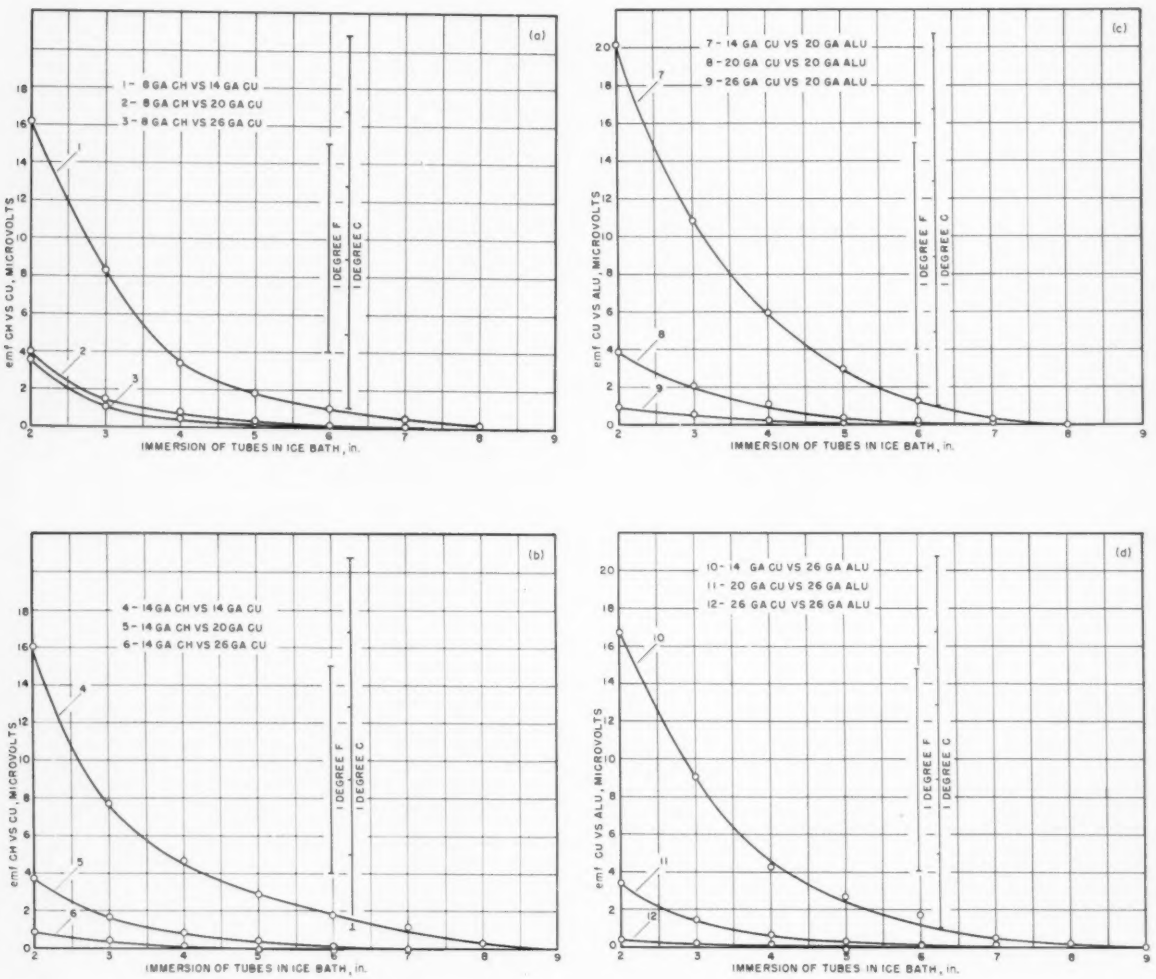
(a)
1- 8 GA CH VS 14 GA CU
2- 8 GA CH VS 20 GA CU
3- 8 GA CH VS 26 GA CU
emf CH VS CU, MICROVOLTS
IMMERSION OF TUBES IN ICE BATH, in.
1 DEGREE F
1 DEGREE C
(c)
7- 14 GA CU VS 20 GA ALU
8- 20 GA CU VS 20 GA ALU
9- 26 GA CU VS 20 GA ALU
emf CU VS ALU, MICROVOLTS
IMMERSION OF TUBES IN ICE BATH, in.
1 DEGREE F
1 DEGREE C
(b)
4- 14 GA CH VS 14 GA CU
5- 14 GA CH VS 20 GA CU
6- 14 GA CH VS 26 GA CU
emf CH VS CU, MICROVOLTS
IMMERSION OF TUBES IN ICE BATH, in.
1 DEGREE F
1 DEGREE C
(d)
10- 14 GA CU VS 26 GA ALU
11- 20 GA CU VS 26 GA ALU
12- 26 GA CU VS 26 GA ALU
emf CU VS ALU, MICROVOLTS
IMMERSION OF TUBES IN ICE BATH, in.
1 DEGREE F
1 DEGREE C

FIGURE 3. *Thermal emf of 14-, 20-, and 26-gage copper versus Alumel at various depths of immersion in an ice bath.*

a. 8-gage Alumel.
b. 14-gage Alumel.
c. 20-gage Alumel.
d. 26-gage Alumel.

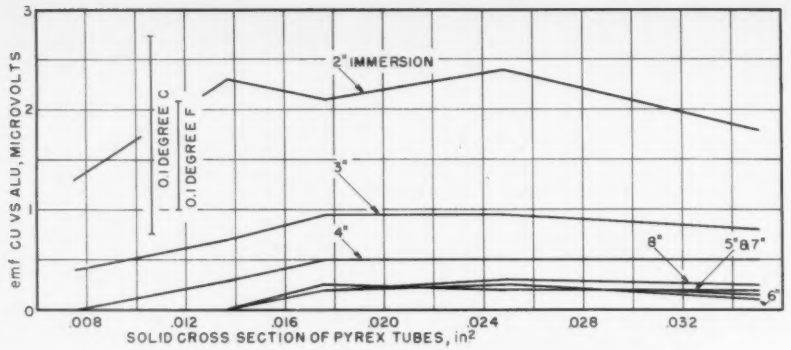

FIGURE 4. *Effect of solid cross section of Pyrex tubes on thermal emf of copper versus Alumel at various depths of immersion in an ice bath.*

Copper was 22-gage SE; Alumel was 22-gage.

section of the Pyrex reference junction tubes had no discernible effect. The largest copper wire used, 14-gage, was responsible for an error at an immersion of 2 in. of about ¾ °C for 8-gage Chromel and 1 °C (1.8 °F) for 8-gage Alumel. At the same immersion and for the 8-gage type K wires, 20-gage copper was responsible for errors of 0.2 °C or less when used with Chromel and up to 0.4 °C with Alumel. A depth of 4 in. is sufficient to reduce the error with either Chromel or Alumel of 14 gage or smaller and copper of 20 gage or smaller to 0.05 °C or less. With two exceptions where the error was 0.02 °C, immersion of the 26-gage copper wire to a depth of 3 in. gave an error of 0.01 °C or less. The errors resulting from use of copper leads of the latter two sizes at an immersion of 6 in. always are less than 0.01 °C.

The data of figure 4 were taken to determine the effect if any of the solid cross section of the Pyrex tubes on the temperature of the reference junction. The thermocouple used here was copper versus Alumel, both 22 gage; and the 22-gage copper was single silk, enamel insulated. Each curve of the chart is for a specific immersion of the top of the mercury in the tube into the ice bath.

Although the emfs developed here are generally lower at immersions up to 4 in. than are the approximately corresponding values of figure 3, the curves of figure 4 do point out the relative insensitivity of the junction temperature to the size of the Pyrex tubes used. In using the procedure described earlier to correct for any residual emf, the emf at 9 in. immersion was made to be 0 μV. The emfs at immersions from 5 to 8 in. as a result, then turned out to be from 0.1 to 0.3 μV for tube cross sections down to about 0.018 in.[2] The values for the two largest tubes are bracketed above by those for 8 in. immersion and for 6 in. immersion below. Practically, this latter emf is of such a magnitude that the spread undoubtedly is within the limits of precision of the observations; thus the error over an immersion of from 5 to 8 in. can be considered constant at 0.2 μV or so. This corresponds to about 0.01 °C. Another set of data similar to this, but with 26-gage Alumel showed the spread to be from 0 to about 0.5 μV for immersions of 5 to 9 in., or about 0.02 °C. The wider spread here, as in some other instances, may have been caused by inhomogeneities introduced by greater cold working of the smaller wire.

Data presented in figure 5 are intended to point out any difference that might result from the use of different types of insulation. Curve 1 (solid circles) is for bare 22-gage Alumel and 22-gage single silk, enamel insulated copper in tube E, and Curve 2 (open circles) is for the same wires with the silk insulation carefully removed. The difference in

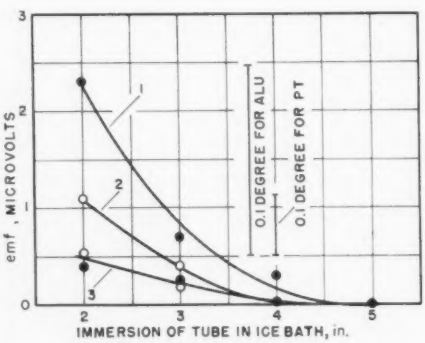

FIGURE 5. *Effects of insulation of copper leads on thermal emf of copper versus Alumel and copper versus platinum at various depths of immersion in an ice bath.*

●, denotes 22-gage SE Cu, versus 22-gage Alu in curve 1 and versus 24-gage Pt in curve 3.
○, denotes 22-gage EN Cu, versus 22-gage Alu in curve 1 and versus 24-gage Pt in curve 3.

thermal emf at an immersion of 2 in. corresponds to about 0.06 °C. Similar observations were taken with copper versus platinum thermocouples. The difference in this case, in the reverse direction, is so small as probably to be within the limit of precision. The one curve (3) drawn through the observations thus can be taken as an indication of errors to be encountered when using 24-gage platinum and a 22-gage copper wire lead. The error corresponds to about 0.07 °C at an immersion of 2 in., 0.03 °C at 3 in., and vanishes at 4 in.

5. Conclusions

The foregoing data point out that the errors caused by insufficient immersion in an ice bath, even under the extreme conditions of large wires and glass tubes, can be small enough that they will not be the primary causes of inaccuracy in many cases of engineering measurements. In those cases where the errors are of an intolerable magnitude, use of smaller wires and greater depth of immersion of the junction below the surface of the ice bath can reduce the error practically to the vanishing point. The size of the Pyrex tube used to contain the reference junction can be varied, within reasonable limits, without any appreciable effect on the temperature of the reference junction.

The type of insulation on the copper wire, single silk enamel or enamel alone were seen in the case of Alumel apparently to have a measurable effect on the temperature of the reference junction, but in a similar test with platinum, no such result was found. These results are, therefore, somewhat inconclusive although it does seem reasonable that an effect of the type of insulation used on moderate sized wires should be seen.

6. References

[1] SAE Aerospace Information Report No. 46, The preparation and use of Chromel-Alumel Thermocouples for turbojet engines, Committee AE–2, Temperature Measurement Sensing, Society of Automotive Engineers, Inc., 485 Lexington Avenue, New York 17, N.Y., March 15, 1956.

[2] SAE Aerospace Recommended Practice No. 691, Recommended ice bath for reference junctions, Committee AE–2, Temperature Measurement Sensing, Society of Automotive Engineers, Inc., 485 Lexington Avenue, New York 17, N.Y., August 1, 1964.

[3] D. L. McElroy, Progress Report 1. Thermocouple research report for the period November 1, 1956 to October 31, 1957, ORNL 2467.

(Paper 69C2–189)

JOURNAL OF RESEARCH of the National Bureau of Standards—C. Engineering and Instrumentation
Vol. 69C, No. 2, April-June 1965

Superimposed Birefractory Plates

L. H. Adams* and R. M. Waxler

(November 30, 1964)

A study is made of the relations among the parameters involved in the passage of a beam of plane-polarized light through a pair of birefractory plates. For a pair of plates having known phase lags and a known angle between their principal axes, the angle of inclination necessary for a plane-polarized beam to emerge plane-polarized is determined. In addition, the conditions for producing circularly polarized light are developed and presented in a simple and convenient form. It turns out that the "combination" quarter-wave plate shows a striking similarity in several respects, to the ordinary quarter-wave plate. It is shown how the "combination" plates can be used to construct several novel polarimetric half-shades.

1. Introduction

Many optical instruments employ polarized light and associated birefractory plates as essential elements in their operation. For example a pair of quarter-wave plates is used in photoelastic stress analysis in order to observe a system of isochromatic lines in a stressed plate irrespective of the azimuth of the plate [1, 2].[1] Exact quarter-wave compensators are especially needed for devices such as the one developed by Goranson and Adams [3] (based on the classical method first fully described by Friedel [4]) which was used initially to measure birefringence in stressed glass, and later for determining the effect of pressure on the release of birefringence in some transparent materials [5]. Jerrard [6] has developed a similar instrument. The Friedel method has also been adapted in constructing an interference microscope [7].

The full advantage of the extraordinarily precise Friedel methods is realized only when using a compensator the optical retardation of which is almost exactly one-quarter wavelength. There are various procedures for constructing precise quarter-wave compensators. One of these is to utilize a suitable combination of two birefractory plates of arbitrary phase lag [8, 2]. A consideration of the properties of such a two plate combination brings out some relations which are of great interest and also provides a method for constructing such compensators.

2. Combining Two Plates

When a beam of plane-polarized light passes through a birefractory plate the emerging beam, as is well known, will be found in general to be elliptically polarized. In treating this problem and the problem of passing the beam through two superimposed plates we shall follow the development of Goranson and Adams [3] using their notation with some additions (see table 1). For the passage of plane-polarized light through a single plate, the four quantities, ϵ', θ_1', Φ_I and $\underline{i}_1$ which are defined in table 1 are related by the equations [2]

$$\sin 2\epsilon' = \sin 2\underline{i}_1 \sin \Phi_I, \tag{1}$$

$$\cos 2\underline{i}_1 = \cos 2\epsilon' \cos 2\theta_1', \tag{2}$$

$$\cot \Phi_I = \cot 2\epsilon' \sin 2\theta_1', \tag{3}$$

$$\tan 2\theta_1' = \tan 2\underline{i}_1 \cos \Phi_I. \tag{4}$$

[2] Equations (1), (2), and (3) above have been obtained from eqs (6), (7), and (8) in the paper by Goranson and Adams [3] using the substitutions which they have indicated. Equation (4) above has been derived from eq (5) of Goranson and Adams following their procedures and making appropriate substitutions.

TABLE 1. *Definitions of the symbols used in the text* [a]

Plates I, II—are the first and second doubly refracting plate in the path of a beam of plane-polarized light.

α_1' and γ_1'—are the vibrational directions of the faster and slower wave respectively in plate I. These directions form a set of mutually perpendicular reference axes.

α_2' and γ_2'—are the vibrational directions of the faster and slower wave respectively in plate II. These directions form a second set of mutually perpendicular reference axes.

ψ—is the angle which denotes the orientation of plate I with respect to plate II and is measured from α_2' to α_1' or from γ_2' to α_1'. ψ is always positive and is limited to the first quadrant, i.e., $0° \leq \psi \leq 90°$.

[a] The definitions given in this table correspond to those given by Goranson and Adams [3] with some additions. It may be noted that the definitions given here pertain to the special case where the principal directions of plates I and II have been chosen as the reference axes, and as a result are simpler than those of Goranson and Adams in many instances.

* Retired.

[1] Figures in brackets indicate the literature references on page 113.

ψ_c—is the value of ψ when plates I and II are superposed to produce a compound quarter-wave plate.

ϵ', ϵ''—are the ellipticities of the light emergent from plates I and II respectively. The ellipticity is defined as the angle whose tangent is $\pm(b/a)$ where a and b denote the major and minor axes respectively. By convention, with the light coming toward one, ϵ is positive when the light vector along the emergent elliptical vibration moves counterclockwise and negative when clockwise. $-45° \leq \epsilon \leq 45°$.

$\underline{i}_1$—is the angle between the vibrational direction of the entering plane-polarized light and α_1'. $-90° \leq \underline{i}_1 \leq +90°$.

$\underline{i}_2$—is the angle between the vibrational direction of the entering plane polarized light and α_2' or γ_2'. $-90° \leq \underline{i}_2 \leq +90°$.

$\underline{i}_{p_1}$, $\underline{i}_{p_2}$—are the values of $\underline{i}_1$ and $\underline{i}_2$ respectively when the emergent beam of light is linearly polarized after passing through plates I and II.

$\underline{i}_{c_1}$, $\underline{i}_{c_2}$—are the values of $\underline{i}_1$ and $\underline{i}_2$ respectively when the emergent beam of light is circularly polarized after passing through plates I and II. [It is understood in this case that plates I and II have been superimposed at the angle, ψ_c, to make a compound quarter-wave plate.]

θ_1'—refers to light which has passed through plate I and is the angle between the major axis of the elliptical vibration and α_1'. $-90° \leq \theta_1' \leq +90°$.

θ_2'—refers to light which has passed through plate I and is the angle between the major axis of the elliptical vibration and α_2' or γ_2'. $-90° \leq \theta_2' \leq +90°$.

θ_2''—refers to light which has passed through plates I and II and is the angle between the major axis of the elliptical vibration and α_2' or γ_2'. $-90° \leq \theta_2'' \leq +90°$.

Φ—is the phase lag of a given birefractory plate. $0° \leq \Phi \leq 360°$.

Φ_{I}, Φ_{II}—are the phase lags for plates I and II respectively.

When a beam of elliptically polarized light such as the one emerging from plate I passes through a second birefractory plate, the emerging beam, as is well known, is also elliptically polarized. For an elliptically polarized beam of a given ellipticity and azimuth entering a birefractory plate of a given phase lag and azimuth the ellipticity and azimuth of the emerging beam are uniquely determined. Goranson and Adams have shown that the following relations hold:

$$\sin 2\epsilon'' = \sin 2\epsilon' \cos \Phi_{\mathrm{II}} \pm \cos 2\epsilon' \sin 2\theta_2' \sin \Phi_{\mathrm{II}} \quad (5)$$

and

$$\tan 2\theta_2'' = \tan 2\theta_2' \cos \Phi_{\mathrm{II}} \mp \frac{\tan 2\epsilon'}{\cos 2\theta_2'} \sin \Phi_{\mathrm{II}}, \quad (6)$$

where again the parameters are defined in table 1.

These equations in conjunction with tables 1 and 2 and with proper regard to the significance of the $\pm$ and $\mp$ signs, are adequate to determine the correct and unique values of ϵ'' and θ_2'' as follows: Where an alternative in sign occurs (and where it occurs in other equations throughout the paper) the sign chosen depends on which of the two principal directions of plate II is chosen as the reference axis. If ψ is measured from α_2' the upper sign is used, if ψ is measured from γ_2' the lower sign is used.

When either the upper or lower sign is used in (5), it will be found that the solution for ϵ'' is unique because, by definition, $-45° \leq \epsilon'' \leq +45°$. When either the upper or lower sign is used in eq (6) it will be found that there are still two solutions for θ_2'', but physical considerations show that only one solution is valid. The correct solution for θ_2'' may be found by referring to table 2.

TABLE 2. *Limits on the correct values of $2\theta_2''$ which may be used to find a unique solution for eq (6)*

$\cot \Phi_a \equiv \cot 2\epsilon' \sin 2\theta_2'$

where $0° < \Phi_a < 180°$ if $\epsilon' > 0°$ and $180° < \Phi_a < 360°$ if $\epsilon' < 0°$

$(\Phi_{\mathrm{II}} + \Phi_a)$	$2\theta_2''$
$0° < (\Phi_{\mathrm{II}} \pm \Phi_a) < 90°$	$0° < 2\theta_2'' < 180°$
$90° < (\Phi_{\mathrm{II}} \pm \Phi_a) < 270°$	$-180° < 2\theta_2'' < 0°$
$270° < (\Phi_{\mathrm{II}} \pm \Phi_a) < 360°$	$0° < 2\theta_2'' < 180°$

3. Restoration to Plane-Polarization

First we determine what are the relations between the variables in order for the beam, originally plane-polarized, to pass through the two plates and to emerge plane-polarized.

Here $\epsilon'' = 0$. Hence by (5)

$$\tan 2\epsilon' = \mp \tan \Phi_{\mathrm{II}} \sin 2\theta_2'. \quad (7)$$

Applying (3) we have

$$\tan \Phi_{\mathrm{I}} \sin 2\theta_1' = \mp \tan \Phi_{\mathrm{II}} \sin 2\theta_2'. \quad (8)$$

Since the angle between the corresponding principal directions of the two plates is ψ, it follows that

$$\theta_2' = \theta_1' + \psi. \quad (9)$$

Substituting (9) and (4) in (8), we have (noting that ϵ'' is zero, and that $\underline{i}$ becomes $\underline{i}_{p_1}$ the inclination that will result in emerging plane-polarized light)

$$\cot 2\underline{\mathbf{i}}_{p_1}=\left(\mp\frac{\tan\Phi_I}{\tan\Phi_{II}}-\cos 2\psi\right)\frac{\cos\Phi_I}{\sin 2\psi}. \quad (10)$$

After the correct minus or plus value has been determined for use in eq (10), there will be two values of $\underline{\mathbf{i}}_{p_1}$, differing by 90°, which will satisfy the equation. These two solutions are both valid and can be associated generally with the principal axes of a single birefractory plate. For each of these solutions there will be separate values of θ_1', θ_2', and θ_2''. These two sets of values will be separated from each other by 90° just as the $\underline{\mathbf{i}}_{p_1}$ values are. The following relations are useful: From (6) and (7) we find

$$\tan 2\theta_2''=\tan 2\theta_2'(\cos\Phi_{II}+\tan\Phi_{II}\sin\Phi_{II}).$$

Multiplying and dividing by $\cos\Phi_{II}$ we obtain:

$$\tan 2\theta_2''=\tan 2\theta_2'/\cos\Phi_{II}. \quad (11)$$

From (4) and (10) we obtain

$$\cot 2\theta_1'=\left(\mp\frac{\tan\Phi_I}{\tan\Phi_{II}}-\cos 2\psi\right)\frac{1}{\sin 2\psi}. \quad (12)$$

We are now in a position, having two plates with Φ_I and Φ_{II}, and placed at angle ψ to determine what inclination $\underline{\mathbf{i}}_{p_1}$ of the entering plane-polarized beam will cause the emerging beam to be plane-polarized; and also to calculate θ_2'', the azimuth of the emerging beam. Formally stated the problem is: *Given* Φ_I, Φ_{II}, and ψ to calculate $\underline{\mathbf{i}}_{p_1}$ so that the beam will emerge plane-polarized; and also to calculate θ_2''. *Solution*, calculate $\underline{\mathbf{i}}_{p_1}$ from (10), θ_1' from (12), θ_2' from (9) and θ_2'' from (11).

3.1. Special Case for $\Phi_I=\Phi_{II}$

In many instances it would be convenient to superimpose two identical strips or slabs. Here we would have $\Phi_I=\Phi_{II}$, which we may call simply Φ. For this case eq (12) becomes

$$\cot 2\theta_1'=-\cot\psi \text{ or } \cot(90-\psi)$$

from which

$$2\theta_1'=-\psi,\ -\psi+180° \text{ or } 90°-\psi,\ 90°-\psi+180°. \quad (12a)$$

Similarly, from (10)

$$\cot 2\underline{\mathbf{i}}_{p_1}=-\cot\psi\cos\Phi \text{ or } \tan\psi\cos\Phi, \quad (10a)$$

and, from (9) and (12a)

$$2\theta_2'=\psi,\ \psi+180° \text{ or } 90°+\psi,\ 90°+\psi+180°. \quad (9a)$$

Also (incidentally) from (8) with $\Phi_I=\Phi_{II}$

$$\sin 2\theta_2'/\sin 2\theta_1'=\mp 1.$$

From (11) and (9a) it follows that

$$\tan 2\theta_2''=\tan\psi/\cos\Phi \text{ or } -\cot\psi/\cos\Phi, \quad (11a)$$

and, from (11a) and (10a) when $\Phi_I=\Phi_{II}=\Phi$

$$2\theta_2''=-2\underline{\mathbf{i}}_{p_1} \text{ or } -2\underline{\mathbf{i}}_{p_1}+180°. \quad (13a)$$

For this simplified case (when Φ and ψ are given), the procedure for determining $\underline{\mathbf{i}}_{p_1}$ and θ_2'' is to calculate $\underline{\mathbf{i}}_{p_1}$ from (10a) and θ_2'' from (13a). If desired, we may obtain θ_1' from (12a) and θ_2' from (9a).

The values of the parameters of interest are presented in two illustrative examples in table 3. In both cases $\Phi_I=\Phi_{II}=\Phi=70°$; in one example ψ has been set arbitrarily at 30°, and the second example refers to the situation where $\psi_c=41.20°$ which is the angle needed to construct a composite quarter-wave plate. (It will be shown in section 4 how the value of ψ_c is found.) Figure 1 shows the relationships of the azimuths for transmitting plane-polarized light with two superimposed plates when $\Phi_I=\Phi_{II}=\Phi=70°$ and $\psi_c=41.20°$.

TABLE 3. *Values of the parameters of interest in producing plane-polarized light and circularly polarized light when it is given that* $\Phi_I=\Phi_{II}=\Phi=70°$

Two examples are shown: (1) for an arbitrary $\psi=30°$, and, (2) for the required $\psi_c=41.20°$. (The values are given for the situation where the α'-direction of plate II is chosen as the reference axis.)

	$\psi=30°$	$\psi_c=41.20°$
Plane-polarized light	$\underline{\mathbf{i}}_{p_1}=-29.68°, 60.32°$ $\underline{\mathbf{i}}_{p_2}=0.32°, -89.68°$ $\theta_2''=29.68, -60.32°$ $\theta_1'=-15°, 75°$ $\theta_2'=15, -75°$	$\underline{\mathbf{i}}_{p_1}=-34.33°, 55.67°$ $\underline{\mathbf{i}}_{p_2}=6.87°, -83.13$ $\theta_2''=34.33°, -55.67°$ $\theta_1'=-20.60°, 69.40°$ $\theta_2'=20.60°, -69.40°$
Circularly polarized light	Note: For Circularly-polarized light $\psi(=\psi_c)=41.20°$	$\underline{\mathbf{i}}_{c_1}=10.67°, -79.33°$ $\underline{\mathbf{i}}_{c_2}=51.87°, -38.13°$ θ_2'' is undefined $\theta_1'=3.80°, -86.20°$ $\theta_2'=45.00°, -45.00°$

The parameters are obtained from the following equations (particularly applicable in this simple form since $\Phi_I=\Phi_{II}$):

Plane-polarized light	Circularly polarized light
(1) $\underline{\mathbf{i}}_{p_1}$, ... eq (10a)	(1) ψ_c ..... eq (19a)
(2) $\underline{\mathbf{i}}_{p_2}$, ... $\underline{\mathbf{i}}_{p_2}=\underline{\mathbf{i}}_{p_1}+\psi$	(2) $\underline{\mathbf{i}}_{c_1}$ ..... eq (17a)
(3) θ_2'', ... eq (13a)	(3) $\underline{\mathbf{i}}_{c_2}$ ..... $\underline{\mathbf{i}}_{c_2}=\underline{\mathbf{i}}_{c_1}+\psi$
(4) θ_1', ... eq (12a)	(4) θ_2'' ..... is undefined
(5) θ_2', ... eq (9a)	(5) θ_1' ..... eq (18a)
	(6) θ_2' ..... is given as $\theta_2'=45°$

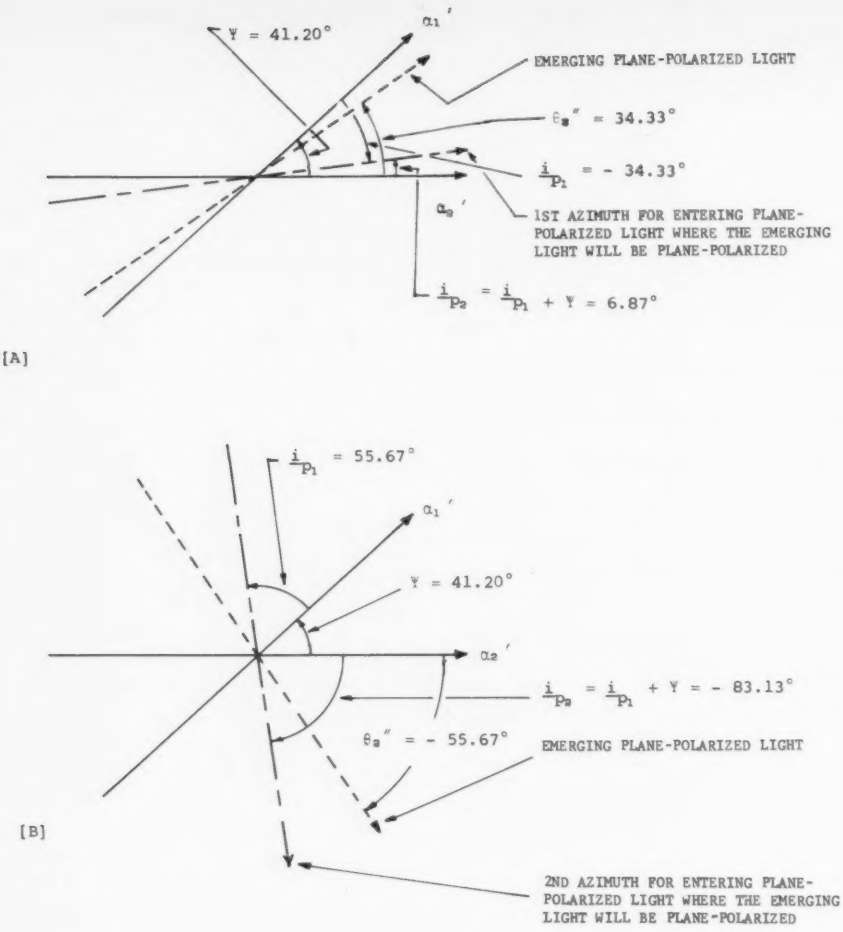
Ψ = 41.20°
α1′
EMERGING PLANE-POLARIZED LIGHT
θ2″ = 34.33°
ip1 = - 34.33°
α2′
1ST AZIMUTH FOR ENTERING PLANE-POLARIZED LIGHT WHERE THE EMERGING LIGHT WILL BE PLANE-POLARIZED
ip2 = ip1 + Ψ = 6.87°
[A]
ip1 = 55.67°
α1′
Ψ = 41.20°
α2′
ip2 = ip1 + Ψ = - 83.13°
θ2″ = - 55.67°
EMERGING PLANE-POLARIZED LIGHT
[B]
2ND AZIMUTH FOR ENTERING PLANE-POLARIZED LIGHT WHERE THE EMERGING LIGHT WILL BE PLANE-POLARIZED

FIGURE 1. *Illustration of the azimuthal relationships in the transmission of plane-polarized light by two superimposed doubly refracting plates when* $\Phi=70°$ *and* $\Psi=\Psi_c=41.20°$.

It is shown in [A] and [B] that there are two mutually perpendicular entering azimuths for which plane-polarized light will emerge plane-polarized and that the vibration direction will be rotated through the angle $(\theta_2''-\underset{\sim}{i}_{p_2})$ which is the same for both.

For any combination of birefractory plates, therefore, there can be found two mutually perpendicular azimuths for incident plane-polarized light such that the emergent light is also plane-polarized. In this respect such a combination is like a single birefractory plate. The effect of the combination differs (in general), however, from that of a single plate in that the combination rotates the vibration direction through the angle $(\theta_2''-\underset{\sim}{i}_{p_2})$. It turns out that the sense of this rotation will be either positive (counterclockwise) or negative (clockwise) depending on whether the plates are combined so that ψ is measured from the α_2' or γ_2' direction. In table 4 are presented values of the parameters for emerging plane-polarized light when the two plates have different $\Phi_{\mathrm{I}}=\Phi_{\mathrm{II}}=\Phi$, but with the arbitrary parameter, ψ, set at 30° for all cases.

TABLE 4. *Values of $\underline{i}_{p_1}$ and other parameters of interest in producing plane-polarized from two plates having different $\Phi_I = \Phi_{II} = \Phi$ but with the arbitrary parameter ψ set at 30° for all cases*

(The values are given for the situation where the α'-direction of plate II is chosen as the reference axis.)

Φ	0	15	30	45	60	75	90	105	120	135	150	165	180
Ψ	30	30	30	30	30	30	30	30	30	30	30	30	30
$2\underline{i}_{p_1}$	−30.0	−30.9	−33.7	−39.2	−49.2	−65.8	−90.0	65.8	49.2	39.2	33.7	30.9	30.0
	150.0	149.1	146.3	140.8	130.8	114.2	90.0	−114.2	−130.8	−140.8	−146.3	−149.1	−150.0
$2\theta_1'$	−30.0	−30.0	−30.0	−30.0	−30.0	−30.0	−30.0	−30.0	−30.0	−30.0	−30.0	−30.0	−30.0
	150.0	150.0	150.0	150.0	150.0	150.0	150.0	150.0	150.0	150.0	150.0	150.0	150.0
$2\theta_2''$	30.0	30.9	33.7	39.2	49.2	65.8	90.0	−65.8	−49.2	−39.2	−33.7	−30.9	−30.0
	−150.0	−149.1	−146.3	−140.8	−130.8	−114.2	−90.0	114.2	130.8	140.8	146.3	149.1	150.0
$2\theta_2'$	30.0	30.0	30.0	30.0	30.0	30.0	30.0	30.0	30.0	30.0	30.0	30.0	30.0
	−150.0	−150.0	−150.0	−150.0	−150.0	−150.0	−150.0	−150.0	−150.0	−150.0	−150.0	−150.0	−150.0

The parameters are obtained from the following equations (particularly applicable in this simple form since $\Phi_I = \Phi_{II}$):

(1) $2\underline{i}_{p_1}'$ ---------- eq (10a)
(2) $2\theta_1'$ ---------- eq (12a)
(3) $2\theta_2''$ ---------- eq (13a)
(4) $2\theta_2'$ ---------- eq (9a)

4. Simple Method for Producing Circularly Polarized Light

A simple method for getting ψ_c and $\underline{i}_{c_1}$ for given Φ_I and Φ_{II} begins as follows: Suppose we let θ'_2 equal 45°. Then, from (5) with $\epsilon''=45°$, sin $(2\epsilon'+\Phi_{II})=1$, and therefore

$$\epsilon' = 45 \mp \Phi_{II}/2. \tag{14}$$

If $\underline{i}_1$ is chosen to give ϵ' given by eq (14), then θ_1' can be calculated and $\psi=\psi_c$ can be calculated by eq (9) to give $\theta_2'=45°$. This combination of $\underline{i}_1$ and ψ_c will (by the conditions leading up to eq (14)) yield $\epsilon''=45°$, i.e., emergent laevorotary circularly polarized light.

By (14)—for this case of emerging circularly polarized light—

$$\sin 2\epsilon' = \pm\cos \Phi_{II} \tag{15}$$

and

$$\tan 2\epsilon' = \pm\cot \Phi_{II}. \tag{16}$$

From (1) and (15) we have

$$\sin 2\underline{i}_{c_1} = \pm\cos \Phi_{II}/\sin \Phi_I, \tag{17}$$

and from (3) and (16)

$$\sin 2\theta_1' = \pm\cot \Phi_{II}/\tan \Phi_I. \tag{18}$$

and from (9) and the above assumption that $\theta_2'=45°$

$$\psi_c = 45° - \theta_1'. \tag{9b}$$

It is important to note the following points in regard to eqs (17), (18), and (9b) and the "combination" plate considered here: (1) The equations admit solutions only if $90° \leq \Phi_I + \Phi_{II} \leq 270°$. (2) Careful examination shows that only one pair of solutions is valid in each equation, although there are additional apparent solutions. (3) The two solutions for ψ_c are complementary. One solution for ψ_c is obtained if α_2' is chosen as the reference axis, the second solution is obtained if γ_2' is chosen as the reference axis. (4) As noted in section 3.1 there will be a rotation of the principal directions of vibration for this "combination" plate, the sense of this rotation depends upon the choice of ψ_c. (5) The equations were developed to produce left-handed circularly polarized light, i.e., $\epsilon''=45°$. However, for a given "combination" plate, light incident at azimuth, $\underline{i}=\underline{i}_c+90°$ will emerge as right-handed circularly polarized light, i.e., $\epsilon''=-45°$.

4.1. Special Case for $\Phi_I=\Phi_{II}$

For two similar plates we put $\Phi_I=\Phi_{II}=\Phi$, and (17) becomes

$$\sin 2\underline{i}_{c_1} = \pm\cot \Phi \tag{17a}$$

and (18) becomes

$$\sin 2\theta_1' = \pm\cot^2 \Phi. \tag{18a}$$

Now from (9) $\sin 2\theta_1' = \cos 2\psi$; therefore from (18a)

$$\cos 2\psi_c = \pm\cot^2 \Phi. \tag{19a}$$

Then, from (17a) and (19a) we may readily calculate the impinging azimuth and the requisite separation, ψ_c, to give emerging circularly polarized light. Incidentally, it should be noted that a solution for ψ_c is obtained when Φ ranges from 45 to 135° but not from 0 to 45° or from 135 to 180°.

As a supplement to the example shown in figure 1, figure 2 shows the relationships of the azimuths for producing circularly polarized light from two superimposed plates when $\Phi_I=\Phi_{II}=\Phi=70°$. Figure 3 shows the rotation of the principal planes of vibration in a "combination" quarter-wave plate when $\Phi=70°$. As shown, the rotation may be either positive or negative depending on whether the upper or lower sign is chosen in eq (19a) when solving for ψ_c.

Table 5 gives values of ψ_c, $\underline{i}_{c_1}$, and $\underline{i}_{p_1}$ for various values of Φ when two similar plates are combined to make a quarter-wave plate. Here it is evident that

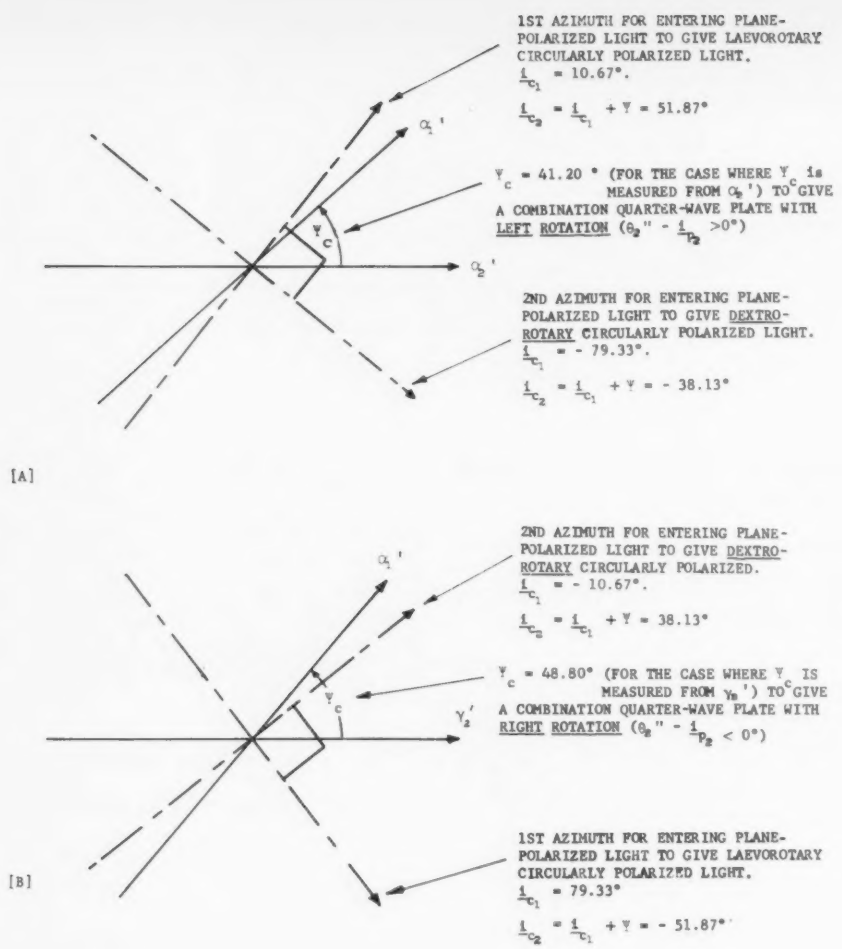
1ST AZIMUTH FOR ENTERING PLANE-POLARIZED LIGHT TO GIVE LAEVOROTARY CIRCULARLY POLARIZED LIGHT.
i_{c_1} = 10.67°.
$i_{c_2} = i_{c_1} + \Psi$ = 51.87°
Ψ_c = 41.20° (FOR THE CASE WHERE Ψ IS MEASURED FROM α_2') TO GIVE A COMBINATION QUARTER-WAVE PLATE WITH LEFT ROTATION ($\theta_2'' - i_{p_2} > 0°$)
α_1'
Ψ_c
α_2'
2ND AZIMUTH FOR ENTERING PLANE-POLARIZED LIGHT TO GIVE DEXTRO-ROTARY CIRCULARLY POLARIZED LIGHT.
i_{c_1} = - 79.33°.
$i_{c_2} = i_{c_1} + \Psi$ = - 38.13°
[A]
2ND AZIMUTH FOR ENTERING PLANE-POLARIZED LIGHT TO GIVE DEXTRO-ROTARY CIRCULARLY POLARIZED.
i_{c_1} = - 10.67°.
$i_{c_2} = i_{c_1} + \Psi$ = 38.13°
α_1'
Ψ_c = 48.80° (FOR THE CASE WHERE Ψ IS MEASURED FROM γ_2') TO GIVE A COMBINATION QUARTER-WAVE PLATE WITH RIGHT ROTATION ($\theta_2'' - i_{p_2} < 0°$)
Ψ_c
γ_2'
1ST AZIMUTH FOR ENTERING PLANE-POLARIZED LIGHT TO GIVE LAEVOROTARY CIRCULARLY POLARIZED LIGHT.
i_{c_1} = 79.33°
$i_{c_2} = i_{c_1} + \Psi$ = - 51.87°
[B]

FIGURE 2. *Illustration of the azimuthal relationships in the production of circularly polarized light by two superimposed doubly refracting plates when $\Phi = 70°$.*

In case [A], $\Psi = \Psi_c$ is measured from α_2' and rotates the principal vibration directions to the left. In case [B], $\Psi = \Psi_c = 48.80°$ is measured from γ_2' and rotates the principal vibration directions to the right by an equal amount (see fig. 3). It is shown in each case that there exist mutually perpendicular azimuths of incidence which yield laevo- and dextro-rotary circularly polarized light respectively, which are at 45° to the azimuths for the production of plane-polarized light (fig. 3).

the choice of ψ_c is fixed by the phase lags of the plates. A striking feature of the relation of $\underline{i}_{c_1}$ to $\underline{i}_{p1}$ is brought out by the table, namely that $(\underline{i}_{c_1} - \underline{i}_{p_1})$ appears to be always $\pm 45°$. As a matter of fact in a pair of plates adjusted to transform plane-polarized light into circularly polarized light the difference between the two $\underline{i}$'s is exactly 45°. That is, it may be readily shown that

$$\sin^2 2\underline{i}_{c_1} = \cos^2 2\underline{i}_{p_1} \tag{20}$$

The proof of relation (20) may be found in appendix 1. In this respect the "combination" quarter-wave plate behaves like an ordinary single plate with 90° retardation.

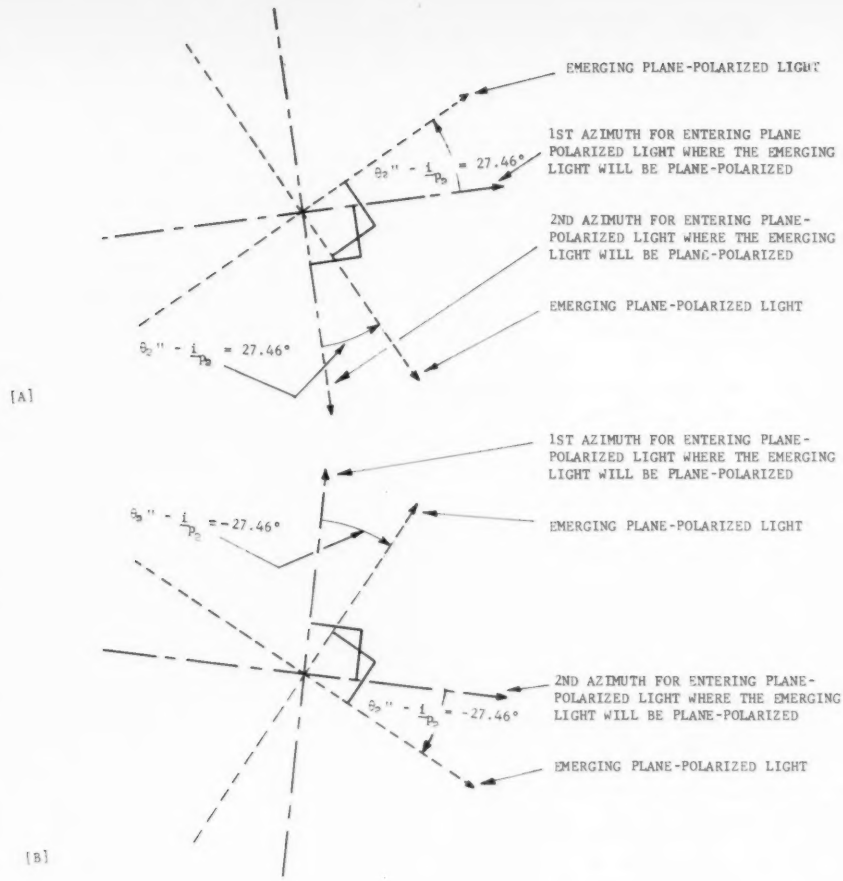
EMERGING PLANE-POLARIZED LIGHT
1ST AZIMUTH FOR ENTERING PLANE POLARIZED LIGHT WHERE THE EMERGING LIGHT WILL BE PLANE-POLARIZED
2ND AZIMUTH FOR ENTERING PLANE-POLARIZED LIGHT WHERE THE EMERGING LIGHT WILL BE PLANE-POLARIZED
EMERGING PLANE-POLARIZED LIGHT
[A]
1ST AZIMUTH FOR ENTERING PLANE-POLARIZED LIGHT WHERE THE EMERGING LIGHT WILL BE PLANE-POLARIZED
EMERGING PLANE-POLARIZED LIGHT
2ND AZIMUTH FOR ENTERING PLANE-POLARIZED LIGHT WHERE THE EMERGING LIGHT WILL BE PLANE-POLARIZED
EMERGING PLANE-POLARIZED LIGHT
[B]

FIGURE 3. *Illustration of the rotation of the principal vibration directions in combination quarter-wave plates when* $\Phi = 70°$.

Two situations corresponding to the two solutions of eq (19A) are shown: In [A], $\Psi = \Psi_\epsilon = 41.20°$ and is measured from α_2'; In [B], $\Psi = \Psi_\epsilon = 48.80°$ and is measured from γ_2'. The magnitude of the rotation is the same in both cases. Case [A] is the same as that in figure 1 where the azimuthal relations of the principal vibration directions of the plates are shown. Note that the azimuths in each case are mutually perpendicular and at 45° to those for producing circularly polarized light (fig. 2)

TABLE 5.—*Values of* ψ_ϵ, $\underline{i}_{c_1}$, $\underline{i}_{p_1}$, *and related parameters in producing circularly polarized light from two plates having different* $\Phi_I = \Phi_{II} = \Phi$

(The values are given for the situation where the α'−direction of Plate II is chosen as the reference axis.)

Φ	45	50	60	70	80	90	100	110	120	130	135
$\cot \Phi$	1.000	0.840	0.577	0.3640	0.1762	0	−0.1762	−0.364	−0.577	−0.840	−1.000
$\cot^2 \Phi$	1.000	.704	.333	.1326	.0312	0	.0312	.1326	.333	.706	1.000
$2\underline{i}_{c_1}$	90.00	57.2	35.2	21.34	10.2	0	−10.2	−21.34	−35.2	−57.2	−90.0
	−90.0	−122.8	−144.8	−158.66	−169.8	180	169.8	158.66	144.8	122.8	90.0
$2\psi_\epsilon$	0	45.4	70.6	82.40	88.4	90	88.4	82.40	70.6	45.4	0
ψ_ϵ	0	22.7	35.3	41.20	44.2	45.0	44.2	41.20	35.3	22.7	0
$\cot \psi_\epsilon$	∞	2.42	1.412	1.142	1.028	1.000	1.028	1.142	1.412	2.42	∞
$\cos \Phi$	0.707	0.642	0.500	0.342	0.1736	0	−0.1736	−0.342	−0.500	−.642	−0.707
$-\cot \Psi_\epsilon \cos \Phi$	−∞	−1.55	−.706	−.3918	−.1789	0	.1789	.3918	.706	1.55	∞
$2\underline{i}_{p_1}$	0	−32.8	−54.8	−68.66	−79.8	−90.0	79.8	68.66	54.8	32.8	0
	180.0	147.2	125.2	111.34	100.2	90.0	−100.2	−111.34	−125.2	−147.2	180.0

The parameters are obtained from the following equations (particularly applicable in this simple form since $\Phi_I = \Phi_{II}$):

(1) ψ_ϵ ---------- eq (19a)
(2) $\underline{i}_{c_1}$ ---------- eq (17a)
(3) $\underline{i}_{p_1}$ ---------- eq (10a)

In another respect also the "combination" plate resembles a simple quarter-wave plate, namely that when a beam of plane-polarized light is passed through, the azimuth of the ellipse of the emerging beam is independent of the inclination $\underline{i}_1$ of the entering beam. For proof of this interesting relation see appendix 2.

There is a third way in which the "combination" plate resembles an ordinary quarter-wave plate. To show this, we first recall that by (1) a beam of plane-polarized light passing through a plate with Φ equal to 90° emerges with ϵ equal to $\underline{i}$. For our "combination" plate—let us put

$$\Delta = \underline{i}_1 - \underline{i}_{p_1}. \tag{21}$$

It turns out, as shown in appendix 3, that whereas with the ordinary quarter-wave plate $\epsilon' = \underline{i}$, for the combination quarter-wave plate

$$\epsilon'' = \underline{i}_1 - \underline{i}_{p_1} \equiv \Delta. \tag{22}$$

Thus, there is the same relation, between ϵ'' and Δ as there is between ϵ' and $\underline{i}$ for the simple quarter-wave plate.

5. Design of Half-Shade Systems

Precision measurements in polarimetry usually depend upon making a brightness match between two parts of a field of view. Half-shade devices have been constructed which permit the observer to ascertain very precisely the azimuth of plane-polarized light, and the azimuth and ellipticity of elliptically polarized light [6, 9, 10]. As examples, the Lippich half-nicol and the Cornu-Jellet split nicol are widely known as azimuth half-shades, and the Brace half-shade has been used extensively in the measurement of ellipticity. The superimposition of doubly refracting plates makes it possible to construct several novel half-shade devices. These half-shades, particularly adapted to monochromatic analysis, are interesting in themselves, and they serve to illustrate some interesting features of the "combination" plates discussed thus far.

5.1. Azimuth Half-Shades

The inherent rotation of the principal vibration directions of a "combination" quarter-wave plate which was discussed in sections 3.1 and 4.1 may be used to construct an azimuth half-shade. It is convenient to denote by α'_L and γ'_L the principal directions (after rotation) of a laevorotary compound plate, and by α'_D and γ'_D the principal directions (after rotation) of a dextrorotary compound plate.

(a) In figure 4 it is shown that two compound plates may be cut along γ'_L and γ'_D and these two directions placed in adjacent positions along the vibration direction, P, of a nicol prism. The combination of nicol and two plates in fixed position then acts effectively as an azimuth half-shade with half-shadow angle of $2|\theta''_2 - \underline{i}_{r2}|$. The characteristics of this half-shade are analogous to those of the Lippich half-nicol or the Cornu-Jellet split nicol. As an equivalent arrangement to the one shown in figure 4, α'_L may be interchanged for γ'_L, when, at the same time, α'_D is interchanged for γ'_D.

(b) The half-shade described in section (a) above depends upon the rotation of the optic axes which is a unique feature of "Combination" plates, and the two parts of the biplate may have an arbitrary path difference. On the other hand, half-wave plates have long been known for their ability to rotate the plane of polarization of incident light [11]. The Laurent plate is a half-wave plate placed partly over a polarizing prism and rotated in fixed combination with the prism [11]. Chauvin has described an analyzer consisting of the same combination [9]. The advantage of these half-shade devices lies in the fact that the sensitivity may be varied by varying the angle between the vibration direction of the polarizing prism and one of the principal directions of the half-wave plate.

A half-wave plate may be simply constructed by superposing two of the "combination" quarter-wave plates described in this paper. However one of the quarter-wave plates must be dextrorotary and the other laevorotary and they must have equal amounts of rotation of the optic axes. The two plates must be combined so as to compensate for the inherent rotation of each one.

(c) It is known that when a doubly refracting material is placed with its principal vibration direction in a diagonal position between two crossed quarter-wave plates, that the combination acts as as an optically rotary material [3]. Two specimens may be cut from the same doubly refracting sheet and positioned so that the fast direction of one specimen adjoins the slow direction of the other.

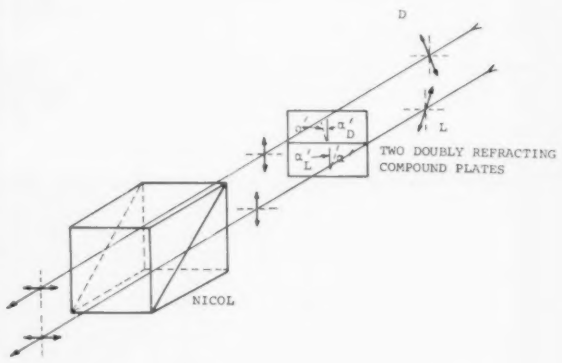

FIGURE 4. *An azimuth half-shade consisting of two compound plates in fixed combination with an analyzing nicol prism.*

Incident plane-polarized light with azimuth shown at D causes the top half of the field of view to show total extinction. Incident plane-polarized light with azimuth shown at L causes the bottom half of the field of view to show total extinction.

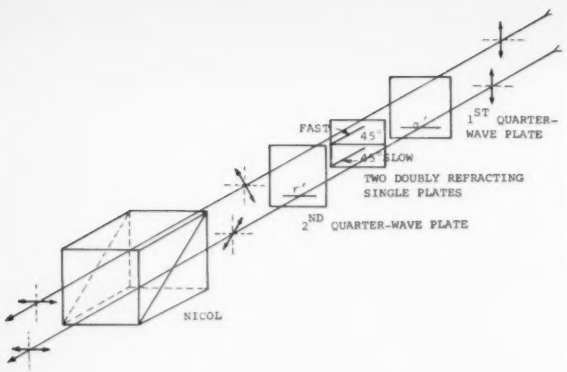

FIGURE 5. *An azimuth half-shade consisting of a divided doubly refracting material between two crossed quarter-wave plates.*

The analyzing nicol rotates independently and is shown in a position where the two halves of the field of view have equal brightness.

If these two plates are placed so that their principal vibration directions are in a diagonal position between two crossed quarter-wave plates, the field of view being evenly divided, this fixed combination may be employed as an azimuth half-shade whose half-shadow angle is equal to Φ, the phase lag of the divided plate. One possible arrangement is shown in figure 5.

This half-shade acts then in a manner analogous to two plates of quartz cut perpendicularly to the optic axis, one plate being laevorotary and the other being dextrorotary. The combination described above acts effectively as a Soliel or Nakamura half-shade [6].

The arrangement shown in figure 5 is correct when using quarter-wave plates with no unusual features. However, in constructing the half-shade from quarter-wave plates described in this paper, the inherent rotations of the plates themselves must be recognized and accounted for. For example, in the arrangement shown in figure 5, it is possible to use a compound laevorotary plate for the first quarter-wave plate, and to set the axes so that α'_L is fixed at the azimuth of α' shown in the figure. In this case a dextrorotary compound plate must be used for the second quarter-wave plate, γ' (not γ'_D) of this second plate will still have the azimuth of γ' shown in the figure.

5.2. An Elliptic Half-Shade

The Bravais biplate is well known as an elliptic half-shade [10]. It consists of two quarter-wave plates with their edges in juxtaposition and the fast ray of one plate parallel to the slow ray of the other. This biplate serves to show when elliptically polarized light has been completely restored to plane-polarized light, because the two halves of the field match at all azimuths, the brightness level

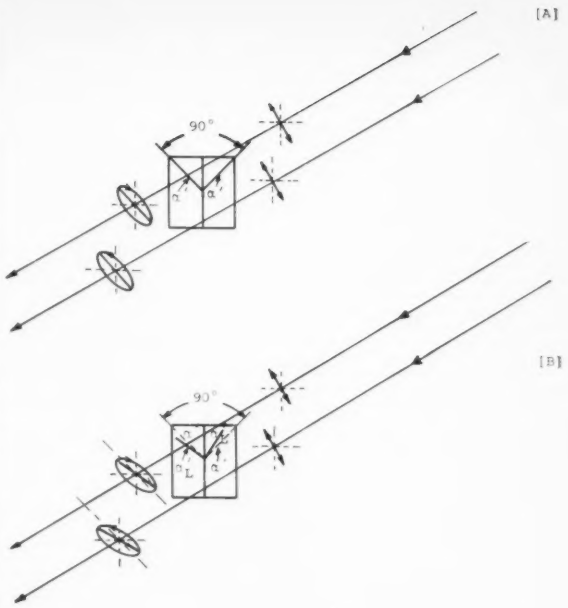

FIGURE 6. *Bravais biplates.*

A An elliptic half-shade in which the two parts are single plates of equal and opposite order (quarter-wave).

B An elliptic half-shade in which the two parts are *compound* plates of equal and opposite order (quarter-wave).

alone varying, but the match is destroyed as soon as the incident light becomes elliptically polarized. A Bravais biplate is shown in figure 6A.

Because the azimuth of this biplate may be varied with respect to the analyzing nicol, it is perfectly all right to use compound quarter-wave plates with their associated rotation of the principal axes. It is important, however, that both halves of the biplate have the same amount and sign of rotation. Figure 6B shows a Bravais biplate constructed from two laevorotary quarter-wave plates. The biplate might as easily be constructed from two dextrorotary quarter-wave plates.

5.3. Half-Shades Uniquely Adapted to the Friedel Method

The third Friedel method has been employed by Goranson and Adams for the precise determination of optical path difference [3]. According to this method, plane-polarized light is made to pass through a doubly refracting specimen with one of the principal vibration directions of the specimen set at 45 deg with respect to the vibration direction of the polarizer. The light is then made to pass through a quarter-wave plate with one of its principal directions parallel to the vibration direction of the original plane-polarized light. The light emergent

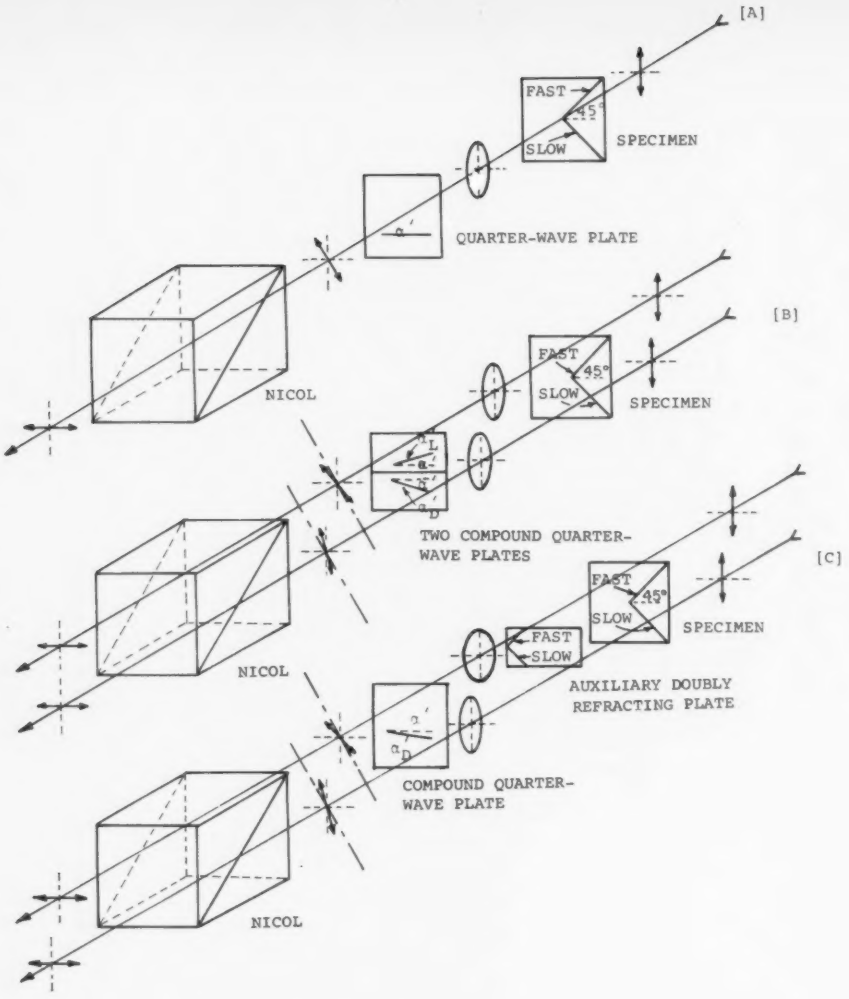

FIGURE 7. *Friedel method III.*

A There is no divided field. The analyzing nicol must be rotated to the left for complete extinction.
B Two compound quarter-wave plates produce a divided field. The analyzing nicol must be rotated to the left to make a brightness match between the two halves of the field.
C A divided field is produced by an auxiliary doubly refracting plate. The analyzing nicol must be rotated to the left to make a brightness match between the two halves of the field.

from the quarter-wave plate is plane-polarized, and an extinction position may be found by rotating the analyzer. The measured angle between the azimuths of the incident and emergent plane-polarized beams of light is equal to one-half the phase angle of the specimen. The arrangement of the optical elements for this method is shown in figure 7A.[3]

One may employ a compound quarter-wave plate described in this paper instead of the more familiar type of quarter-wave plate which is usually obtained by splitting sheets of mica to the proper thickness. In this case, however, it is necessary to know the sign and amount of the inherent rotation of the quarter-wave plate itself and to account for it in setting the zero position of the analyzer.

(a) An effective half-shade may be obtained if two compound quarter-wave plates (one dextrorotary, and one laevorotary) are placed with their

[3] Although no half-shade device is shown in figure 7A the original instrument designed by Goranson and Adams [3] was equipped with a Wright biquartz wedge plate [12].

edges in juxtaposition so as to divide the field and with the α' direction of each alined with the principal vibration direction of the polarizer. This arrangement is shown is figure 7B. In this case there is no correction to be made to the zero position of the analyzer, and, in measuring, the analyzer is rotated until the two halves of the divided field have the same intensity.

(b) Another half-shade device may be obtained if a second doubly refracting plate is placed after the specimen so that it covers half the field and has its principal vibration directions alined with those of the specimen. The auxiliary plate may be selected so that the rotation incurred by its phase lag just balances the inherent rotation of a compound quarter-wave plate. Actually, Φ of this auxiliary plate must have the magnitude $4|\theta_2''-\underline{i}_{p_2}|$, where θ_2'' and $\underline{i}_{p_2}$ refer to the "combination" quarter-wave plate. A typical arrangement is shown in figure 7C for the case of a dextrorotary compound quarter-wave plate. In making a measurement, as with the half-shade device discussed in part (a), the analyzer is rotated until the two halves of the field have the same intensity.

6. References

[1] E. G. Coker and L. N. G. Filon, A Treatise on Photoelasticity (Cambridge University Press, Cambridge, 1957).
[2] H. T. Jessop and F. C. Harris, Photoelasticity (Dover Publications, Inc., New York, 1949).
[3] R. W. Goranson and L. H. Adams, J. Frank. Inst. **216,** 475 (1933).
[4] G. Friedel, Bull. Soc. Min. France **16,** 19 (1893).
[5] R. M. Waxler and L. H. Adams, J. Res. NBS **65A** (Phys. and Chem.) No. 4, 283 (1961).
[6] H. G. Jerrard, J. Opt. Soc. Am. **44,** 289 (1954).
[7] F. H. Smith, Research (London) **8,** 385 (1955).
[8] Z. Tuzi and H. Oosima, Sci. Papers Inst. Phys. Chem. Res. Tokyo **36,** 72 (1939).
[9] H. G. Jerrard, J. Opt. Soc. Am. **38,** 35 (1948).
[10] C. A. Skinner, J. Opt. Soc. Am. and Rev. Sci. Instr. **10,** 491 (1925).
[11] A. C. Hardy and F. H. Perrin, The Principles of Optics (McGraw-Hill Book Company, Inc., New York, 1932).
[12] F. E. Wright, Am. J. Sci. **26,** 377, 391 (1908).

7. Appendix 1. Relation Between $\underline{i}_{c_1}$ and $\underline{i}_{p_1}$ in an "Adjusted" Combination Plate

Given: the four quantities Φ, ψ_c, $\underline{i}_{p_1}$ and $\underline{i}_{c_1}$ and the three equations. (When ψ is measured from α_2')

$$\cos 2\psi_c = +\cot^2 \Phi \tag{19a}$$

$$\tan \psi_c = -\tan 2\underline{i}_{p_1} \cos \Phi \tag{10a}$$

$$\sin 2\underline{i}_{c_1} = \cot \Phi. \tag{17a}$$

To prove:

$$\sin^2 2\underline{i}_{c_1} = \cos^2 2\underline{i}_{p_1} \tag{20}$$

from (19a),

$$\frac{1-\cot^2\Phi}{1+\cot^2\Phi} = \frac{1-\cos 2\psi_c}{1+\cos 2\psi_c}$$

$$\sin^2\Phi - \cos^2\Phi = \frac{\sin 2\psi_c}{\cos 2\psi_c} = \tan^2\psi_c$$

dividing by $\cos^2\Phi$ gives

$$\frac{1}{\cot^2\Phi} - 1 = \frac{\tan^2\psi_c}{\cos^2\Phi}$$

or

$$\cot^2\Phi = \frac{1}{1+\dfrac{\tan^2\psi_c}{\cos^2\Phi}}. \tag{23}$$

From (23) and (10a) we have,

$$\cot^2\Phi = \frac{1}{1+\tan^2 2\underline{i}_{p_1}} = \cos^2 2\underline{i}_{p_1}. \tag{24}$$

From (24) and (17a) we have $\sin^2 2\underline{i}_{c_1} = \cos^2 2\underline{i}_{p_1}$. (The proof when ψ is measured from γ_2' is similar.)

8. Appendix 2

Given eq (6) and other relations pertaining to the "combination" quarter-wave plate, it is required to prove that the resulting azimuth, θ_2'', is independent of the inclination, $\underline{i}_1$, of the entering plane-polarized beam.

By (3) the eq (6) becomes

$$\tan 2\theta_2'' = \tan 2\theta_2' \cos\Phi - \frac{\tan\Phi \sin\theta_1'}{\cos 2\theta_2'} \sin\Phi. \tag{6a}$$

In order to eliminate θ_2' and θ_1', we proceed as follows: By (9) and (4), we have

$$\tan 2\theta_2' = \frac{\tan 2\underline{i}_1 \cos\Phi + \tan 2\psi_c}{1-\tan 2\underline{i}_1 \cos\Phi \tan 2\psi_c}. \tag{25}$$

Also, we obtain from (9)

$$\frac{\sin 2\theta_1'}{\cos 2\theta_2'} = \frac{1}{\cot 2\theta_1' \cos 2\psi_c - \sin 2\psi_c}. \tag{26}$$

From this, with (4) and (19a)

$$\frac{\sin 2\theta_1'}{\cos 2\theta_2'} = \frac{1}{\dfrac{\cot^2\Phi}{\tan 2\underline{i}_1 \cos\Phi} - \sqrt{1-\cot^4\Phi}} \tag{27}$$

and, by (19a)

$$\tan 2\psi_c \left(\equiv \frac{\sin 2\psi_c}{\cos 2\psi_c} \right) = \frac{\sqrt{1-\cot^4\Phi}}{\cot^2\Phi}. \tag{28}$$

Now substitute $\tan 2\psi_c$ from (28) in (25), and put the resulting value of $\tan 2\theta_2'$ and also the value of

$\sin 2\theta_1'/\cos 2\theta_2'$ from (27) in (6a), and we obtain an expression equivalent to the second term of (6) or (6a). Multiply the numerator and denominator by $\sin^2 \Phi$ to get a modified expression, which we call A, i.e.,

$$\tan 2\theta_2'' = A.$$

It will be found that $A \cos \Phi/\sqrt{-\cos 2\Phi}$ turns out to be simply unity (the quantities $\underset{\sim}{\mathbf{i}}_1$ and Φ happily dropping out). Therefore,

$$\tan 2\theta_2'' = \frac{\sqrt{-\cos 2\Phi}}{\cos \Phi} = \tan 2\psi_e \cos \Phi. \qquad (29)$$

The azimuth of the elliptically polarized beam is therefore independent of $\underset{\sim}{\mathbf{i}}_1$.

9. Appendix 3. Ellipticity of a Light Beam Emerging From an "Adjusted" Combination Plate

We have $\Phi_I = \Phi_{II} \equiv \Phi$ and ψ is measured from α_{II}'. By substituting (1) and (2) in (5) we obtain

$$\sin 2\epsilon'' = \sin 2\underset{\sim}{\mathbf{i}}_1 \sin \Phi \cos \Phi + \cos 2\underset{\sim}{\mathbf{i}}_1 \sin \Phi \sin 2\theta_2'/\cos 2\theta_1'. \qquad (30)$$

From (9),

$$\sin 2\theta_2' = \sin 2\theta_1' \cos 2\psi + \cos 2\theta_1' \sin 2\psi, \qquad (9c)$$

and, introducing (9c) into (30),

$$\sin 2\epsilon'' = \sin 2\underset{\sim}{\mathbf{i}}_1 \sin \Phi \cos \Phi + \cos 2\underset{\sim}{\mathbf{i}}_1 \sin \Phi (\tan 2\theta_1' \cos 2\psi + \sin 2\psi). \qquad (31)$$

From (19a),

$$\sin 2\psi_e = \sqrt{1-\cot^4 \Phi}, \qquad (19b)$$

and, introducing (4), (19a), and (19b) into (31),

$$\sin 2\epsilon'' = \sin 2\underset{\sim}{\mathbf{i}}_1 \sin \Phi \cos \Phi + \cos 2\underset{\sim}{\mathbf{i}}_1 \sin \Phi (\tan 2\underset{\sim}{\mathbf{i}}_1 \cos \Phi \cot^2 \Phi + \sqrt{1-\cot^4 \Phi}). \qquad (32)$$

Next, noting that, in general,

$$\sin \Phi \cos \Phi \cot^2 \Phi = \cos^3 \Phi/\sin \Phi$$

and

$$\sin \Phi \cos \Phi + \cos^3 \Phi/\sin \Phi = \cot \Phi$$

also

$$\sin \Phi \sqrt{1-\cot^4 \Phi} = \sqrt{1-\cot^2 \Phi},$$

$$\sin 2\epsilon'' = \sin 2\underset{\sim}{\mathbf{i}}_1 \cot \Phi + \cos 2\underset{\sim}{\mathbf{i}}_1 \sqrt{1-\cot^2 \Phi}. \qquad (33)$$

From (24),

$$\pm \sin 2\underset{\sim}{\mathbf{i}}_{p_1} = \sqrt{1-\cot^2 \Phi}. \qquad (24a)$$

From the geometry the sign can be either plus or minus; taking the case where the sign is minus—

$$\sin 2\epsilon'' = \sin 2\underset{\sim}{\mathbf{i}}_1 \cos 2\underset{\sim}{\mathbf{i}}_{p_1} - \cos 2\underset{\sim}{\mathbf{i}}_1 \sin 2\underset{\sim}{\mathbf{i}}_{p_1}. \qquad (34)$$

$$\sin 2\epsilon'' = \sin (2\underset{\sim}{\mathbf{i}}_1 - 2\underset{\sim}{\mathbf{i}}_{p_1}), \qquad (35)$$

or

$$\epsilon'' = \underset{\sim}{\mathbf{i}}_1 - \underset{\sim}{\mathbf{i}}_{p_1} \equiv \Delta. \qquad (22)$$

(Paper 69C2–190)

JOURNAL OF RESEARCH of the National Bureau of Standards—C. Engineering and Instrumentation
Vol. 69C, No. 2, April–June 1965

A Self-Calibrating Instrument for Measuring Conductance at Radio Frequencies

Leslie E. Huntley*

(January 12, 1965)

Accuracies obtainable in measuring resistance (conductance) at radio frequencies have lagged behind those obtainable in measuring reactance (susceptance), because frequency-dependent changes in the values of resistors are not as well known as are such changes in capacitors, and because no satisfactory method has existed for comparing resistors to capacitors at radio frequencies. An instrument based on the twin T null circuit can be made self-calibrating at a given frequency, allowing conductances in the proper range to be measured directly in terms of a change in capacitance, without any need for accurate knowledge of the values of the circuit elements. Analysis of a practical circuit shows that such an instrument is potentially capable of measuring conductance to within a few parts in 10^6 at frequencies below about 15 MHz, and that accuracies actually obtained will be limited only by the accuracy to which changes in effective capacitance are known. Conductances between 0.01 and 0.0001 mho were measured at 10^7 radians/sec with an estimated error of 0.05 percent, which is the error associated with the measurement of changes in effective capacitance at that frequency.

1. Introduction

It has long been known that capacitors are superior to either inductors or resistors for use as impedance standards at high frequencies, because changes in their effective values with increasing frequency can be more accurately and more easily evaluated than can such changes in either resistors or inductors. For this reason, the High Frequency Impedance Group in the Electronic Calibration Center at NBS-Boulder, has decided to refer all its measurements of impedance at high frequencies to standards of capacitance [1].[1] While either null or resonance techniques can be used to compare capacitors and inductors to derived standards of capacitance, no satisfactory technique has existed for comparing resistors to capacitors at radio frequencies. The existing null techniques for measuring resistance require prior knowledge of the effective values of at least one resistor at the frequency at which the measurement is to be made. The resonance techniques, while theoretically capable of measuring resistance directly in terms of a change in capacitance, are at present capable of high accuracy only when measuring very high or very low values of resistance. Because of the lack of a satisfactory measurement technique, the accuracies obtainable in resistance measurements have lagged behind those obtainable in the measurement of reactance.

An investigation of the twin T null circuit has shown that it is possible to construct an instrument capable of measuring resistance directly in terms of a change of capacitance, without prior knowledge of the values of any of the circuit elements.

This paper describes an instrument which was constructed for this purpose, and presents results which indicate that resistances, in the proper range, can be measured to an accuracy which is limited only by the accuracy to which the change in capacitance is known.

2. Circuit Equations

2.1. Ideal Case (No Residual Impedances)

The circuit to be considered (fig. 1) is adapted from one which was described by Tuttle [2], and applied to a commercial instrument by Sinclair [3], in 1940. The circuit is essentially the one which Woods [4] used in his VHF Dual Admittance Bridge in 1950. Tuttle has shown

* Radio Standards Engineering Division, NBS Boulder Laboratories, Boulder, Colo.
[1] Figures in brackets indicate the literature references at the end of this paper.

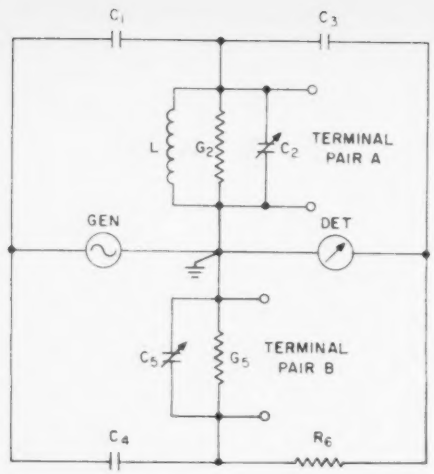

FIGURE 1. *Twin* T *circuit using pure components.*

that the condition for zero transmission through the twin T (null condition) is given by

$$Z_1+Z_3+\frac{Z_1Z_3}{Z_2}+Z_4+Z_6+\frac{Z_4Z_6}{Z_5}=0. \tag{1}$$

In the present case, $Z_1=\frac{1}{j\omega c_1}$, $Z_3=\frac{1}{j\omega c_3}$, etc., and the real and imaginary parts of (1) give the two null equations:

$$C_1+C_2+C_3+\frac{C_1C_3}{C_4}(1+R_6G_5)=\frac{1}{\omega^2L} \tag{2}$$

and

$$\omega^2R_6C_1C_3\left(1+\frac{C_5}{C_4}\right)=G_2. \tag{3}$$

As in the Woods Bridge, a measurement can be made by connecting an unknown admittance $Y_x=G_x+j\omega C_x$, either to terminal-pair A, or to terminal-pair B. When Y_x is connected to terminal-pair A, C_2 must be replaced by $C_2'+C_x$, G_2 by $G_2'+G_x$, and C_5 by C_5', in the null equations. Similar changes (indicated by double primes) must be made when Y_x is connected to terminal-pair B. Subtracting the initial null equations from the final ones yields the four expressions

$$C_{xA}=-\Delta C_2 \tag{4}$$

$$C_{xB}=-\Delta C_5' \tag{5}$$

$$G_{xA}=\omega^2\left(R_6\frac{C_1C_3}{C_4}\right)\Delta C_5 \tag{6}$$

$$G_{xB}=\frac{-\Delta C_2'}{\left(R_6\frac{C_1C_3}{C_4}\right)}, \tag{7}$$

where

$$\Delta C_2=C_2'-C_2 \qquad \Delta C_2'=C_2''-C_2$$

$$\Delta C_5=C_5'-C_5 \qquad \Delta C_5'=C_5''-C_5,$$

and subscripts A and B denote the terminal-pair to which Y_x is connected.

If P is defined as

$$P \equiv R_6 \frac{C_1 C_3}{C_4},$$

then

$$G_{xA} = \omega^2 P \Delta C_5 \tag{8}$$

and

$$G_{xB} = \frac{-1}{P} \Delta C_2'. \tag{9}$$

If a conductance is measured first on terminal-pair A, then on terminal-pair B,

$$G_{xA} = G_{xB}$$

and

$$\omega^2 P \Delta C_5 = -\frac{1}{P} \Delta C_2'$$

$$P^2 = -\frac{1}{\omega^2} \frac{\Delta C_2'}{\Delta C_5}.$$

If P is adjustable so that it can be made equal to $\frac{1}{\omega}$,

$$\frac{1}{\omega^2} = \frac{-1}{\omega^2} \frac{\Delta C_2'}{\Delta C_5},$$

and

$$\Delta C_5 = -\Delta C_2'.$$

If P is adjusted to make the same change in capacitance necessary to null the instrument when G_x is measured on terminal-pair A, as when it is measured on terminal-pair B, then $P = \frac{1}{\omega}$, and

$$G_{xA} = \omega \Delta C_5 \tag{10}$$

$$G_{xB} = -\omega \Delta C_2''. \tag{11}$$

While P has not been eliminated from the calculation of G_x, it is possible to evaluate it with great accuracy, allowing conductance to be measured with accuracies limited only by the accuracy to which a change in capacitance is known.

It should be mentioned that a conductance may be measured in terms of a change in capacitance without making P equal to $1/\omega$. If $G_{xA} = G_{xB} = G_x$, multiplying eq (8) by eq (9) yields the expression

$$G_x^2 = -\omega^2 \Delta C_2' \Delta C_5,$$

and P is eliminated from the calculation of G_x. Because the number of measurements needed to determine G_x is doubled, and because accuracy decreases as the value of P departs from $1/\omega$, this method is less effective than the other, especially when more than a few measurements are to be made at a given frequency.

2.2. Realistic Circuit (Including Residual Impedances)

In general, residual impedances cause the effective values of the circuit elements to change with frequency and cause losses in the fixed capacitors, variable losses in the variable capacitors, and some reactance to be associated with the fixed resistors.

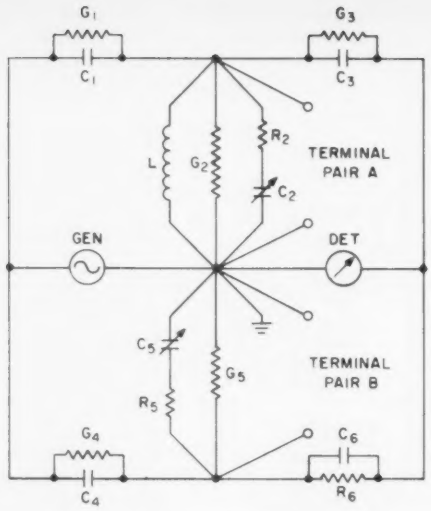

FIGURE 2. *Twin T circuit using impure components.*

The circuit of figure 2 is a more realistic representation of the actual circuit. In the figure, the value of each circuit element is taken as its effective value at the frequency at which the instrument is used. If R_2 is lumped with G_2 for the present, and R_5 with G_5, the null equations for the circuit of figure 2 are

$$G_1G_3\left(G_4+G_5+\frac{1}{R_6}\right)-\omega^2(C_1G_3+C_3G_1)(C_4+C_5+C_6)-\omega^2C_1C_3\left(G_4+G_5+\frac{1}{R_6}\right)$$

$$+\frac{G_4}{R_6}(G_1+G_2+G_3)-\omega^2\left(\frac{C_4}{R_6}+C_6G_4\right)\left(C_1-\frac{1}{\omega^2L}+C_2+C_3\right)-\omega^2C_4C_6(G_1+G_2+G_3)=0, \quad (12)$$

and

$$G_1G_3(C_4+C_5+C_6)+(C_1G_3+C_3G_1)\left(G_4+G_5+\frac{1}{R_6}\right)-\omega^2C_1C_3(C_4+C_5+C_6)$$

$$+\frac{G_4}{R_6}\left(C_1-\frac{1}{\omega^2L}+C_2+C_3\right)+\left(\frac{C_4}{R_6}+C_6G_4\right)(G_1+G_2+G_3)-\omega^2C_4C_6\left(C_1-\frac{1}{\omega^2L}+C_2+C_3\right)=0. \quad (13)$$

In the appendix, these equations are reduced to give the four expressions

$$G_{xA}\approx\omega^2\left(R_6\frac{C_1C_3}{C_4}\right)\Delta C_5-\omega^2(R_4C_4-R_6C_6)(\Delta C_2+C_{xA})-\Delta G_2, \quad (14)$$

$$G_{xB}\approx\frac{-\Delta C_2'}{\left(R_6\frac{C_1C_3}{C_4}\right)}[1-\omega^2R_2(C_2+C_2')(R_4C_4-R_6C_6)]-\omega^2(R_1C_1+R_3C_3)(\Delta C_5'+C_{xB})-\Delta G_5, \quad (15)$$

$$C_{xA}\approx-\Delta C_2[1-\omega^2R_2(C_2+C_2')(R_4C_4-R_6C_6)]-[R_1C_1+R_3C_3-R_4C_4+R_6C_6+R_5(C_5+C_5')]G_{xA}, \quad (16)$$

and

$$C_{xB}\approx-\Delta C_5'+[R_1C_1+R_3C_3-R_4C_4+R_6C_6-R_2(C_2+C_2')]G_{xB}. \quad (17)$$

For the instrument whose construction is described later, these equations are accurate to within a few parts in 10^6. If the instrument is to be self-calibrating for conductance

measurements, eqs (14) and (15) must be reduced to the form

$$G_{xA}+\Delta G_2=\omega^2 P\Delta C_5,$$

and

$$G_{xB}+\Delta G_5=\frac{-\Delta C_2'}{P}.$$

In order to accomplish this, define

$$K\equiv R_1C_1+R_3C_3-R_4C_4+R_6C_6. \tag{18}$$

Equations (16) and (17) then become

$$C_{xA}\approx -\Delta C_2[1-\omega^2R_2(C_2+C_2')(R_4C_4-R_6C_6)]-[K+R_5(C_5+C_5')]G_{xA} \tag{19}$$

and

$$C_{xB}\approx -\Delta C_5'+[K-R_2(C_2+C_2')]G_{xB}. \tag{20}$$

When measuring a nearly pure conductance, sufficient accuracy is obtained for C_{xA} if the term $\omega^2R_2(C_2+C_2')(R_4C_4-R_6C_6)$ is neglected. Then (19) becomes

$$C_{xA}\approx -\Delta C_2-[K+R_5(C_5+C_5')]G_{xA}. \tag{21}$$

If a nearly pure conductance is measured on terminal-pair A, then on terminal-pair B, using the same capacitor operated over an identical range for both measurements, then

$$G_{xA}=G_{xB}=G_x$$

and

$$R_5(C_5+C_5')=R_2(C_2+C_2')=R(C+C').$$

Since $C_{xA}=C_{xB}$,

$$-\Delta C_2-[K+R(C+C')]G_x=-\Delta C_5'+[K-R(C+C')]G_x$$

from which is obtained

$$K=\frac{\Delta C_5'-\Delta C_2}{2G_x}, \tag{22}$$

which can be evaluated.

Now, R_1C_1, R_3C_3, and R_4C_4 are likely to be at least an order of magnitude smaller than R_6C_6. When this is true, $K\approx R_6C_6$,

$$C_{xA}+\Delta C_2\approx -[K+R_5(C_5+C_5')]G_{xA},$$

and

$$C_{xB}+\Delta C_5'\approx [K-R_2(C_2+C_2')]G_{xB}.$$

Equations (14) and (15) can now be rewritten

$$G_{xA}\approx \omega^2P\Delta C_5-\omega^2K[K+R_5(C_5+C_5')]G_{xA}-\Delta G_2$$

and

$$G_{xB}\approx \frac{-\Delta C_2'}{P}[1+\omega^2KR_2(C_2+C_2')]-\omega^2(R_1C_1+R_3C_3)[K-R_2(C_2+C_2')]G_{xB}-\Delta G_5.$$

If the terms $\omega^2K[K+R_5(C_5+C_5')]$, $\omega^2KR_2(C_2+C_2')$, and $\omega^2(R_1C_1+R_3C_3)[K-R_2(C_2+C_2')]$ are insignificant compared to unity, the expressions for the conductance reduce to the desired form.

If $\Delta G_2=\Delta G_5$, or if both are insignificant compared to G_x, P can be determined as it was in the ideal case. It is possible to insure that $\Delta C_2=\Delta C_5$, and that $\Delta G_2=\Delta G_5$ in the two measure-

ments, by using the same variable capacitors operated over an identical range to measure G_x and C_x in both cases. This requires both G_x and the capacitors which measure G_x and C_x to be switched from terminal to terminal.

It is possible to adjust P to within the limits of stability and resettability of the capacitor used to measure G_x. In a good two-terminal air capacitor equipped with a precision coaxial connector, the error is no more than a few parts in 10^5 of the maximum capacitance. Since changes in effective capacitance are not known to better than several parts in 10^4 at present, adjusting P in this way allows one to measure conductance to the same accuracy as that to which a change in effective capacitance is known.

With the constants of the instrument known, it is only necessary to evaluate the residual impedances associated with the external variable capacitors, perhaps by the method of Field and Sinclair [5], in order to make quite good measurements of either conductance or reactance.

3. Construction of the Instrument

In converting the twin T circuit to a working instrument, several facts must be considered. Since it is necessary to move the standard capacitors from one pair of terminals to the other when evaluating the constants of the instrument, the standard capacitors cannot be made an integral part of the instrument. If the capacitors are not to be built in, more than one pair of terminals must be provided to allow paralleling the unknown admittance and the capacitor which measures C_x. Multiple terminals are also desirable because they simplify calibration of the variable capacitors used with the instrument. If multiple terminals are to be used, it is desirable for each pair to connect to a common point, the "bridge corner," and for the conductors to be mutually perpendicular in order to reduce mutual impedances as much as possible. The fact that it is possible to connect external variable capacitors of different ranges for C_2 and C_5 requires changing the values of L and G_2 necessary to provide initial balance. Since multiple terminals are already necessary, it is just as well to provide for the attachment of external standards for L and G_2. As a result, the actual instrument becomes very simple. It is only necessary to provide for mounting the four fixed elements, the series elements of the T, in a base to which are attached the two sets of multiple terminals.

As actually constructed, the instrument takes the form shown in figures 3, 5, and 6. The four series elements are mounted in holes bored parallel to the four sides of a 2 in. by 6 in. brass block. The holes are extended through the edges of the block to provide access to the components from one end, and to form the outer conductor of a short section of 3/4 in. coaxial line on the other. Holes bored through diagonally opposite corners from face to face provide the outer conductors for two more short sections of line. When center conductors are added, six short sections of coaxial line, whose center conductors meet in a point, are formed at two diagonally opposite corners of the block. Two of these line sections connect to the series components, and the other four are equipped with NBS-Woods [6] precision coaxial connectors to provide the bridge terminals. The junction point of the six line sections forms the "bridge corner."

Capacitors C_1 and C_3 are coaxial capacitors with nominal values of 10 pF. C_4 is a parallel plate capacitor whose nominal value is 1 pF. R_6 is a commercial metal film resistor whose value is selected to give the proper value of P at the frequency at which the instrument is to be used.

Since it is necessary to adjust P, one or more of the series elements must be adjustable. C_4 is provided with two adjustments. Each plate has one half its surface cut about $\frac{1}{32}$ in. lower than the other half, so that rotating one plate with respect to the other causes a change of about 10 percent in its capacitance. Final adjustment of P is accomplished by means of a trimming screw which extends into the space between the two plates. Gross changes in P can be accomplished by replacing the resistor R_6 with another of different value.

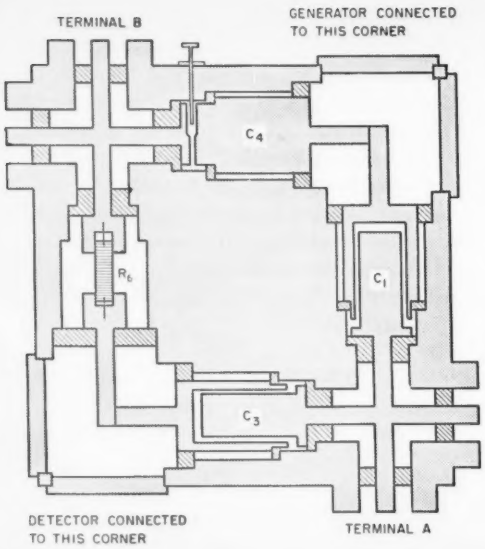

FIGURE 3. *Cross section through the brass block showing construction of the instrument.*

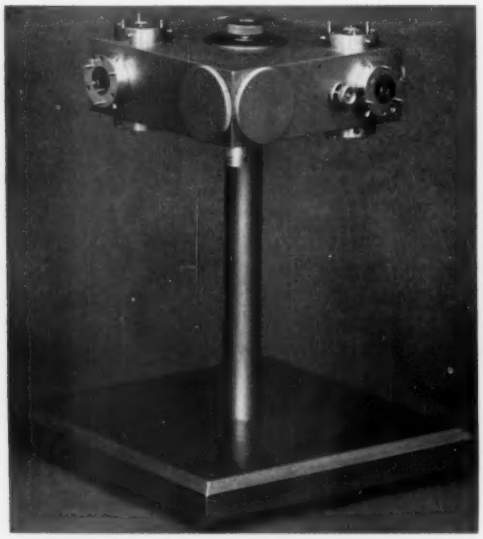

FIGURE 5. *The basic instrument showing connector details and C_4 trimmer.*

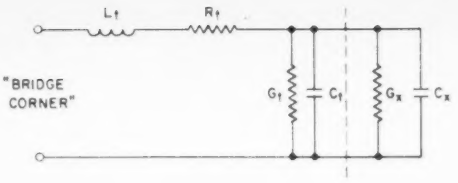

FIGURE 4. *Equivalent circuit used in calculating the effect of terminal impedances on measured Y_x.*

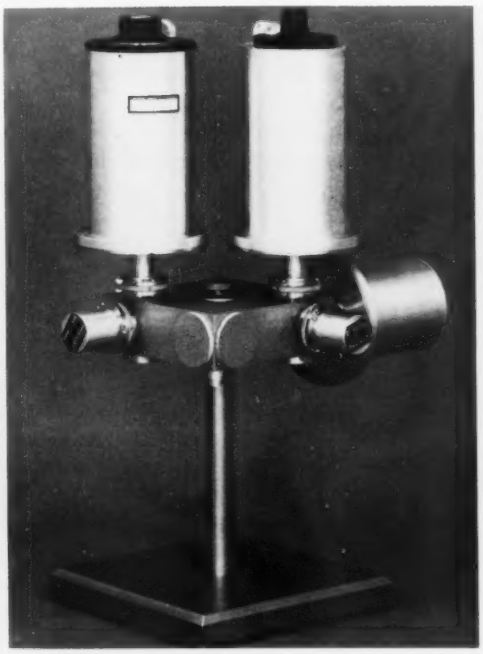

FIGURE 6. *The basic instrument with standards attached for measuring a 200-ohm resistor.*

4. Experimental Results

P was adjusted to equal $\frac{1}{\omega}$, at $\omega = 10^7$ radians/sec, by measuring a 1000 Ω resistor using a 10 to 110 pF variable standard capacitor. This resistor, as were those used later, is a high quality commercial metal-film resistor mounted in a shielding can which is equipped with a NBS-Woods Precision Coaxial Connector. The three standard capacitors used are equipped with similar connectors.

When P had been adjusted to the point that the capacitance change on one terminal was within a few parts in 10^5 of that on the other, over an identical capacitance range, P was considered to be adjusted to within a few parts in 10^5. The adjustment was checked by measuring a 2000 Ω resistor using the same capacitor, a 20,000 Ω resistor using a 7 to 17 pF capacitor, and 100, 200, and 500 Ω resistors using a 100 to 1100 pF capacitor. The results are summarized in table 1. Since the error in resetting the capacitors is a few parts in 10^5 of their maximum capacitance, the adjustment of P is probably correct to within a few parts in 10^5.

With the values obtained for ΔC_5, or $\Delta C_2'$, in checking the adjustment of P, and knowing that P is $10^{-7} \pm$ a few parts in 10^5, it is possible to calculate the effective conductance of each of the resistors at 10^7 radians/sec. The results of the calculations appear in table 2. The measurements of C_x obtained in checking the adjustment of P may be used to calculate a value for K. The results of the calculations appear in table 3.

TABLE 1. *Verification of the adjustment of* P

Resistors measured	Terminal used	Capacitor used	ΔC	% Diff. $=\left(\frac{\Delta C_2}{\Delta C_2}-1\right)100$
Ω		*pF*	*pF*	
100	*A*	100–1100	999.40	+0.003
100	*B*	100–1100	999.37	
200	*A*	100–1100	499.00	+.012
200	*B*	100–1100	498.94	
500	*A*	100–1100	192.92	.000
500	*B*	100–1100	192.92	
1000	*A*	10–110	100.050	−.001
1000	*B*	10–110	100.051	
2000	*A*	10–110	50.206	−.004
2000	*B*	10–110	50.208	
20,000	*A*	7–17	4.9994	+.006
20,000	*B*	7–17	4.9991	
20,000	*A*	7–17	4.9976	−.030

Percentage error in P is ½×(% diff.).

TABLE 2. *Comparison of measured resistance to d-c resistance*

ΔC	$G=\omega\Delta C$	$R_f=\frac{1}{G}$	R_{dc}	% diff. $=\left(\frac{R_f}{R_{dc}}-1\right)100$
pF	*Mho*			
1000.44	1.00044×10^{-2}	99.956	99.971	−0.015
499.71	4.9971×10^{-3}	200.12	200.155	−.018
199.84	1.9984×10^{-3}	500.40	500.428	−.006
100.031	1.00031×10^{-3}	999.69	999.853	−.016
50.029	5.0029×10^{-4}	1998.8	1999.52	−.036
5.0180	5.0180×10^{-5}	19928	19998.4	−.353

TABLE 3. *Calculation of K from measured capacitance*

G_x	$\Delta C'_5$	ΔC_2	$K=\frac{\Delta C'_5-\Delta C_2}{2G_x}$
Mho	*pF*	*pF*	
0.01	3.503	−5.942	4.72×10^{-10}
.005	−0.125	−4.821	4.70×10^{-10}
.002	−2.440	−4.308	4.67×10^{-10}
.001	−2.3145	−3.2559	4.71×10^{-10}
.0005	−2.4132	−2.8826	4.69×10^{-10}

The admittance measured by the instrument is the effective admittance at the "bridge corners." In order to calculate Y_x accurately, it is necessary to know the effect of the residual impedances between the terminal and the "bridge corner." The equivalent circuit of figure 4 is a reasonable representation of the residual impedances associated with the terminal.

When the instrument is nulled initially with the terminal open, the effective admittance at the "bridge corner" is given by

$$Y_e=\frac{G_t(1+R_tG_t)+\omega^2R_tC_t^2+j\omega[C_t-L_tG_t^2-\omega^2L_tC_t^2]}{(1+R_tG_t-\omega^2L_tC_t)^2+\omega^2(R_tC_t+L_tG_t)^2}.$$

For the purpose of estimating the magnitudes of the residual impedances, the terminal can be considered to be 1⅜ in. of 50Ω, ¾ in., brass air line. Since the series resistance and inductance in similar sections of line have been determined to be 0.8 milliohm/in. and 4.4×10^{-9} H/in. at 10^7 radians/sec, R_t is about 1.1 milliohms, and L_t about 6.2×10^{-9} H. C_t is about 2.5 pF, and G_t is less than 1 μmho. Using these values for the residual impedances, the equation can be reduced to

$$Y_e\approx G_t+j\omega C_t, \text{ at } \omega=10^7 \text{ radians/sec.}$$

When an unknown admittance, $Y_x=G_x+j\omega C_x$, is connected to the terminal, the effective admittance at the "bridge corner" is given by

$$Y'_e=\frac{(G_t+G_x)[1+R_t(G_t+G_x)]+\omega^2R_t(C_t+C_x)^2+j\omega[C_t+C_x-L_t(G_t+G_x)^2-\omega^2L_t(C_t+C_x)^2]}{[1+R_t(G_t+G_x)-\omega^2L_t(C_t+C_x)]^2+\omega^2[R_t(C_t+C_x)+L_t(G_t+G_x)]^2}.$$

For $G_x \leq 10^{-2}$ and $C_x < 10^{-11}$, this reduces to

$$Y'_e \approx G_t + G_x + j\omega(C_t + C_x - L_t G_x^2)$$

and

$$\Delta Y_e = Y'_e - Y_e \approx G_x + j\omega(C_x - L_t G_x^2).$$

The error in the measured conductance is insignificant, and the measured capacitance is in error by the term $(-L_t G_x^2)$. Before the reactance associated with a nearly pure conductance can be accurately measured, it is necessary to evaluate this inductance, as well as the series resistance associated with the capacitor used to measure the conductance. It should be mentioned that these residual impedances cause no error in evaluating the constants of the instrument if care is taken to make all the terminals as nearly identical as possible.

5. Discussion

The measurements of P, which are summarized in table 1, indicate that it is possible to adjust P to within a few parts in 10^5 of $1/\omega$. The limit on the accuracy of adjustment of P is the limit of stability and resettability of the standard capacitors used in making the adjustment.

Comparison of resistance measured at 10^7 radians/sec with that measured at zero frequency (table 2) indicates that the instrument is capable of measuring resistance to within a few hundredths of a percent. The very close agreement between rf and d-c values must be considered fortuitous at present because changes in capacitance are not known to much better than ± 0.05 percent.

The values calculated for K (table 3) have a scatter of less than 1 percent of K. This indicates that it will be possible to make quite good measurements of the reactance associated with a nearly pure conductance. Apparently, the accuracy of such measurements will be limited by the accuracy to which the series resistance associated with the standard capacitors and the series inductance associated with the terminal can be determined.

While the instrument has been proved only at a frequency of 10^7 radians/sec, there is no apparent reason why the same principle can not be used at much higher, or at much lower, frequencies. The main deficiency of the instrument lies in the range of conductance which can be measured accurately. At present the range is limited, by the relationship $G_x = \omega \Delta C$, to two or three decades of conductance by the range of capacitance changes which is easily obtainable. Since the magnitude of the conductance measurable by a given capacitor depends on the frequency, the range of conductances measurable by the instrument is frequency dependent. The deficiency need not be too serious if it proves feasible to use the instrument to measure conductances for use as standards when calibrating other instruments capable of covering a greater conductance range.

The instrument has demonstrated its ability to make conductance measurements limited in accuracy only by the accuracy to which changes in capacitance are known. This being the case, it is possible to immediately realize an order of magnitude increase in the accuracy of those conductance measurements which are within the range of the instrument. Of greater significance is the fact that the instrument demonstrates a principle which makes it possible to refer resistance measurements directly to standards of capacitance, thus placing the measurement of resistance and reactance on a common basis.

6. Appendix

The null equations for the circuit of figure 2 are

$$G_1 G_3 \left(G_4 + G_5 + \frac{1}{R_6}\right) - \omega^2 (C_1 G_3 + C_3 G_1)(C_4 + C_5 + C_6) - \omega^2 C_1 C_3 \left(G_4 + G_5 + \frac{1}{R_6}\right)$$

$$+ \frac{G_4}{R_6}(G_1 + G_2 + G_3) - \omega^2 \left(\frac{C_4}{R_6} + C_6 G_4\right)\left(C_1 - \frac{1}{\omega^2 L} + C_2 + C_3\right) - \omega^2 C_4 C_6 (G_1 + G_2 + G_3) = 0, \quad \text{(A1)}$$

and

$$G_1G_3(C_4+C_5+C_6)+(C_1G_3+C_3G_1)\left(G_4+G_5+\frac{1}{R_6}\right)-\omega^2C_1C_3(C_4+C_5+C_6)$$

$$+\frac{G_4}{R_6}\left(C_1-\frac{1}{\omega^2L}+C_2+C_3\right)+\left(\frac{C_4}{R_6}+C_6G_4\right)(G_1+G_2+G_3)-\omega^2C_4C_6\left(C_1-\frac{1}{\omega^2L}+C_2+C_3\right)=0. \quad \text{(A2)}$$

A measurement can be made by connecting an unknown admittance, $Y_x=G_x+j\omega C_x$, either to terminal-pair A, or to terminal-pair B. When Y_x is connected to terminal-pair A, C_2 must be replaced by $C_2'+C_x$, G_2 by $G_2'+G_x$, G_5 by G_5', and C_5 by C_5' in the null equations. Similar changes must be made when the unknown admittance is connected to terminal-pair B. If $\Delta C_2=C_2'-C_2$, $\Delta G_2=G_2'-G_2$, $\Delta C_5=C_5'-C_5$, and $\Delta G_5=G_5'-G_5$, and subscripts A and B denote the terminal-pair to which the unknown admittance is connected, subtracting the initial null equations from the final ones yields the four expressions

$$C_{xA}\left[1+\frac{R_6G_4C_6}{C_4}\right]=-\left[1+\frac{R_6G_4C_6}{C_4}\right]\Delta C_2+\left[\frac{R_6G_1G_3}{\omega^2C_4}-\frac{R_6}{C_4}C_1C_3\right]\Delta G_5$$

$$+\left[\frac{G_4}{\omega^2C_4}-R_6C_6\right](\Delta G_2+G_x)-\frac{R_6}{C_4}(C_1G_3+C_3G_1)\Delta C_5, \quad \text{(A3)}$$

$$C_{xB}\left[\frac{\omega^2R_6C_1C_3}{C_4}-\frac{R_6G_1G_3}{C_4}\right]=-\left[\frac{\omega^2R_6C_1C_3}{C_4}-\frac{R_6G_1G_3}{C_4}\right]\Delta C_5+\left[1+\frac{R_6G_4C_6}{C_4}\right]\Delta G_2$$

$$+\frac{R_6}{C_4}(C_1G_3+C_3G_1)(\Delta G_5+G_x)+\left(\frac{G_4}{C_4}-\omega^2R_6C_6\right)\Delta C_2, \quad \text{(A4)}$$

$$G_{xA}\left[1+\frac{R_6G_4C_6}{C_4}\right]=\left[\frac{\omega^2R_6C_1C_3}{C_4}-\frac{R_6G_1G_3}{C_4}\right]\Delta C_5+\left[\omega^2R_6C_6-\frac{G_4}{C_4}\right](\Delta C_2+C_x)$$

$$-\frac{R_6}{C_4}(C_1G_3+C_3G_1)\Delta G_5-\left(1+\frac{R_6G_4C_6}{C_4}\right)\Delta G_2, \quad \text{(A5)}$$

and

$$G_{xB}\left[\frac{R_6C_1C_3}{C_4}-\frac{R_6G_1G_3}{\omega^2C_4}\right]=-\left(1+\frac{R_6G_4C_6}{C_4}\right)\Delta C_2-\frac{R_6}{C_4}(C_1G_3+C_3G_1)(\Delta C_5+C_x)$$

$$+\left[\frac{R_6G_1G_3}{\omega^2C_4}-\frac{R_6C_1C_3}{C_4}\right]\Delta G_5+\left[\frac{G_4}{\omega^2C_4}-R_6C_6\right]\Delta G_2. \quad \text{(A6)}$$

If C_1, C_3, and C_4 are good three-terminal capacitors, their losses will be due entirely to series resistance, in which case,

$$G_1\approx\omega^2R_1C_1^2,\ G_3\approx\omega^2R_3C_3^2,$$

and

$$G_4\approx\omega^2R_4C_4^2.$$

If C_2 and C_5 are good two-terminal capacitors, changes in their conductance will be due entirely to series resistance, and

$$\Delta G_2\approx\omega^2R_2(C_2'^2-C_2^2)=\omega^2R_2(C_2+C_2')\Delta C_2,$$

$$\Delta G_5\approx\omega^2R_5(C_5+C_5')\Delta C_5.$$

In the instrument described,

$$C_1\approx C_3\approx 10\text{ pF}$$

$$C_4\approx 1\text{ pF}$$

$$C_2 \leq 1000 \text{ pF}$$

$$C_5 \leq 1000 \text{ pF}$$

$$R_6 \approx 1000\Omega \text{ at } 10^7 \text{ radians/sec}$$

and

$$R_6 \approx 100\Omega \text{ at } 10^8 \text{ radians/sec.}$$

It is not unreasonable to assume $R_1 \approx R_2 \approx R_3 \approx R_4 \approx R_5 < 0.1\Omega$ and

$$C_6 \approx 1 \text{ pF.}$$

The null equations can then be reduced by using the following approximations:

$$\left[1+\frac{G_4 R_6 C_6}{C_4}\right] \approx \left[1+\frac{\omega^2 R_4 C_4^2 R_6 C_6}{C_4}\right] \approx 1+\omega^2 R_4 R_6 C_4 C_6 \approx 1, \tag{a}$$

$$\left[\frac{R_6 G_1 G_3}{\omega^2 C_4}-\frac{R_6 C_1 C_3}{C_4}\right] \approx \frac{R_6 C_1 C_3}{C_4}\left[\omega^2 R_1 R_3 C_1 C_3 - 1\right] \approx -\frac{R_6 C_1 C_3}{C_4}, \tag{b}$$

$$\left[\frac{\omega^2 R_6 C_1 C_3}{C_4}-\frac{R_6 G_1 G_3}{C_4}\right] = \omega^2\left[\frac{R_6 C_1 C_3}{C_4}-\frac{R_6 G_1 G_3}{\omega^2 C_4}\right] \approx \omega^2 \frac{R_6 C_1 C_3}{C_4}, \tag{c}$$

$$\left[\frac{G_4}{\omega^2 C_4}-R_6 C_6\right] \approx \left[\frac{\omega^2 R_4 C_4^2}{\omega^2 C_4}-R_6 C_6\right] \approx R_4 C_4 - R_6 C_6, \tag{d}$$

$$\left[\frac{G_4}{C_4}-\omega^2 R_6 C_6\right] = \omega^2\left[\frac{G_4}{\omega^2 C_4}-R_6 C_6\right] \approx \omega^2[R_4 C_4 - R_6 C_6]. \tag{e}$$

$$[C_1 G_3 + C_3 G_1] \approx [\omega^2 R_3 C_3^2 C_1 + \omega^2 R_1 C_1^2 C_3] \approx \omega^2 C_1 C_3 (R_1 C_1 + R_3 C_3). \tag{f}$$

Using expressions (a), (b), (d), and (f), eq (A3) is reduced to

$$C_{xA} \approx -\Delta C_2 - \frac{R_6 C_1 C_3}{C_4}\Delta G_5 + (R_4 C_4 - R_6 C_6)(\Delta G_2 + G_{xA}) - \frac{\omega^2 R_6 C_1 C_3}{C_4}(R_1 C_1 + R_3 C_3)\Delta C_5.$$

Since

$$\Delta G_5 \approx \omega^2 R_5 (C_5 + C_5')\Delta C_5,$$

$$\Delta G_2 \approx \omega^2 R_2 (C_2 + C_2')\Delta C_2,$$

and

$$\omega^2 R_6 \frac{C_1 C_3}{C_4}\Delta C_5 \approx G_{xA},$$

$$C_{xA} \approx -\Delta C_2[1-\omega^2 R_2(C_2+C_2')(R_4 C_4 - R_5 C_6)] - [R_1 C_1 + R_3 C_3 - R_4 C_4 + R_6 C_6 + R_5(C_5+C_5')]G_{xA}, \tag{A7}$$

which is eq (16).

Using (a), (c), (e), and (f), eq (A4) is reduced to

$$C_{xB} \approx -\Delta C_5 + (R_1 C_1 + R_3 C_3)(\Delta G_5 + G_{xB}) + \frac{\Delta C_2 (R_4 C_4 - R_6 C_6)}{\left(R_6 \frac{C_1 C_3}{C_4}\right)} + \frac{\Delta G_2}{\omega^2\left(R_6 \frac{C_1 C_3}{C_4}\right)}.$$

Since

$$\frac{\Delta C_2}{R_6 \frac{C_1 C_3}{C_4}} \approx -G_{xB},$$

and

$$\omega^2 (R_1 C_1 + R_3 C_3) R_5 (C_5 + C_5') << 1,$$

this can be further reduced to

$$C_{xB} \approx -\Delta C_5 + [R_1C_1 + R_3C_3 - R_4C_4 + R_6C_6 - R_2(C_2 + C_2')]G_{xB}, \tag{A8}$$

which is eq (17).

Using (a), (c), (e), and (f), eq (A5) is reduced to

$$G_{xA} \approx \frac{\omega^2 R_6 C_1 C_3}{C_4} \Delta C_5 - \omega^2 (R_4C_4 - R_6C_6)(\Delta C_2 + C_{xA}) \frac{-\omega^2 R_6 C_1 C_3}{C_4} (R_1C_1 + R_3C_3)\Delta G_5 - \Delta G_2.$$

Since

$$\Delta G_5 \approx \omega^2 R_5 (C_5 + C_5')\Delta C_5$$

and

$$\omega^2 (R_1C_1 + R_3C_3) R_5 (C_5 + C_5') << 1,$$

this reduces to

$$G_{xA} \approx \frac{\omega^2 R_6 C_1 C_3}{C_4} \Delta C_5 - \omega^2 (R_4C_4 - R_6C_6)(\Delta C_2 + C_{xA}) - \Delta G_2 \tag{A9}$$

which is eq (14).

Using expressions (a), (b), (d), and (f), eq (A6) is reduced to

$$G_{xB} \approx \frac{-\Delta C_2}{R_6 \dfrac{C_1C_3}{C_4}} - \omega^2 (R_1C_1 + R_3C_3)(\Delta C_5 + C_{xB}) - \Delta G_5 + \frac{(R_4C_4 - R_6C_6)\Delta G_2}{R_6 \dfrac{C_1C_3}{C_4}}.$$

Since

$$\Delta G_2 \approx \omega^2 R_2 (C_2 + C_2')\Delta C_2,$$

$$G_{xB} \approx -\frac{\Delta C_2}{R_6 \dfrac{C_1C_3}{C_4}} [1 - \omega^2 R_2 (C_2 + C_2')(R_4C_4 - R_6C_6)] - \omega^2 (R_1C_1 + R_3C_3)(\Delta C_5 + C_{xB}) - \Delta G_5, \tag{A10}$$

eq (15). Equations (A7), (A8), (A9), and (A10) should be accurate to within a few parts in 10^6 at frequencies up to 10^8 radians/sec for the instrument described.

7. References

[1] Powell, R. C., Jickling, R. M., and Hess, A. E., High frequency impedance standards at the National Bureau of Standards. IRE Trans. Instr. **I-7,** Nos. 3 & 4, 270 (Dec. 1958).

[2] Tuttle, W. N., Bridged-T and parallel-T null circuits for measurements at radio frequencies, Proc. IRE **28,** 23 (Jan. 1940).

[3] Sinclair, D. B., The Twin T–A new type of null instrument for measuring impedance at frequencies up to 30 megacycles. Proc. IRE **28,** 310 (July 1940).

[4] Woods, D., A precision V.H.F. twin-T dual admittance bridge and associated standards, Report No. A.I.D. Rad. Elec. **17** (Jan. 1950).

[5] Field, R. F., and Sinclair, D. B., A method for determining the residual inductance and resistance of a variable air condenser at radio frequencies, Proc. IRE, **24,** No. 2, 255–274 (Feb. 1936).

[6] Woods, D., A coaxial connector system for precision R.F. measuring instruments and standards. Proc. IEE, **108B**, Paper No. 3499E, pp. 205–213 (Mar. 1961).

(Paper 69C2–191)

JOURNAL OF RESEARCH of the National Bureau of Standards—C. Engineering and Instrumentation
Vol. 69C, No. 2, April–June 1965

Exact Inductance Equations for Rectangular Conductors With Applications to More Complicated Geometries

Cletus Hoer* and Carl Love*

(January 11, 1965)

Exact equations are given for the calculation of the self-inductance of rectangular conductors and of the mutual inductance between combinations of parallel filaments, thin tapes and rectangular conductors. A general procedure is also given for calculating the self-inductance of complicated geometries by dividing the geometry into simple elements whose inductances can be calculated. This general procedure is valid for conductors having nonuniform, as well as uniform current densities.

1. Introduction

It is the purpose of this paper to give a number of exact equations for the self- and mutual inductance of rectangular conductors, and also to show how these equations may be combined to obtain exact inductance solutions for more complicated geometries. These equations were derived during a recent investigation of thin tapes as possible high frequency inductance standards.

A number of approximate equations exist for calculating the inductance of rectangular conductors [1–5].[1] The usual method is to calculate the mutual inductance between two filaments spaced a distance apart equal to the geometric-mean-distance [6] of the conductor or conductors. This method assumes that the length is much greater than the other dimensions. However, when the length is no larger than ten times the next largest dimension, the error from this method may be as large as several percent. It is for those cases where a high degree of accuracy is needed that the equations in this paper have been derived.

2. Mutual Inductance Calculations

In general, the mutual inductance between two conductors will be a function of the current distribution in each conductor. A conductor having a constant cross-sectional area [2] along its length may be thought of as a bundle of parallel filaments, each having a cross-sectional area dA and carrying a current JdA. The current density, J, is assumed to be constant along the length of each filament but to vary from filament to filament. The mutual inductance, M, between two conductors having constant cross-sectional areas A_1 and A_2 and carrying currents I_1 and I_2 may be derived from energy considerations and is

$$M=\frac{1}{I_1 I_2}\int_{A_1}\int_{A_2} M_{12}J_1J_2dA_1dA_2, \tag{1}$$

where M_{12} is the mutual inductance between a filament carrying a current J_1dA_1 in the first conductor and a filament carrying a current J_2dA_2 in the second conductor. Since it is assumed that the current is constant along the length of each filament, the mutual inductance between

*Radio Standards Engineering Division, NBS Boulder Laboratories, Boulder, Colo.
[1] Figures in brackets indicate the literature references at the end of this paper.
[2] I.e., the cross-section dimensions do not change.

any two of the filaments is given by Neumann's formula,

$$M_{12}=0.001 \int_{l_1} \int_{l_2} \frac{\vec{dl_1} \cdot \vec{dl_2}}{r}. \tag{2}$$

The distance r is between two elements of length dl_1 and dl_2 which are along two filaments having total length l_1 and l_2, respectively. For dimensions in centimeters, M_{12} is in microhenrys. Since inductance cannot be calculated or specified except for a closed circuit, the integrals of (2) are usually over a closed path. However, the self- and mutual inductance of parts of a closed circuit (such as those to follow) may be calculated, provided that the total inductance of the circuit includes the contribution from each part.

If the current density is constant throughout each conductor, (1) reduces to

$$M=\frac{1}{A_1 A_2} \int_{A_1} \int_{A_2} M_{12} dA_1 dA_2 \tag{3}$$

which is independent of the current in either conductor and a function of only their dimensions. Using (2) and (3), the mutual inductance between any two conductors having constant cross-sectional areas and uniform (but not necessarily equal) current densities may be evaluated.

Results obtained from (2) and (3) are quite useful even though the current densities are not uniform. In many cases, the conductors may be subdivided into elements small enough so that each element may be considered as having a uniform current density. The mutual inductances between the smaller elements are then properly summed to get the total mutual inductance. Results from (2) and (3) are also useful when the cross-sectional area of a conductor is not uniform along its length. In this case the conductor is subdivided into sections, each of which has a constant cross-sectional area along its length. The mutual inductances between sections are then properly summed to get the total mutual inductance. The technique of subdividing conductors into smaller elements whose inductance can be calculated is developed at the end of this paper.

2.1. Mutual Inductance Between Parallel Filaments

The first step in calculating the mutual inductance between parallel tapes or bars is to calculate the mutual inductance between parallel filaments using Neumann's formula. The mutual inductance, M_f, between two parallel filaments of length l_1 and l_2 spaced in any relative position is

$$M_f=0.001 \left[z \ln (z+\sqrt{z^2+\rho^2}) - \sqrt{z^2+\rho^2} \right]_{l_3+l_2-l_1,\, l_3}^{l_3-l_1,\, l_3+l_2} (z) \tag{4}$$

where

$$\left[f(z) \right]_{s_2,\, s_4}^{s_1,\, s_3} (z) \equiv \sum_{k=1}^{4} (-1)^{k+1} f(s_k).$$

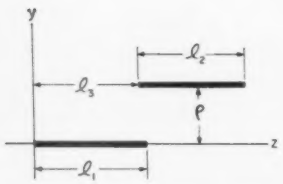

FIGURE 1. *Two parallel filaments whose mutual inductance is given by eq (4).*

The dimensions are defined in figure 1. If the left end of l_2 is to the left of the y-axis, the value of l_3 will be negative. The value of M_f is in microhenrys for dimensions in centimeters. This one equation covers all possible positions of two parallel filaments. It is given in its expanded form for special cases elsewhere in the literature [1, 7].

2.2. Mutual Inductance Between a Thin Tape and a Filament

The mutual inductance, M_{tf}, between a filament and a thin tape parallel to the filament such as shown in figure 2 is obtained by putting M_f into (3) and integrating over the width of the thin tape.

$$M_{tf}=\frac{1}{a}\int_0^a M_f dx, \tag{5}$$

where $\rho^2=P^2+(E-x)^2$ in M_f.

Since z in M_f is not a function of x (that is, the limits of integration s_1, s_2, s_3, and s_4 are independent of x), it is unnecessary to expand M_f, and the two terms inside of the brackets of (4) can be integrated as they are. This integration gives

$$M_{tf}=\frac{0.001}{a}\left[\left[\frac{z^2-P^2}{2}\ln\left(x+\sqrt{x^2+P^2+z^2}\right)+xz\ln\left(z+\sqrt{x^2+P^2+z^2}\right)\right.\right.$$
$$\left.\left.-Pz\,\mathrm{Tan}^{-1}\frac{xz}{P\sqrt{x^2+P^2+z^2}}-\frac{x}{2}\sqrt{x^2+P^2+z^2}\right]_{E-a}^{E}\right]_{l_3+l_2-l_1,\,l_3}^{l_3-l_1,\,l_3+l_2}(x)(z) \tag{6}$$

where

$$\left[\left[f(x,z)\right]_{q_2}^{q_1}(x)\right]_{s_2,\,s_4}^{s_1,\,s_3}(z)\equiv\sum_{i=1}^{2}\sum_{k=1}^{4}(-1)^{i+k}f(q_i,s_k).$$

The positive directions for E, P, and l_3 are taken as the positive directions of the x, y, and z axes, respectively. If the back end of the filament is in any octant other than that shown in figure 2, some or all of the values of E, P, and l_3 will be negative. In this equation and in those following, the principal value of the inverse tangent is to be used.

2.3. Mutual Inductance Between Two Thin Tapes

To obtain the mutual inductance, M_t, between two parallel thin tapes of zero thickness, such as shown in figure 3, M_f is integrated over all filaments in both tapes.

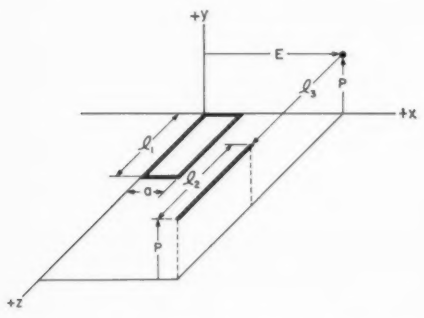

FIGURE 2. *A filament parallel to a thin tape whose mutual inductance is given by eq (6).*

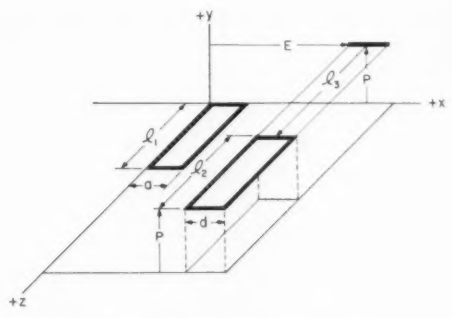

FIGURE 3. *Two parallel thin tapes whose mutual inductance is given by eq (8).*

$$M_t=\frac{1}{ad}\int_E^{E+d}\int_0^a M_f dx_1 dx_2 \tag{7}$$

where $\rho^2=P^2+(x_2-x_1)^2$ in M_f. This integration gives

$$M_t=\frac{0.001}{ad}\left[\left[\frac{x^2-P^2}{2}z\ln(z+\sqrt{x^2+P^2+z^2})+\frac{z^2-P^2}{2}x\ln(x+\sqrt{x^2+P^2+z^2})\right.\right.$$
$$\left.\left.-\frac{1}{6}(x^2-2P^2+z^2)\sqrt{x^2+P^2+z^2}-xPz\,\mathrm{Tan}^{-1}\frac{xz}{P\sqrt{x^2+P^2+z^2}}\right]_{E+d-a,\,E}^{E-a,\,E+d}{}_{(z)}{}_{l_3+l_2-l_1,\,l_3}^{l_3-l_1,\,l_3+l_2}\right. \tag{8}$$

where

$$\left[\left[f(x,z)\right]_{q_2,\,q_4}^{q_1,\,q_3}{}_{(x)}\right]_{s_2,\,s_4}^{s_1,\,s_3}{}_{(z)}\equiv\sum_{i=1}^{4}\sum_{k=1}^{4}(-1)^{i+k}f(q_i,s_k).$$

The distance E is measured from the yz, plane to the left edge of the second tape. If the back left corner of the second tape is in any octant other than that shown in figure 3, some or all of the values of E, P, and l_3 will be negative.

The mutual inductance, $M_{t\perp}$, between two thin tapes whose axes are parallel but whose widths are perpendicular to one another such as shown in figure 4 is

$$M_{t\perp}=\frac{1}{ac}\int_P^{P+c}\int_0^a M_f dx dy=\frac{1}{c}\int_P^{P+c}M_{tf}dy, \tag{9}$$

where P in M_{tf} has been replaced by the variable y. This integration gives

$$M_{t\perp}=\frac{0.001}{ac}\left[\left[\left[\left(\frac{z^2}{2}-\frac{y^2}{6}\right)y\ln(x+\sqrt{x^2+y^2+z^2})+\left(\frac{z^2}{2}-\frac{x^2}{6}\right)x\ln(y+\sqrt{x^2+y^2+z^2})\right.\right.\right.$$
$$+xyz\ln(z+\sqrt{x^2+y^2+z^2})-\frac{xy}{3}\sqrt{x^2+y^2+z^2}-\frac{z^3}{6}\mathrm{Tan}^{-1}\frac{xy}{z\sqrt{x^2+y^2+z^2}}$$
$$\left.\left.\left.-\frac{x^2z}{2}\mathrm{Tan}^{-1}\frac{yz}{x\sqrt{x^2+y^2+z^2}}-\frac{y^2z}{2}\mathrm{Tan}^{-1}\frac{xz}{y\sqrt{x^2+y^2+z^2}}\right]_{E-a}^{E}{}_{(y)}\right]_{P}^{P+c}{}_{(z)}\right]_{l_3+l_2-l_1,\,l_3}^{l_3-l_1,\,l_3+l_2} \tag{10}$$

where

$$\left[\left[\left[f(x,y,z)\right]_{q_2}^{q_1}{}_{(x)}\right]_{r_2}^{r_1}{}_{(y)}\right]_{s_2,\,s_4}^{s_1,\,s_3}{}_{(z)}\equiv\sum_{i=1}^{2}\sum_{j=1}^{2}\sum_{k=1}^{4}(-1)^{i+j+k+1}f(q_i,r_j,s_k).$$

The distance P is measured from the xz plane to the bottom of the second tape.

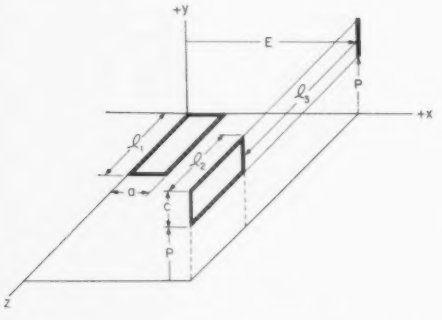

FIGURE 4. *Two thin tapes whose axis are parallel but whose widths are perpendicular.*
The mutual is given by eq (10).

2.4. Mutual Inductance Between a Bar and a Filament

The mutual inductance, M_{bf}, between a rectangular bar and a filament parallel to the bar such as shown in figure 5 is obtained by integrating M_{tf} over all thin tapes in the bar. Equation (3) gives

$$M_{bf}=\frac{1}{ab}\int_0^b\int_0^a M_f dxdy=\frac{1}{b}\int_{P-b}^{P} M_{tf}dY, \tag{11}$$

where P in M_{tf} is now replaced by the variable $Y\equiv P-y$. The integration of (11) is identical to the integration of (9) except for the limits of integration and the constant.

$$M_{bf}=\frac{0.001}{ab}\left[\left[\left[\left[f(x,y,z)\right]_{E-a}^{E}{}_{(x)}\right]_{P-b}^{P}{}_{(y)}\right]_{l_3+l_2-l_1,\ l_3}^{l_3-l_1,\ l_3+l_2}{}_{(z)}\right], \tag{12}$$

where $f(x, y, z)$ is the expression within the inner brackets of (10). The distance P in (12) is measured from the xz plane to the filament.

2.5. Mutual Inductance Between Rectangular Bars

To obtain the mutual inductance, M_b, between two rectangular bars, M_t is integrated over all thin tapes in both bars.

$$M_b=\frac{1}{bc}\int_P^{P+c}\int_0^b M_t dy_1 dy_2, \tag{13}$$

where P in M_t is replaced by the variable (y_2-y_1). Since the x and z limits of integration on M_t are independent of y, the four terms inside the brackets of (8) may be integrated as they are. After a lengthy integration, (13) yields an exact expression for the mutual inductance between two parallel rectangular bars spaced in any relative position.

$$\begin{aligned}M_b=\frac{0.001}{abcd}\Bigg[\Bigg[\Bigg[\Bigg[&\left(\frac{y^2z^2}{4}-\frac{y^4}{24}-\frac{z^4}{24}\right)x\ln\left(\frac{x+\sqrt{x^2+y^2+z^2}}{\sqrt{y^2+z^2}}\right)+\left(\frac{x^2z^2}{4}-\frac{x^4}{24}-\frac{z^4}{24}\right)y\ln\left(\frac{y+\sqrt{y^2+z^2+x^2}}{\sqrt{z^2+x^2}}\right)\\&+\left(\frac{x^2y^2}{4}-\frac{x^4}{24}-\frac{y^4}{24}\right)z\ln\left(\frac{z+\sqrt{z^2+x^2+y^2}}{\sqrt{x^2+y^2}}\right)+\frac{1}{60}(x^4+y^4+z^4-3x^2y^2-3y^2z^2-3z^2x^2)\sqrt{x^2+y^2+z^2}\\&-\frac{xyz^3}{6}\operatorname{Tan}^{-1}\frac{xy}{z\sqrt{x^2+y^2+z^2}}-\frac{xy^3z}{6}\operatorname{Tan}^{-1}\frac{xz}{y\sqrt{x^2+y^2+z^2}}\\&-\frac{x^3yz}{6}\operatorname{Tan}^{-1}\frac{yz}{x\sqrt{x^2+y^2+z^2}}\Bigg]_{E+d-a,\ E}^{E-a,\ E+d}{}_{(x)}\Bigg]_{P+c-b,\ P}^{P-b,\ P+c}{}_{(y)}\Bigg]_{l_3+l_2-l_1,\ l_3}^{l_3-l_1,\ l_3+l_2}{}_{(z)}\end{aligned} \tag{14}$$

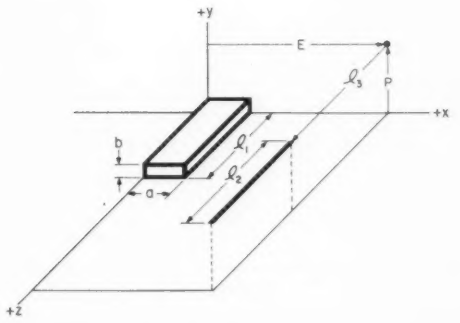

FIGURE 5. *A filament parallel to a rectangular bar whose mutual inductance is given by eq (12).*

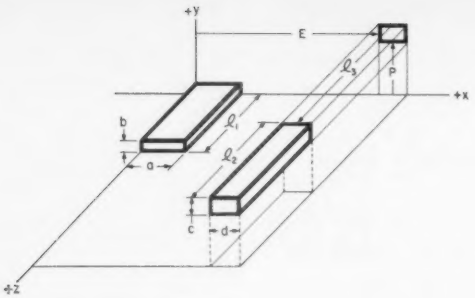

FIGURE 6. *Two parallel rectangular bars whose mutual inductance is given by eq (14).*

where $$\left[\left[\left[f(x, y, z) \right]_{q_3,\, q_4}^{q_1,\, q_2} (x) \right]_{r_2,\, r_4}^{r_1,\, r_3} (y) \right]_{s_2,\, s_4}^{s_1,\, s_3} (z) \equiv \sum_{i=1}^{4} \sum_{j=1}^{4} \sum_{k=1}^{4} (-1)^{i+j+k+1} f(q_i, r_j, s_k).$$

The dimensions are defined in figure 6. Either bar may be placed so that its back lower left corner is at the origin. The second bar may fall in any of the octants. If the back lower left corner of the second bar falls in any octant other than that shown in figure 6, some or all of the values of E, P, and l_3 will be negative. The distance E is measured from the yz plane to the left side of the second bar; P is measured from the xz plane to the bottom of the second bar, and l_3 is measured from the xy plane to the back of the second bar.

The mutual inductance equations (4) through (14) have intentionally been left in their rather complicated form because it is in this form that one can most efficiently program them on a computer. For most cases, considerable effort is required to evaluate these expressions without the aid of a computer. If the dimensions vary greatly in magnitude, the positive terms may very nearly cancel with the negative terms, and care must be taken to calculate each term to an accuracy sufficient to assure the required accuracy in the result.

It should also be noted that if either x or y or z approaches zero, all inverse tangents in (6) through (14) go to zero.[3] If any two of the variables x, y, and z approach zero, all terms in (14) go to zero except the square root term.

3. Self-Inductance Calculations

The self-inductance of a conductor is a special case of the mutual inductance between two conductors. We can think of the self-inductance of a conductor as the mutual inductance between two identical conductors which coincide with each other. The discussion on mutual inductance calculations may then be applied to self-inductance calculations. The self-inductance, L, of a conductor having a constant cross-sectional area, A, and carrying a current I is given by (1) where the two integrations are now over the same conductor.

$$L=\frac{1}{I^2}\int_A\int_A M_{12}J_1J_2dA_1dA_2. \tag{16}$$

The mutual inductance, M_{12}, between two filaments in the conductor is given by (2) if the current JdA in each filament is constant along the length of the filament.

If the current density is constant throughout the conductor, (16) reduces to

$$L=\frac{1}{A^2}\int_A\int_A M_{12}dA_1dA_2, \tag{17}$$

which is a function only of the dimensions of the conductor.

[3] In eqs (6) and (8), $y=P$.

For the self-inductance, L_t, of a thin tape of width "a" and length "l", (17) gives

$$L_t=\frac{1}{a^2}\int_0^a\int_0^a M_f dx_1 dx_2,$$

where $\rho^2=(x_2-x_1)^2$ in M_f. This integration gives

$$L_t=\frac{0.002}{3a^2}\left[3a^2 l\ln\frac{l+\sqrt{l^2+a^2}}{a}-(l^2+a^2)^{3/2}+3l^2a\ln\frac{a+\sqrt{a^2+l^2}}{l}+l^3+a^3\right]. \tag{18}$$

This result may also be obtained from (8), the expression for the mutual between two thin tapes, by setting $d=a$ and $E=P=l_3=0$.

The self-inductance, L_b, of a rectangular bar of sides "a" and "b" and length "l" is most readily obtained from (14), the expression for the mutual inductance between rectangular bars, by setting $d=a$, $c=b$, and $E=P=l_3=0$. These substitutions give

$$L_b=\frac{0.001}{a^2b^2}\left[\left[\left[\left[f(x,y,z)\right]_0^{-a,a}(x)\right]_{0,0}^{-b,b}(y)\right]_{0,0}^{-l,l}(z),\right. \tag{19}$$

where $f(x, y, z)$ is the expression within the inner brackets of (14). It can be shown that $f(x, y, z)$ is an even function of x, of y, and of z. This result allows one to use the absolute value of the limits of integration, thereby reducing (19) to

$$L_b=\frac{0.008}{a^2b^2}\left[\left[\left[\left[f(x,y,z)\right]_0^{a}(x)\right]_0^{b}(y)\right]_0^{l}(z),\right. \tag{20}$$

where

$$\left[\left[\left[\left[f(x,y,z)\right]_{q_2}^{q_1}(x)\right]_{r_2}^{r_1}(y)\right]_{s_2}^{s_1}(z)\equiv\sum_{i=1}^{2}\sum_{j=1}^{2}\sum_{k=1}^{2}(-1)^{i+j+k+1}f(q_i,r_j,s_k)\right.$$

For bars with a thickness-to-width ratio less than 0.1, the self-inductance L_b may be calculated from the empirical equation

$$L_b=L_t-Kl\frac{b}{a}10^{-3}, \tag{21}$$

where L_t is calculated from (18). The values of K given in table 1 are sufficiently accurate to calculate L_b to an uncertainty of 1 ppm for the range covered by the table. These values were obtained by forcing (21) to give results equal to that obtained from (20).

TABLE 1. *Values of* K, μh/*cm*

b/a \ l/a	2	5	10	20	50	100
0.002	2.087	2.088	2.088	2.089	2.089	2.089
.005	2.077	2.080	2.081	2.082	2.082	2.082
.010	2.0633	2.0686	2.0703	2.0712	2.0717	2.0719
.015	2.0508	2.0581	2.0605	2.0617	2.0624	2.0630
.020	2.0392	2.0482	2.0513	2.0529	2.0538	2.0542
.030	2.0176	2.0300	2.0342	2.0364	2.0376	2.0377
.040	1.9978	2.0131	2.0184	2.0210	2.0226	2.0232
.050	1.9792	1.9973	2.0035	2.0066	2.0085	2.0091
.060	1.9616	1.9822	1.9893	1.9929	1.9950	1.9957
.070	1.9448	1.9678	1.9757	1.9797	1.9821	1.9829
.080	1.9287	1.9540	1.9627	1.9671	1.9697	1.9706
.090	1.9132	1.9406	1.9501	1.9548	1.9577	1.9587
.100	1.8983	1.9277	1.9379	1.9430	1.9461	1.9472

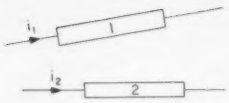

FIGURE 7. *Two arbitrary circuit elements carrying currents* i_1 *and* i_2.

4. Inductance of Complicated Geometries

The inductance of complicated geometries or of conductors having nonuniform current densities often can be calculated from a consideration of the magnetic energy of the conductor. Consider the two circuit elements shown in figure 7. The instantaneous energy, w, stored in the magnetic field created by the sinusodial currents i_1 and i_2 may be written

$$w=\tfrac{1}{2}L_1i_1^2+\tfrac{1}{2}L_2i_2^2+M_{12}i_1i_2, \tag{22}$$

where L_1 and L_2 are the self-inductances of elements "1" and "2", respectively, and M_{12} is the mutual inductance between these two elements. In (22) the currents are the instantaneous values

$$i_k=i_{k0}\sin(\omega t+\phi_k), \qquad k=1,2,$$

where i_{k0} is the maximum value of i_k and ϕ_k is the phase angle.

It is often more convenient to use the complex notation

$$I_1=a_1+jb_1, \quad I_2=a_2+jb_2.$$

Using this notation, the average magnetic energy W stored in the system of figure 7 may be written

$$W=\tfrac{1}{2}L_1I_1\cdot I_1+\tfrac{1}{2}L_2I_2\cdot I_2+M_{12}I_1\cdot I_2. \tag{23}$$

It is assumed that the currents I_1 and I_2 have the same frequency but not necessarily the same phase angle. The pseudo vector notation $I_1\cdot I_2$ has been used to take care of the difference in phase angle.

$$I_1\cdot I_2=a_1a_2+b_1b_2=\frac{i_{10}i_{20}}{2}\cos(\phi_1-\phi_2).$$

Equation (23) for the average magnetic energy of two circuit elements may also be written in summation form as

$$W=\frac{1}{2}\sum_{i=1}^{2}\sum_{j=1}^{2}M_{ij}I_i\cdot I_j \tag{24}$$

where M_{ii}=self-inductance of element i.

For a circuit having n elements, the average magnetic energy of the total circuit is

$$W_n=\frac{1}{2}\sum_{i=1}^{n}\sum_{j=1}^{n}M_{ij}I_i\cdot I_j. \tag{25}$$

The equivalent inductance, L_n, of a closed circuit having n elements is that inductance which will give the same average energy, W_n, when the same total current, I_T, is flowing through the circuit.

$$W_n=\tfrac{1}{2}L_nI_T\cdot I_T. \tag{26}$$

Solving (25) and (26) for the equivalent self-inductance gives

$$L_n=\frac{1}{I_T\cdot I_T}\sum_{i=1}^{n}\sum_{j=1}^{n}M_{ij}I_i\cdot I_j. \tag{27}$$

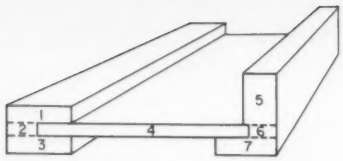

FIGURE 8. *A conductor of complicated cross-sectional area divided into elements whose inductances can be calculated.*

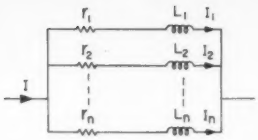

FIGURE 9.—*An equivalent circuit of the conductor shown in figure 8.*

This equation can be used to calculate not only the equivalent self-inductance of a closed circuit but also the equivalent self-inductance of part of a circuit if there is negligible interaction between the part under consideration and the rest of the circuit. The self-inductance of conductors having complicated geometries, therefore, may be calculated from (27). The procedure is to subdivide the conductors into simple geometries whose inductances can be calculated, and then sum these values with (27).

For example, let us calculate the equivalent self-inductance of the conductor shown in figure 8, assuming that there is negligible interaction between it and the rest of the circuit. There are no formulas for the self-inductance of such a geometry, so divide the conductor into elements whose inductances can be calculated. Since the self- and mutual inductance of parallel rectangular bars in any position can be calculated, divide the conductor into $n=7$ rectangular bars. The conductor now looks like the circuit in figure 9 with $n=7$ elements in parallel. The voltage drop across each element can be written

$$e=I_k r_k+j\omega \sum_{i=1}^{n} M_{ki} I_i, \tag{28}$$

where r_k and M_{kk} are the resistance and self-inductance of element k, and M_{ki} is the mutual between elements k and i. Since the desired self-inductance is independent of the value of e, set $e=1+j0$ for simplicity. Equation (28) gives n equations which may be solved for the n unknown currents I_1 through I_n. With the currents known, the equivalent inductance can be calculated from (27);

$$L=\frac{1}{I\cdot I}\sum_{i=1}^{n}\sum_{j=1}^{n} M_{ij} I_i \cdot I_j, \qquad n=7, \tag{29}$$

where, for this example,

$$I=\sum_{i=1}^{n} I_i, \qquad n=7.$$

At low frequencies (28) becomes

$$e\approx I_k r_k,$$

in which case (29) reduces to

$$L=R^2\sum_{i=1}^{n}\sum_{j=1}^{n}\frac{M_{ij}}{r_i r_j}, \tag{30}$$

where R is the total resistance of the conductor. Since the conductor is assumed to have a constant cross-sectional area along its length, each element will have a common length, l. The total resistance, R, may be calculated from

$$\frac{1}{R}=\sum_{k=1}^{n}\frac{1}{r_k}=\frac{1}{l}\sum_{k=1}^{n}\frac{A_k}{\rho_k}, \tag{31}$$

where A_k is the area of element k which has a resistivity ρ_k. Equation (30) shows that at low frequency the inductance of a conductor is not only a function of its dimensions but also of the resistivities of its different elements. When the resistivities of all elements are the same, however, (30) reduces to

$$L=\frac{1}{A^2}\sum_{i=1}^{n}\sum_{j=1}^{n}M_{ij}A_iA_j, \tag{32}$$

which is a function of only the dimensions. If the 3 sections of the conductor in figure 8 all have the same resistivity, the low frequency inductance may be calculated directly from (32) where the total area A is

$$A=\sum_{i=1}^{n}A_i, \qquad n=7.$$

The procedure outlined in this example is valid for a conductor of any arbitrary constant cross-sectional area, provided of course that the conductor can be subdivided into n elements whose inductances can be calculated, and that there is negligible interaction between this conductor and the rest of the circuit.

If the interaction is not negligible between the part being calculated and the rest of the circuit, the whole circuit must be considered. If there is interaction between the conductor of the previous example and, say, m other conductors in the circuit, the sum from $i=1$ to n in (28) becomes $i=1$ to $n+m$. There would then be $n+m$ currents to be evaluated, after which the equivalent inductance of the conductor could be calculated from (29), i and j going from 1 to n as before.

If exact values of inductance are not required, the equivalent self-inductance often may be calculated easier using geometric-mean-distances [1–7] (abbreviated g.m.d.). It should be remembered, however, that even exact equations for the g.m.d. gives approximate values of inductance because all g.m.d. formulas assume that lengths are infinite.

5. Conclusions

Exact equations have been given for the mutual inductance between the following parallel conductors: a filament and a thin tape, a filament and a rectangular bar, two thin tapes, and two rectangular bars. There is no restriction on the size or spacing of the conductors. Exact equations have also been given for the self-inductance of a thin tape and of a rectangular bar. Since these equations are quite long, they have been put in a form most suited for programming on high speed computers.

These equations for simple rectangular conductors may be used to calculate the self-inductance of any other more complicated geometry if that geometry can be divided into simple rectangular elements. A general procedure for calculating the self-inductance of complicated geometries has been given. The mutual inductance between complicated geometries may also be calculated using a procedure similar to that used for self-inductance.

In deriving the equations given in this paper, the assumption was made that the current density was uniform throughout the conductor (or throughout each element in the case of complicated geometries). This restriction is not a severe one however, since in many cases the conductor may be divided into elements small enough so that the current density in each element may be considered uniform. Applications of these equations to the calculation of high frequency inductances where the current density is not uniform are given in a forthcoming paper by Brooke, Hoer, and Love [8].

6. References

[1] F. W. Grover, Inductance Calculations, pp. 34–35 (D. Van Nostrand Co., Inc., 1946).

[2] A. Gray, Absolute Measurements in Electricity and Magnetism, pp. 475–498, 2d ed. (Macmillan & Co., London, 1921).

[3] E. B. Rosa and F. W. Grover, Formulas and tables for the calculation of mutual and self-inductance, BS Sci. Pap. **169,** revised 3d ed, 1948.

[4] E. B. Rosa, The self and mutual-inductance of linear conductors, Bul. BS **4,** 301–344 (1908).

[5] F. B. Silsbee, Notes on the design of 4-terminal resistance standards for alternating currents, J. Res. NBS **4,** 73–107, (1930).

[6] E. B. Rosa, On the geometrical mean distances of rectangular areas and the calculation of self-inductance, Bul. BS **3,** 1–41 (1907).

[7] C. Snow, Formulas for computing capacitance and inductance, NBS Circ. **544,** (1954).

[8] R. Brooke, C. Hoer, and C. Love, Inductance and characteristic impedance of strip line (to be published).

(Paper 69C2-192)

JOURNAL OF RESEARCH of the National Bureau of Standards—C. Engineering and Instrumentation
Vol. 69C, No. 2, April–June 1965

Common Volume of Two Intersecting Cylinders

J. H. Hubbell

(October 29, 1964)

The volume common to two cylinders of radii $r_1 \leq r_2$ with axes intersecting at angle β is found to be $r_2^3 v(k)/\sin\beta$, where $k = r_1/r_2$ and $v(k)$ may be evaluated (1) as the hypergeometric series

$$2\pi k^2 {}_2F_1(-\tfrac{1}{2}, \tfrac{1}{2}; 2; k^2) = 4\pi \sum_1^\infty \binom{\frac{1}{2}}{n}\binom{\frac{1}{2}}{n-1} k^{2n},$$

(2) as the combination of complete elliptic integrals $(8/3)[(1+k^2)E(k) - (1-k^2)K(k)]$ or (3) as the cumulative integral

$$8\int_0^k kE(k)\,dk.$$

A table of $v(k)$ to 8 decimals over the range $0 \leq k(0.01) \leq 1.00$, including δ_m^2 modified second central differences, is presented. This volume integral was useful in interpreting a gamma-ray albedo experiment involving a collimated source and a collimated detector, and may also be applicable to crossed-beam experiments. Two series useful for k close to unity are provided, one of which involves differencing against the series

$$16/3 = 4\pi \sum_1^\infty \binom{\frac{1}{2}}{n}\binom{\frac{1}{2}}{n-1}.$$

1. Introduction

In crossed-beam experiments [1][1] using the high-intensity accelerators now becoming available, the "geometrical target," or volume common to the two colliding beams, is a useful parameter for interpreting the measured data. An evaluation of this volume in terms of an infinite series was recently exhumed for possible application to an x-ray free-air ionization chamber having a cylindrical sensitive volume intersected by a pencil of x rays [2]. This evaluation had been used in the analysis of a gamma-ray beam back-scattering experiment [3] for making a theoretical estimate of the single-scattered component of the radiation "seen" by a collimated detector.

Evaluations of the volume common to two circular cylinders of unequal radii with axes intersecting at right angles [4, 5, 6], and of equal radii with axes intersecting at an arbitrary angle [7], have frequently been offered as calculus textbook exercises. However, a combined treatment does not seem to appear in the technical literature in a form convenient for easy application to practical problems. The following results provide formulas, a table, and a graph for such applications.

The series used in [3] is here corrected, expressed in terms of binomial coefficients, and identified as a hypergeometric series. For nearly equal cylinder radii, convergence can be accelerated by use of the difference-series technique [8]. An alternative series for this region, derived from the right-angle elliptic-integral solution [4, 5, 6], is more complicated but also more rapidly convergent.

[1] Figures in brackets indicate the literature references at the end of this paper.

2. Volume Integral

The integral for the common volume of two cylinders of radii $r_1 \leq r_2$ with axes intersecting at angle β (see fig. 1) is found as follows. The cross section parallel to the cylinder axes, at a distance x from them, is a parallelogram of height $2(r_2^2 - x^2)^{1/2}$ and base $2(r_1^2 - x^2)^{1/2}/\sin\beta$. Hence the volume integral is

$$V(r_1, r_2, \beta) = \int_{-r_1}^{r_1} 2(r_2^2 - x^2)^{1/2} \cdot \frac{2(r_1^2 - x^2)^{1/2}}{\sin\beta}\,dx \qquad (1a)$$

$$= \frac{8}{\sin\beta}\int_0^{r_1} (r_2^2 - x^2)^{1/2} \cdot (r_1^2 - x^2)^{1/2} dx. \qquad (1b)$$

3. Common Volume When $r_1 = r_2$

For equal cylinder radii $r_1 = r_2 = r$, the integral in (1b) reduces to the familiar result [7]

$$V(r, \beta) = \frac{8}{\sin\beta}\int_0^r (r^2 - x^2)\,dx \qquad (2)$$

$$= \frac{16r^3}{3\sin\beta}. \qquad (3)$$

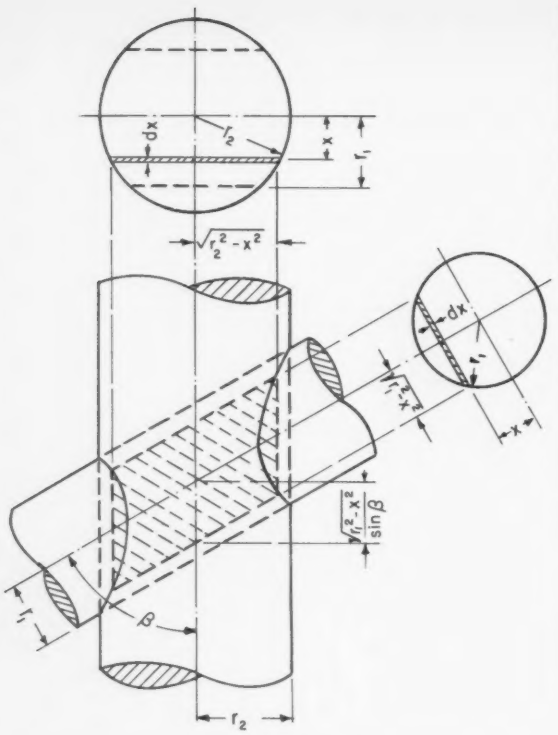

FIGURE 1. *Three-view sketch of the common volume of cylinders with radii r_1 and r_2 axially intersecting at angle β.*

The area of the shaded parallelogram parallel to the plane of the axes in the lower left view comprises the integrand in eq (1a) and is integrated over the range $-r_1 \leq x \leq r_1$ shown in the other two views.

4. Common Volume When $r_1 \leq r_2$

4.1. Series Solution

The factor $(r_2^2 - x^2)^{1/2}$ in the integral in (1b) may be expanded as a power series [9, p. 2, eq 5.3] in x/r_2, since $x \leq r_1 \leq r_2$. The volume integral then becomes

$$V(r_1, r_2, \beta) = \frac{8r_2}{\sin\beta} \sum_{n=0}^{\infty} \binom{\frac{1}{2}}{n} \int_0^{r_1} \left(-\frac{x^2}{r_2^2}\right)^n (r_1^2 - x^2)^{1/2} dx \quad (4)$$

which may be integrated term by term.

The resulting series solution is

$$V(r_1, r_2, \beta) = \frac{4\pi r_2^3}{\sin\beta} \left\{ \frac{1}{2}\left(\frac{r_1}{r_2}\right)^2 - \frac{1}{4}\left(\frac{1}{2}\right)^2 \left(\frac{r_1}{r_2}\right)^4 - \frac{3}{6}\left(\frac{1}{2\cdot 4}\right)^2 \left(\frac{r_1}{r_2}\right)^6 - \frac{5}{8}\left(\frac{1\cdot 3}{2\cdot 4\cdot 6}\right)^2 \left(\frac{r_1}{r_2}\right)^8 - \frac{7}{10}\left(\frac{1\cdot 3\cdot 5}{2\cdot 4\cdot 6\cdot 8}\right)^2 \left(\frac{r_1}{r_2}\right)^{10} - \ldots \right\}$$

$$= \frac{4\pi r_2^3}{\sin\beta} \sum_{n=1}^{\infty} \binom{\frac{1}{2}}{n} \binom{\frac{1}{2}}{n-1} \left(\frac{r_1}{r_2}\right)^{2n}. \quad (5)$$

This same result may be obtained by casting the integral in (1b) in the form

$$V(r_1, r_2, \beta) = (r_2^3/\sin\beta) 4 \left(\frac{r_1}{r_2}\right)^2 \times \int_0^1 t^{-1/2}(1-t)^{1/2} \left(1 - \frac{r_1^2}{r_2^2} t\right)^{1/2} dt, \quad (6)$$

where $t = x^2/r_1^2$, which is now recognizable as the integral representation of the hypergeometric series [10]

$$V(r_1, r_2, \beta) = (r_2^3/\sin\beta) 2\pi \left(\frac{r_1}{r_2}\right)^2 {}_2F_1\left(-\frac{1}{2}, \frac{1}{2}; 2; \frac{r_1^2}{r_2^2}\right) \quad (7)$$

identifiable with (5).

Since (5) is somewhat slowly convergent when $r_1 \cong r_2$, under some circumstances it may be advantageous to difference this series against a $1/\pi$-series (16) discussed in the appendix, giving

$$V(r_1, r_2, \beta) = \frac{4\pi r_2^3}{\sin\beta} \left\{ \frac{4}{3\pi} - \sum_{n=1}^{\infty} \binom{\frac{1}{2}}{n} \binom{\frac{1}{2}}{n-1} \left[1 - \left(\frac{r_1}{r_2}\right)^{2n}\right] \right\}. \quad (8)$$

The convergence rate of the series-term in (8) is not improved over that of (5). However, for $r_1 \cong r_2$ this sum is small compared to the constant term $4/3\pi$, identifiable with the equal-radii solution (3), hence resulting in higher precision of $V(r_1, r_2, \beta)$ for the same number of terms. An alternative series solution for this region is given at the end of the following section.

4.2. Elliptic Integral Solution

An alternative solution of the integral in (1b) may be obtained as a combination of complete elliptic integrals [11] of the first and second kinds, $K(k)$ and $E(k)$. Applying formulas (219.11) and (361.03) from Byrd and Friedman [12] the result is found to be[2]

$$V(r_1, r_2, \beta) = \frac{8r_2^3}{3\sin\beta} [(1+k^2)E(k) - (1-k^2)K(k)] \quad (9)$$

where

$$k = r_1/r_2.$$

Except for the angle factor $1/\sin\beta$ this result is the standard textbook solution [5, 6] for cylinders intersecting at right angles. Also, the formulation in (9) is related to the indefinite integral [12, eq (611.01)]

$$\int_0^k kE(k)dk = \frac{1}{3}[(1+k^2)E(k) - (1-k^2)K(k)]. \quad (10)$$

[2] This integral is part of the "G factor" used for interpreting gas scattering experiments in which a circular-aperture detector views a gas target transversed by a cylindrical beam. In this context this elliptic integral solution has been given by E. A. Silverstein, Nucl. Instr. and Meth. **4,** 53 (1959) and by D. F. Herring and K. W. Jones, Nucl. Instr. and Meth. **30,** 88 (1964).

A partial check on (9) is obtained by expanding $E(k)$ and $K(k)$ as power series in k according to reference [9], eqs (773.1) and (774.1). Combining like powers of k and substituting back r_1/r_2 for k the resulting series is identical with (5). An additional check is provided by the identity of eqs (9) and (3) in the limit as $k \to 1$. Also, eq (9) can be obtained from (7) by use of the tenth Gauss recursion formula on page 9 of reference [10].

For k close to unity, a series which converges more rapidly than (8) may now be derived by substituting in (9) the series in equations (773.3) and (774.3) in reference [9] for $K(k)$ and $E(k)$. The first few terms of this series are

$$V(r_1, r_2, \beta) = (r_2^3/\sin\beta) \cdot \frac{16}{3} \left\{ 1 - \frac{3}{4} k'^2 - \frac{1}{2^2 \cdot 4} \left(\ln \frac{4}{k'} - \frac{1}{4} \right) k'^4 - 2 \cdot \frac{1^2 \cdot 3}{2^2 \cdot 4^2 \cdot 6} \left(\ln \frac{4}{k'} - \frac{11}{12} \right) k'^6 - 3 \cdot \frac{1^2 \cdot 3^2 \cdot 5}{2^2 \cdot 4^2 \cdot 6^2 \cdot 8} \left(\ln \frac{4}{k'} - \frac{43}{40} \right) k'^8 - 4 \cdot \frac{1^2 \cdot 3^2 \cdot 5^2 \cdot 7}{2^2 \cdot 4^2 \cdot 6^2 \cdot 8^2 \cdot 10} \left(\ln \frac{4}{k'} - \frac{967}{840} \right) k'^{10} - \ldots \right\} \quad (11)$$

where $k'^2 = 1 - k^2 = 1 - (r_1/r_2)^2$. Using only the terms given in (11) the sum for $r_1/r_2 = 0.90$, without the factor $(r_3^3/\sin\beta)$, gives 4.49991482 as compared with the exact value of 4.49991288 . . ., and the convergence improves as r_1/r_2 goes toward unity. The series in (11) may be obtained in general form, if desired, by use of the appropriate transformation [13] on the hypergeometric series given in (7).

5. Numerical Results

In table 1, the dimensionless factor

$$v(k) = \frac{\sin\beta}{r_2^3} V(r_1, r_2, \beta), \quad (12a)$$

$$= 4\pi \sum_{n=1}^{\infty} \binom{\frac{1}{2}}{n} \binom{\frac{1}{2}}{n-1} k^{2n}, \quad (12b)$$

$$= 2\pi k^2 \, {}_2F_1(-\tfrac{1}{2}, \tfrac{1}{2}; 2; k^2), \quad (12c)$$

$$= 8 \int_0^k kE(k)dk, \quad (12d)$$

$$= \tfrac{8}{3}[(1+k^2)E(k) - (1-k^2)K(k)], \quad (12e)$$

where $k = r_1/r_2$ is tabulated to 8 decimal places for $0 \le k(0.01) \le 1.00$, computed using (12e) and $K(k)$ and $E(k)$ from [11]. Hence, for many practical applications, the common volume of two cylinders with radii $r_1 \le r_2$ and axes intersecting at angle β may be computed as

$$V(r_1, r_2, \beta) = \frac{r_2^3}{\sin\beta} v(k) \quad (13)$$

in which values of $v(k)$ are interpolated from table 1.

TABLE 1. *Values of* v(k), *defined in eq (12a–e), over the range* $0 \le k(0.01) \le 1.00$, *valid to the 8D given*

Modified second central differences δ_m^2 are provided for interpolation using auxiliary tables.

k	$v(k)$	δ_m^2	k	$v(k)$	δ_m^2
0.00	0.0000 0000	+12 5665			
.01	0.0006 2831	12 5656	0.51	1.5792 3625	+9 8789
.02	0.0025 1315	12 5627	.52	1.6394 2033	9 7607
.03	0.0056 5423	12 5580	.53	1.7005 8043	9 6391
.04	0.0100 5109	12 5514	.54	1.7627 0439	9 5142
.05	0.0157 0305	12 5429	.55	1.8257 7969	9 3854
.06	0.0226 0928	12 5325	.56	1.8897 9346	9 2530
.07	0.0307 6874	12 5203	.57	1.9547 3247	9 1167
.08	0.0401 8019	12 5061	.58	2.0205 8308	8 9766
.09	0.0508 4222	12 4900	.59	2.0873 3128	8 8323
.10	0.0627 5321	12 4720	.60	2.1549 6262	8 6837
.11	0.0759 1138	12 4520	.61	2.2234 6226	8 5308
.12	0.0903 1471	12 4302	.62	2.2928 1490	8 3734
.13	0.1059 6104	12 4065	.63	2.3630 0478	8 2112
.14	0.1228 4797	12 3807	.64	2.4340 1570	8 0441
.15	0.1409 7294	12 3530	.65	2.5058 3093	7 8719
.16	0.1603 3316	12 3234	.66	2.5784 3325	7 6943
.17	0.1809 2569	12 2917	.67	2.6518 0490	7 5113
.18	0.2027 4735	12 2581	.68	2.7259 2757	7 3222
.19	0.2257 9478	12 2224	.69	2.8007 8235	7 1272
.20	0.2500 6441	12 1848	.70	2.8763 4974	6 9258
.21	0.2755 5248	12 1451	.71	2.9526 0957	6 7174
.22	0.3022 5502	12 1034	.72	3.0295 4102	6 5020
.23	0.3301 6786	12 0595	.73	3.1071 2253	6 2791
.24	0.3592 8660	12 0136	.74	3.1853 3179	6 0481
.25	0.3896 0667	11 9656	.75	3.2641 4571	5 8086
.26	0.4211 2326	11 9154	.76	3.3435 4031	5 5600
.27	0.4538 3135	11 8632	.77	3.4234 9073	5 3016
.28	0.4877 2572	11 8087	.78	3.5039 7111	5 0328
.29	0.5228 0092	11 7520	.79	3.5849 5457	4 7527
.30	0.5590 5129	11 6932	.80	3.6664 1308	4 4605
.31	0.5964 7093	11 6320	.81	3.7483 1740	4 1550
.32	0.6350 5373	11 5686	.82	3.8306 3696	3 8350
.33	0.6747 9336	11 5029	.83	3.9133 3972	3 4992
.34	0.7156 8323	11 4348	.84	3.9963 9206	3 1456
.35	0.7577 1654	11 3644	.85	4.0797 5861	2 7725
.36	0.8008 8626	11 2915	.86	4.1634 0199	2 3774
.37	0.8451 8508	11 2163	.87	4.2472 8265	1 9574
.38	0.8906 0549	11 1385	.88	4.3313 5853	1 5089
.39	0.9371 3970	11 0582	.89	4.4155 8469	1 0276
.40	0.9847 7969	10 9753	.90	4.4999 1288	+ 5075
.41	1.0335 1716	10 8899	.91	4.5842 9096	− 586
.42	1.0833 4356	10 8017	.92	4.6686 6213	6811
.43	1.1342 5009	10 7108	.93	4.7529 6390	1 3730
.44	1.1862 2764	10 6171	.94	4.8371 2665	2 1554
.45	1.2392 6686	10 5207	.95	4.9210 7158	3 0381
.46	1.2933 5809	10 4213	.96	5.0047 0740	4 1308
.47	1.3484 9141	10 3191	.97	5.0879 2495	5 4606
.48	1.4046 5657	10 2137	.98	5.1705 8678	−7 1824
.49	1.4618 4304	10 1053	.99	5.2525 0293	----
.50	1.5200 3999	+9 9937	1.00	5.3333 3333	----

Modified second central differences δ_m^2 are included for interpolation by Everett's formula

$$v(k_i + p\Delta k) = (1-p)v(k_i) + pv(k_{i+1}) + E_2(p)\delta_{m,i}^2 + F_2(p)\delta_{m,i+1}^2 + \ldots, \quad (14)$$

where p is the interpolation fraction of the interval of tabulation Δk, and $\delta_{m,i}^2$, $\delta_{m,i+1}^2$ are the modified second differences at the tabular points i and $i+1$ and were evaluated from the second and fourth differences according to

$$\delta_m^2 = \delta^2 - 0.184\delta^4.$$

Everett's coefficients $E_2(p)$ and $F_2(p)$ are available in standard tables [14, 15] and are identical with Lagrangian interpolation coefficients A^1_{-1} and A^1_2 [16, table 25.1].

The general behavior of $v(k)$ is shown by the curve in figure 2. Values of $v(k)$ can be taken directly from this curve for use in rough calculations where only two- or three-figure accuracy is required.

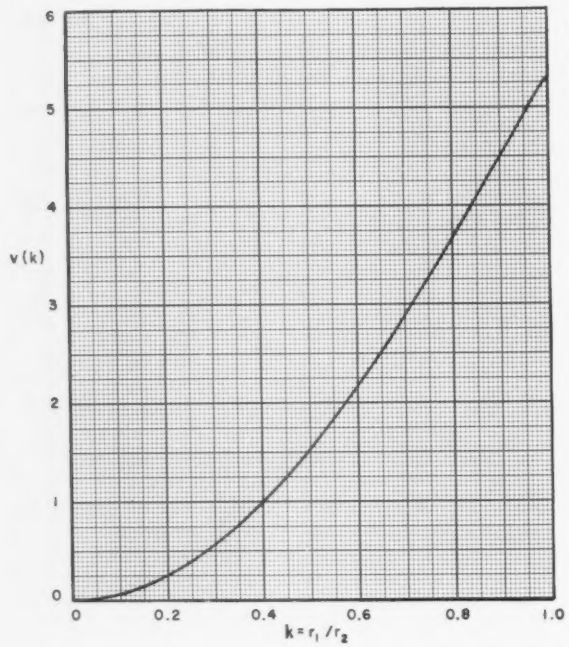

FIGURE 2. *Graph of* v(k) *showing the general behavior of the function and suitable for rough calculations.*

6. Appendix. Two Series for $1/\pi$

The series evaluation (5) for $V(r_1,r_2,\beta)$ contains a factor of π and the formula (3) for $V(r,\beta)$ does not. Thus, for $r_1=r_2=r$, the right-hand side of (5) can be equated to the right-hand side of (3) to form

$$\frac{16r^3}{3\sin\beta}=\frac{4\pi r^3}{\sin\beta}\sum_{n=1}^{\infty}\binom{\frac{1}{2}}{n}\binom{\frac{1}{2}}{n-1} \tag{15}$$

from which

$$\frac{4}{3\pi}=\sum_{n=1}^{\infty}\binom{\frac{1}{2}}{n}\binom{\frac{1}{2}}{n-1}=\frac{1}{2}-\frac{1}{4}\left(\frac{1}{2}\right)^2-\frac{3}{6}\left(\frac{1}{2\cdot 4}\right)^2-\frac{5}{8}\left(\frac{1\cdot 3}{2\cdot 4\cdot 6}\right)^2-\cdots \tag{16}$$

This series can now be used to form the difference-series in eq (8).

An additional $1/\pi$-series, which also does not appear in standard compilations of series [17], can be obtained by combining (16) with a series discussed by Bromwich [18], [17, eq 274]

$$\frac{4}{\pi}=\sum_{n=1}^{\infty}\binom{\frac{1}{2}}{n-1}^2=1+\left(\frac{1}{2}\right)^2+\left(\frac{1}{2\cdot 4}\right)^2+\left(\frac{1\cdot 3}{2\cdot 4\cdot 6}\right)^2+\cdots \tag{17}$$

to form

$$\frac{4}{3\pi}+\frac{4}{\pi}=\sum_{n=1}^{\infty}\binom{\frac{1}{2}}{n-1}\left[\binom{\frac{1}{2}}{n}+\binom{\frac{1}{2}}{n-1}\right]. \tag{18}$$

Using the addition theorem

$$\binom{m}{n}+\binom{m}{n-1}=\binom{m+1}{n} \tag{19}$$

the result is

$$\frac{16}{3\pi}=\sum_{n=1}^{\infty}\binom{\frac{1}{2}}{n-1}\binom{\frac{3}{2}}{n}=1\cdot\frac{3}{2}+\frac{1}{2}\cdot\frac{3\cdot 1}{2\cdot 4}+\frac{1}{2\cdot 4}\cdot\frac{3\cdot 1\cdot 1}{2\cdot 4\cdot 6}+\frac{1\cdot 3}{2\cdot 4\cdot 6}\cdot\frac{3\cdot 1\cdot 1\cdot 3}{2\cdot 4\cdot 6\cdot 8}+\frac{1\cdot 3\cdot 5}{2\cdot 4\cdot 6\cdot 8}\cdot\frac{3\cdot 1\cdot 1\cdot 3\cdot 5}{2\cdot 4\cdot 6\cdot 8\cdot 10}+\cdots. \tag{20}$$

The author thanks E. Hayward for suggesting the problem, and P. Lamperti and L. W. B. Jolley for their stimulating interest in the cylinder intersection and $1/\pi$ series, respectively. The author is also indebted to F. W. J. Olver, I. A. Stegun, L. F. Epstein, and A. Fletcher for suggestions and comments, and especially to Mrs. Ruth Capuano for computing table 1.

7. References

[1] A. Schoch, A discussion of colliding beam techniques, Nuclear Instr. and Methods **11,** 40 (1961).
[2] P. Lamperti, private communication.
[3] E. Hayward and J. H. Hubbell, The backscattering of the Co^{60} gamma rays from infinite media, J. of Appl. Phys. **25,** 506 (1954).
[4] W. E. Byerly, Elements of the Integral Calculus (Ginn and Co., Boston, 1902), p. 281, ex. (5a), which is incorrect.
[5] H. Hancock, Elliptic Integrals p. 89, ex. (6) (John Wiley & Sons, New York, N.Y., 1917).
[6] P. Franklin, Methods of Advanced Calculus, p. 299, ex. 77 (McGraw-Hill, New York and London, 1944).
[7] See, for example, J. Edwards, A Treatise on the Integral Calculus. I., p. 793, ex. (23) (MacMillan, London, 1921).

[8] L. F. Epstein and N. E. French, Improving the convergence of series: Application to some elliptic integrals, Am. Math. Monthly **63,** 698 (1956); also L. F. Epstein and J. H. Hubbell, Evaluation of a generalized elliptic-type integral, J. Res. NBS **67**B, 1 (1963).

[9] See, for example, H. B. Dwight, Tables of Integrals and Other Mathematical Data, 3d ed. p. 2, eq (5.3). (MacMillan, New York, 1957).

[10] W. Magnus and F. Oberhettinger, Formulas and Theorems for the Special Functions of Mathematical Physics, p. 8 (Chelsea Publ. Co., New York, 1949).

[11] A. Fletcher, A table of complete elliptic integrals, Phil. Mag. (7) **30,** 516 (1940), in which $K(k)$ and $E(k)$ are conveniently tabulated for $0 \leq k(0.01) \leq 1.00$ to ten decimals.

[12] P. F. Byrd and M. D. Friedman, Handbook of Elliptic Integrals for Engineers and Physicists (Springer-Verlag, Berlin, 1954).

[13] A. Erdelvi, W. Magnus, F. Oberhettinger and F. G. Tricomi, Higher Transcendental Functions Vol. **1,** p. 110, eq (12). (Bateman Manuscript Project).

[14] H. T. Davis, Tables of the Higher Mathematical Functions, Vol. **1,** pp. 126–127 (Principia Press, Bloomington, Indiana, 1933)

[15] Nautical Almanac Office, Interpolation and Allied Tables, pp. 44–53 (H.M. Stationery Office, London, 1956).

[16] M. Abramowitz and I. A. Stegun, eds., Handbook of Mathematical Functions, NBS Applied Math. Series 55, pp. 880, 901–3 (June, 1964).

[17] See, for example, L. W. B. Jolley, Summation of Series (Dover, New York, revised 2d edition, 1961). Note that eq (409), p. 76 of this reference is identical with (274) p. 50 if the limiting sum is changed from $(11/\pi)-4$ to the correct value of $(16/\pi)-4$.

[18] T. J. Bromwich, Introduction to the Theory of Infinite Series, p. 190 (MacMillan Co., London, 1926).

(Paper 69C2–193)

JOURNAL OF RESEARCH of the National Bureau of Standards—C. Engineering and Instrumentation
Vol. 69C, No. 2, April-June 1965

Steady-State Heat Conduction in an Exposed Exterior Column of Rectangular Cross Section

B. A. Peavy

(February 3, 1965)

This paper presents a mathematical analysis of two-dimensional steady-state heat conduction in a solid of rectangular cross section, two parallel surfaces of which are exposed to separate temperature environments with respective surface heat transfer coefficients. For the other two parallel surfaces, the temperature environment and surface heat transfer coefficients are assumed to vary as a function of position on these surfaces. A particular application of this analysis has been to determine the temperature distribution in a transverse cross section of exposed concrete columns.

1. Introduction

Modern architectural treatment of exterior columns of high-rise buildings involves the use of columns exposed to temperature extremes on the outside face and relatively constant temperatures on the interior. The temperature extremes give rise to dimensional changes in the column which can best be determined from temperature distribution in the column. In connection with a request from the Federal Housing Administration, an investigation was made for determining the temperature distributions in an exposed exterior column.

This paper presents a mathematical analysis of two-dimensional steady-state heat conduction in an exposed exterior column which may be represented by a solid of rectangular cross section, two parallel surfaces of which are exposed to separate temperature environments with respective surface heat transfer coefficients. For the other two parallel surfaces, the temperature environment and surface heat transfer coefficient are assumed to vary as a function of transverse position on these surfaces.

An analysis for general application is presented, along with the statement and numerical results for four specific problems.

2. Analysis for General Problem

Because the heat-transfer problem in a rectangular solid may have a more general application than that cited in the previous section, the following analysis is based on boundary conditions, arbitrary in nature, which may be adapted to specific applications. Section 3 presents the assumed boundary conditions for heat transfer in an exposed exterior column.

For steady-state, two-dimensional heat conduction in a rectangular homogeneous solid with no flow of heat in the direction of the third dimension, it is assumed that the rate of heat flow at each of the four boundary surfaces is proportional to the temperature difference between the temperature of the surface and that of the ambient adjacent to the surface. The proportionality factor may be prescribed as a function of the distance along the surface. A convenient placement of coordinate axes for the type of problem to be considered is as shown in figure 1, where the boundary conditions at the four surfaces, $x=\pm l$, and $y=\pm a$, are shown adjacent to the surfaces.

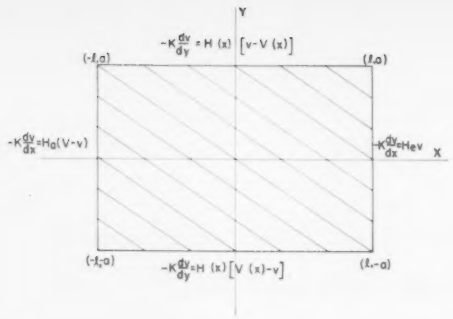

FIGURE 1. *Transverse section of rectangular solid, showing boundary conditions on* $x=\pm 1$ *and* $y=\pm a$.

The temperature potentials V and $V(x)$ are the temperature differences between the temperatures of the ambient adjacent to various surface positions and that of the ambient adjacent to $x=l$; the temperature potential v is the temperature difference between a temperature in the solid and that of the ambient adjacent to $x=l$. The proportionality constants H_a and H_e represent the coefficients of heat transfer between the surface and the ambient at the surfaces $x=-l$, and $x=l$, respectively. For the purposes of this paper the variable heat transfer coefficient $H(x)$ and temperature potential $V(x)$ are considered to be piece-wise continuous on $-l\leq x\leq l$, where $H(x)=H_i(x)$ and $V(x)=V_i(x)$ are continuous on $x_{i-1}\leq x\leq x_i$ and $i=1, 2, 3, \ldots m$; $x_0=-l$, and $x_m=l$.

The partial differential equation for steady-state heat conduction in a homogeneous solid in a rectangular coordinate system is

$$\frac{\partial^2 v}{\partial x^2}+\frac{\partial^2 v}{\partial y^2}=0. \tag{1}$$

A solution of (1) satisfying the boundary conditions at $x=l$ and $x=-l$ (fig. 1) is

$$\frac{v}{V}=\frac{h_1+h_1h_2(1-x/l)}{h_1+h_2+2h_1h_2}+\sum_{n=1}\frac{A_nR(\beta_nx/l)\cosh\beta_ny/l}{\cosh\beta_na/l} \tag{2}$$

where due to the similar conditions on $y=\pm a$, it is assumed that $\frac{dv}{dy}=0$ on the center line $y=0$. Symbols used in (2) are:

K=thermal conductivity of the solid
$h_1=H_al/K$
$h_2=H_el/K$
A_n=coefficients to be determined from boundary conditions on $y=a$
$R(\beta_nx/l)=\beta_n\cos\beta_n(1+x/l)+h_1\sin\beta_n(1+x/l)$

where β_n are positive roots of $(\beta^2-h_1h_2)\sin 2\beta-\beta(h_1+h_2)\cos 2\beta=0$.

Substitution of boundary conditions on $y=a$ gives m equations

$$\sum_{n=1}^{\infty}A_nR(\beta_nx/l)\left[\beta_n\tanh\beta_na/l+\frac{lH(x)}{K}\right]=\frac{lH(x)}{K}\left[\frac{V(x)}{V}-\frac{h_1+h_1h_2(1-x/l)}{h_1+h_2+2h_1h_2}\right]. \tag{3}$$

Multiplying each equation by $R(\beta_kx/l)$ and integrating from $x=-l$ to $x=l$, yields

$$\sum_{n=1}^{\infty}\left[\beta_nA_n\tanh\beta_na/l\int_{-l}^{l}R(\beta_nx/l)R(\beta_kx/l)dx+\frac{l}{K}\sum_{i=1}^{m}A_n\int_{x_{i-1}}^{x_i}H(x)R(\beta_nx/l)R(\beta_kx/l)dx\right]$$
$$=\frac{l}{K}\sum_{i=1}^{m}\int_{x_{i-1}}^{x_i}H(x)R(\beta_kx/l)\times\left[\frac{V(x)}{V}-\frac{h_1+h_2h_1(1-x/l)}{h_1+h_2+2h_1h_2}\right]dx. \tag{4}$$

Using the orthogonal and other related properties of $R(\beta_n x/l)$ as derived in the appendix, (4) may be put in the form of simultaneous equations

$$B_n A_n + \sum_{\substack{k=1 \\ k \neq n}}^{\infty} C_{n,k} A_k = D_n, \qquad n=1, 2, \ldots \tag{5}$$

where

$$B_n = \beta_n \tanh \beta_n a/l \int_{-l}^{l} R^2(\beta_n x/l)dx + \frac{l}{K}\sum_{i=1}^{m}\int_{x_{i-1}}^{x_i} H(x)R^2(\beta_n x/l)dx$$

$$C_{n,k} = \frac{l}{K}\sum_{i=1}^{m}\int_{x_{i-1}}^{x_i} H(x)R(\beta_n x/l)R(\beta_k x/l)dx$$

$$D_n = \frac{l}{K}\sum_{i=1}^{m}\int_{x_{i-1}}^{x_i}\left[\frac{V(x)}{V} - \frac{h_1+h_1h_2(1-x/l)}{h_1+h_2+2h_1h_2}\right]\times H(x)R(\beta_n x/l)dx.$$

Of particular interest is the mean temperature in the solid, v_m, given by

$$\frac{v_m}{V} = \frac{1}{2al}\int_{-l}^{l}\int_{0}^{a}\frac{v}{V}\,dy\,dx$$

$$\frac{v_m}{V} = \frac{h_1(1+h_2)}{h_1+h_2+2h_1h_2} + \frac{l}{2a}\sum_n \frac{A_n \tanh \beta_n a/l[\beta_n \sin 2\beta_n + h_1(1-\cos 2\beta_n)]}{\beta_n^2}. \tag{6}$$

3. Temperature Distribution in Exposed Concrete Columns

An interesting specific case for solution of (2) is to consider a transverse section of a rectangular concrete column. Here a portion of the boundary surface is exposed to outside weather conditions or design temperature, another portion of the surface is exposed to the ambient temperature maintained within the building, and another portion of the surface is in contact with the walls of the building. A cross section of the column, and an abutting wall in the region $b<x<d$, is shown in the lower portion of figure 2. The $x=l$ face of the column is assumed to be

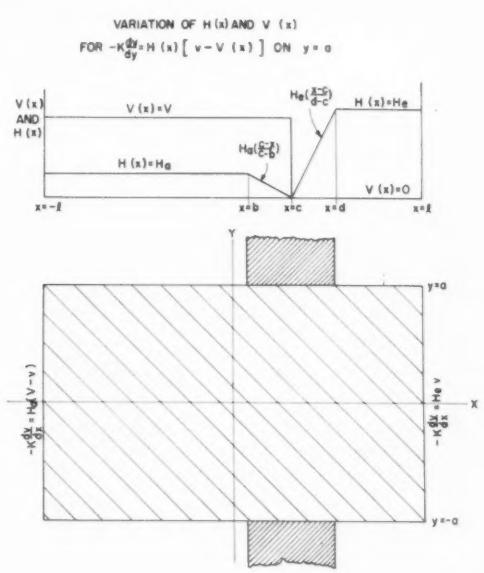

FIGURE 2. *Transverse section of rectangular concrete column with abutting wall separating the inside and outside environment.*

Outside face is located at $x=l$.

the outside face exposed to the outside design temperature which is assumed to be the zero or datum plane temperature from which all other temperature potentials are reckoned; the face $x=-l$ is assumed to be exposed to the indoor temperature potential V.

The upper portion of figure 2 shows the assumed variation of $H(x)$ and $V(x)$ along the surfaces $y=\pm a$. $H(x)$ is assumed constant at H_a in the region $-l\leq x\leq b$; decreases linearly from H_a to zero in going from b to c; increases linearly from zero to H_e in going from c to d; and is constant at H_e in the region $d\leq x\leq l$. $V(x)$ is assumed constant at V from $-l$ to c; and is zero from c to l. In the region of the abutting wall, $b<x<d$, the heat transfer between the wall and the column was assumed to be dependent on the inside and outside temperatures in their region of influence and the surface coefficients decreasing linearly to zero at $x=c$.

$$-K\frac{dv}{dy}=H_a\left(\frac{c-x}{c-b}\right)(v-V) \qquad b<x<c, y=a$$

$$-K\frac{dv}{dy}=H_e\left(\frac{x-c}{d-c}\right)v \qquad c<x<d, y=a.$$

Expressions for D_n, B_n, and $C_{n,k}$ necessary for substitution in (5) are given in the appendix (A13, A14, A15). The solution of (5) for A_n and its substitution in (2) gives the temperature distribution for values of x and y.

Numerical solutions were obtained, using a digital computer, for a 36 in.$\times$14 in. concrete column for four positions of the abutting wall, based on a 100 deg F temperature difference between the inside and outside. Numerical values used, and assumed as constants, were

Thermal conductivity, K=1.0 Btu/hr ft deg F
Inside heat transfer coefficient, H_a=0.5 Btu/hr ft^2 deg F
Outside heat transfer coefficient, H_e=6.0 Btu/hr ft^2 deg F
Width of column, $2a$=14 in.=7/6 ft
Thickness of column, $2l$=36 in.=3 ft
Thickness of wall, $d-b$=8 in.=2/3 ft
Also it was assumed that $d-c=c-b$.

The inside surfaces of the column were assumed to be separated from the inside of the building by suitable interior finish, giving a nominal value for H_a of 0.5 Btu/hr ft^2 deg F. The value H_e=6.0 Btu/hr ft^2 deg F was based on an outside wind velocity of 15 mph.

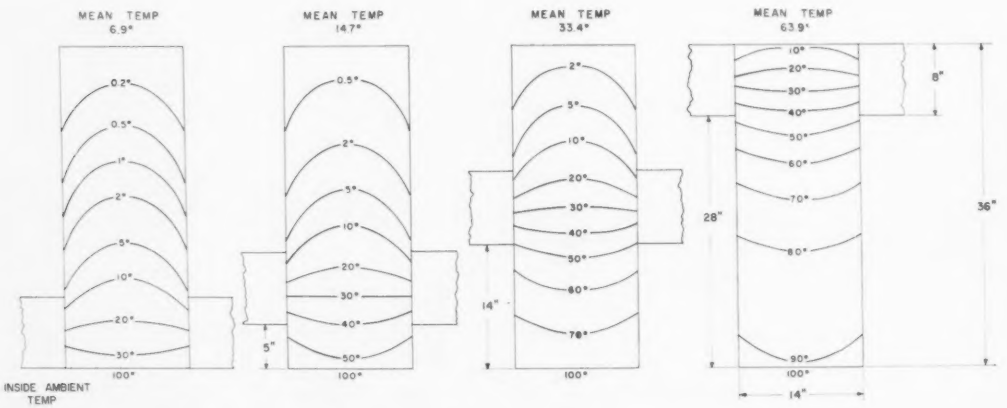

FIGURE 3. *Temperature potential distributions in 36-in. by 14-in. concrete columns for four positions of the abutting walls, based on a 100-deg temperature difference between the inside and outside and the constants cited in the text.*

Figure 3 shows temperature potential isotherms plotted within the column cross section for four positions of the abutting wall. Mean temperatures were computed from (6). Figure 4 shows mean temperatures over the width of the columns plotted against distance measured from the inside surface of the column. Positions of the abutting wall are shown for clarity.

Temperatures in degrees Fahrenheit can be expressed in terms of the temperature potentials, v, of figure 3 by means of the relation

$$t,\ °\mathrm{F} = t_e + (v/100)(t_a - t_e)$$

where t_a is the inside air temperature, and t_e is the outside air temperature, in degrees Fahrenheit.

4. Discussion

The analysis of section 2 assumes similar boundary conditions on the surfaces, $y = \pm a$. For the consideration of a more general case where these conditions are not similar, it is convenient to make a translation of the x–axis of figure 1 to the lower side and rewrite the summation term in (2)

$$\frac{\left[A_n \cosh \beta_n y/l + E_n \cosh \beta_n \left(\frac{2a-y}{l}\right)\right] R(\beta_n x/l)}{\cosh \beta_n 2a/l}.$$

Substitution of boundary conditions at $y=0$ and $y=2a$ will give two sets of simultaneous equations similar to (5), both containing the coefficients A_n and E_n. Solution for A_n and E_n may be obtained by iteration; for example, let $E_n=0$ in one set and solve for A_n, substitute A_n in the second set and solve for E_n, which is substituted in the first set. This process may be continued until A_n and E_n are invariant.

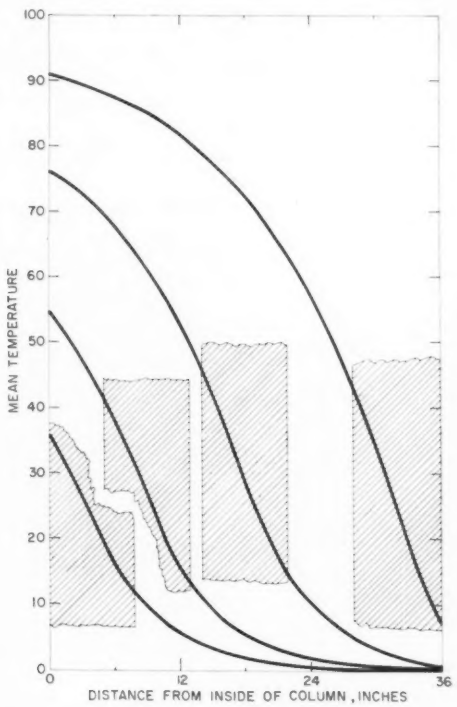

FIGURE 4. *Mean temperatures over the width of the columns against distance measured from the inside surface of the columns.*

Positions of the abutting walls are shown.

The assumption was made that a sufficiently good approximation to the solution of the infinite set of equations (5) in the infinitely many unknowns A_n could be obtained by solving the first forty equations for A_n, $n=1, 2, \ldots, 40$. Solution of the first twenty equations for A_n, $n=1, 2\ldots, 20$ gave results which differed from that for forty A_n by less than 0.1 °F. It therefore appeared that convergence of the approximating sequence of A_n's to the true solution of (5) was sufficiently rapid to justify our assumption.

A computer program in Fortran IV language is available for the problem as set forth in section 3. Data input to this program allows any possible variation in the numerical values for the thermal conductivity, surface coefficients, and dimensions.

4. Appendix. Orthogonal and Other Related Properties of $R(\beta_n x/l)$

To satisfy the boundary condition in (2) at $x=l$, β_n must be the roots of

$$(\beta^2-h_1h_2)\sin 2\beta-\beta(h_1+h_2)\cos 2\beta=0. \tag{A1}$$

Without proof in this paper, the roots β_n will be assumed real and positive. Proof of the real nature of these roots is similar to that for roots of an expression given in Carslaw and Jaeger.[1] It then becomes expedient to develop the orthogonal properties of

$$R(\beta_n x/l)=\beta_n\cos\beta_n(1+x/l)+h_1\sin\beta_n(1+x/l) \tag{A2}$$

where $-l<x<l$. Several expressions useful for later developments are cited below:

$$\sin^2 2\beta=\frac{\beta^2(h_1+h_2)^2}{(\beta^2+h_1^2)(\beta^2+h_2^2)} \tag{A3}$$

$$\cos^2 2\beta=\frac{(\beta^2-h_1h_2)^2}{(\beta^2+h_1^2)(\beta^2+h_2^2)} \tag{A4}$$

$$R^2(\beta x/l)=\frac{\beta^2+h_1^2}{2}+\frac{\beta^2-h_1^2}{2}\cos 2\beta(1+x/l)+h_1\beta\sin 2\beta(1+x/l). \tag{A5}$$

$$R(\beta_n x/l)\,R(\beta_k x/l)=\frac{L_1(x)+L_2(x)}{2} \tag{A6}$$

$$L_1(x)=(\beta_n\beta_k-h_1^2)\cos\phi(1+x/l)+h_1\phi\sin\phi(1+x/l)$$

$$L_2(x)=(\beta_n\beta_k+h_1^2)\cos\psi(1+x/l)-h_1\psi\sin\psi(1+x/l)$$

$$\phi=\beta_n+\beta_k, \qquad \psi=\beta_n-\beta_k$$

$$M_0(x)=\int R(\beta_n x/l)dx=\frac{l}{\beta_n}[\beta_n\sin\beta_n(1+x/l)-h_1\cos\beta_n(1+x/l)] \tag{A7}$$

$$N_0(x)=\int R^2(\beta_n x/l)dx=\frac{x(\beta_n^2+h_1^2)}{2}+\frac{l(\beta_n^2-h_1^2)}{4\beta n}\sin 2\beta_n(1+x/l)-\frac{h_1 l}{2}\cos 2\beta_n(1+x/l) \tag{A8}$$

$$P_0(x)=\int L_1(x)dx=\frac{l}{\phi}[(\beta_n\beta_k-h_1^2)\sin\phi(1+x/l)-h_1\phi\cos\phi(1+x/l)] \tag{A9}$$

$$Q_0(x)=\int L_2(x)dx=\frac{l}{\psi}[(\beta_n\beta_k+h_1^2)\sin\psi(1+x/l)+h_1\psi\cos\psi(1+x/l)]. \tag{A10}$$

[1] Carslaw, H. S., and Jaeger, J. C., Conduction of Heat in Solids, 2d ed., p. 114 (Oxford University Press, London, 1959).

By use of (A3) and (A4), it can be shown that $P_0(l)+Q_0(l)=P_0(-l)+Q_0(-l)=0$; i.e., the integral $\int_{-l}^{l} R(\beta_n x/l)R(\beta_k x/l)dx=0$, showing that $R(\beta_n x/l)$ and $R(\beta_k x/l)$ are orthogonal to each other in the interval $-l<x<l$. Also, using (A3) and (A4),

$$N_0(l)=\frac{l}{2}\frac{(\beta_n^2+h_1^2)(\beta_n^2+h_2^2+h_2)}{(\beta_n^2+h_2^2)}$$

$$-N_0(-l)=\frac{l}{2}(\beta_n^2+h_1^2+h_1).$$

Assuming $H_i(x)$ and $V_i(x)$ to be polynomials in x, then the recurrence

$$M_p(x)=\int x^p R(\beta x/l)dx=xM_{p-1}(x)-\int M_{p-1}(x)dx \tag{A11}$$

and similar relationships for $N_p(x)$, $P_p(x)$ and $Q_p(x)$ may be established for determining B_n, D_n, and $C_{n,k}$ in (5). Assuming a resulting polynomial of the form $S+Tx+Ux^2$ in the solution for D_n, the indefinite integral becomes

$$\int (S+Tx+Ux^2)R(\beta_n x/l)dx=\left(S+Tx+Ux^2-\frac{2l^2U}{\beta_n^2}\right)M_0(x)+\frac{l^2}{\beta_n^2}(T+2Ux)R(\beta_n x/l). \tag{A12}$$

The solution for D_n for the specific case illustrated in figure 2 takes the form

$$D_n=\frac{h_1h_2}{h_1+h_2+2h_1h_2}\sum_{i=1}^{4}\int_{x_{i-1}}^{x_i}(S_i+T_ix+U_ix^2)R(\beta_n x/l)dx$$

where

$S_1=1+h_1$	$T_1=h_1/l$	$U_1=0$
$S_2=cS_1/(c-b)$	$T_2=(cT_1-S_1)/(c-b)$	$U_2=-T_1/(c-b)$
$S_3=-cS_4/(d-c)$	$T_3=(S_4-cT_4)/(d-c)$	$U_3=T_4/(d-c)$
$S_4=-(1+h_2)$	$T_4=h_2/l$	$U_4=0.$

The function in the region $-l<x<l$ is a linear, piecewise continuous function for which the integrals go to zero at the integration limits $x=-l$ and $x=l$, and elsewhere at the other limits only the coefficients of l^2/β_n^2 in (A12) need be considered,

$$D_n=\frac{lh_1h_2}{\beta_n^2(h_1+h_2+2h_1h_2)}[2\{U_2M_0(b)+(U_3-U_2)M_0(c)-U_3M_0(d)\}$$
$$+(T_1+T_2-2U_2b)R(\beta_n b/l)-(T_4-T_3-2U_3d)R(\beta_n d/l)$$
$$+\{T_3-T_2+2c(U_2-U_3)\}R(\beta_n c/l)]. \tag{A13}$$

By a similar analysis

$$\frac{B_n}{l}=\frac{(\beta_n\tanh\beta_n a/l+h_2)(\beta_n^2+h_1^2)(\beta_n^2+h_2^2+h_2)+(\beta_n\tanh\beta_n a/l+h_1)(\beta_n+h_2^2)(\beta_n+h_1^2+h_1)}{2(\beta_n^2+h_2^2)}$$
$$+\frac{1}{4\beta_n^2}\left[\frac{h_2l}{(d-c)}\{R^2(\beta_n d/l)-R^2(\beta_n c/l)\}-\frac{h_1l}{(c-b)}\{R^2(\beta_n c/l)-R^2(\beta_n b/l)\}\right]$$
$$+\frac{(\beta_n^2+h_1^2)}{4}\left[\frac{h_1(c+b)}{l}-\frac{h_2(d+c)}{l}\right] \tag{A14}$$

$$\frac{C_{n,k}}{l}=\frac{h_2l}{2(d-c)}\left[\frac{L_1(d)-L_1(c)}{\phi^2}+\frac{L_2(d)-L_2(c)}{\psi^2}\right]+\frac{h_1l}{2(c-b)}\left[\frac{L_1(c)-L_1(b)}{\phi^2}+\frac{L_2(c)-L_2(b)}{\psi^2}\right]. \tag{A15}$$

(Paper 69C2-194)

JOURNAL OF RESEARCH of the National Bureau of Standards—C. Engineering and Instrumentation
Vol. 69C, No. 2, April-June 1965

Publications of the National Bureau of Standards*

Selected Abstracts

More wavelengths from thorium lamps, W. F. Meggers and R. W. Stanley, *J. Res. NBS* **69A** (*Phys. and Chem.*), *No. 2* (*Mar.–Apr. 1965*), *70 cents.*

For the purpose of supplementing or superseding the spectroscopic secondary standards of wavelength derived since 1910 from an iron arc, Meggers and Stanley, in 1958, reported the first interferometric determinations of wavelengths emitted by a thorium lamp. Those determinations were restricted to 222 intense radiations of thorium with wavelengths ranging from 3288.7356 A to 6991.5839 A. Now the same, and additional, interference spectrograms have been measured to provide improved wavelengths for 511 radiations ranging in wavelength from 3269.6089 A to 7020.504 A. The present list includes many lines of lower intensity than those previously published and fills most of the large intervals in our first report. The accuracy in relative wavelength values of 163 classified thorium lines is tested by the combination principle which indicates that the average error is less than 1 part in 20 to 40 million. Similar measurements of wavelengths emitted by iron-halide lamps have errors that are 3 to 5 times greater.

Splitting of a set of equivalent sites in centrosymmetric space groups into subsets under homogeneous stress, J. B. Wachtman, Jr., and H. S. Peiser, *J. Res. NBS* **69A** (*Phys. and Chem.*), *No. 2* (*Mar.–Apr. 1965*), *70 cents*

It is assumed that the symmetry elements possessed by a homogeneously stressed crystal will be those common to the crystal and to the macroscopic state of stress. Application of stress either leaves a space group unaltered or lowers it to a subgroup. Such lowering can always be considered to take place in successive steps each of which leaves no group intermediate between the starting group and the subgroup. Each such step can be accomplished by a uniaxial stress; for the centrosymmetric space groups, all but one of the symmetry reductions consisting of two or more successive steps can also be accomplished by a uniaxial stress. A set of points all of which are equivalent in the unstrained crystal frequently splits into two or more subsets under stress. For each space group all possibilities are taken into account by considering the behavior of the general position because the behavior of each special position can easily be derived by specializing the description of the general position. The splitting of the general position under homogeneous stress is tabulated for all possibilities for each of the crystallographic space groups possessing centers of symmetry.

Self and mutual admittances of waveguides radiating into plasma layers, J. Galejs, *Radio Science J. Res. NBS/USNC–URSI* **69D**, *No. 2, 179–189 (Feb. 1965) $1.00.*

The self and mutual admittance of waveguide backed slots radiating into a plasma (or dielectric) layer has been formulated in a laterally unbounded geometry. The admittance expression involves integrals that may be approximated by summations for numerical calculations. For a constant mesh size approximation to the integrals the summations are the same as obtained in earlier work, where the plasma layers are considered to be within a wide waveguide. The accuracy of the solution is improved by decreasing the mesh size used for the numerical integration, which is equivalent to increasing the size of the large guide in the waveguide model.

Mutual admittance calculations between two-parallel slots show that the presence of a plasma layer decreases the mutual admittance relative to its free space value.

Electroacoustic waves excited by a space vehicle in ionized atmosphere and its effect on radar return, K.-M. Chen, *Radio Science J. Res. NBS/USNC–URSI* **69D**, *No. 2, 235–241 (Feb. 1965), $1.00.*

When a conducting space vehicle in the ionosphere is illuminated by an incident electromagnetic wave from the ground, a current and charge are induced on the vehicle. The induced current and charge in turn generate two scattered fields in the ionosphere; an electromagnetic (EM) and an electroacoustic (EA) wave. A part of the EA wave is converted to an EM wave across the discontinuity of the ionosphere and reaches the ground. As the result, the Radar return of a space vehicle in the ionosphere is greatly enhanced. In this paper, the case of a conducting cylinder in a plasma and illuminated by an EM wave is considered. The induced current and charge on the cylinder are determined and the scattered EM and EA waves are calculated. The corresponding radar cross sections due to EM and EA waves are defined. It is shown that the enhancement of the radar return due to an EA wave bears some resemblances to the large outbursts of the reflected HF signals from the satellites observed by Kraus.

Insulated and loaded loop antenna immersed in a conducting medium, R. H. Williams, *Radio Science J. Res. NBS/USNC–URSI* **69D**, *No. 2, 287–289 (Feb. 1965), $1.00.*

Previous analyses of the driving-point impedance of a small loop in an insulating radome immersed in a conducting medium are extended to include the effect of a permeable core loading the loop. It is shown that the effective area of the loop is increased by a gain factor previously derived for the loaded loop in free space. The effects of the conducting medium in this factor are negligible.

Electromagnetic waves along an infinitely long and thin conducting wire in a magneto-ionic medium, Y. Mushiake, *Radio Science J. Res. NBS/USNC–URSI* **69D**, *No. 4,* 503–510 (*Apr. 1965*), *$1.00.*

Electromagnetic fields of an infinitely long conducting cylinder in a magneto-ionic medium with axial static magnetic field are theoretically analyzed. Expressions of the electromagnetic fields and the dispersion formulas are obtained. Explicit approximate expressions of the relative propagation constants for the case of an extremely thin wire are derived and their dependence on the plasma and the cyclotron frequencies is discussed. The behavior of the electromagnetic fields around the wire is also discussed.

Excitation of acoustic waves in plasmas, W. A. Saxton, *Radio Science J. Res. NBS/USNC–URSI* **69D**, *No. 4,* 609–616, (*Apr. 1965*), *$1.00.*

This paper reports early results in an experimental study to determine the effects of perturbing weakly-ionized gaseous plasmas with acoustic waves emanating from transducers that operate in the audio and ultrasonic frequency ranges. Compact loudspeakers incorporated into cylindrical plasma discharge tubes provide the source of acoustic signals. Modulation of electromagnetic waves by the acoustically disturbed plasma is measured in a unique rectangular cavity whose output is detected and fed to a wave analyzer. Resultant wave-analyzer responses indicate that the collision frequency is modulated in addition to the plasma frequency, and suggest that the variations in both are proportional to the magnitude of loudspeaker diaphragm deflection, as predicted by simple acoustic theory. Knowing that two forms of modulation occur simultaneously, a calibration scheme was developed to separate the variation Δf_p in the plasma frequency from the total response. Measurements to date indicate that $\Delta N_e/N_e = W\Delta N/N$ (where N_e and N are electron

and neutral-molecule densities, respectively) for slightly-ionized gases which are subjected to low-frequency pressure variations in the order of 10^{-5} mm Hg, and that such variations produce plasma-frequency perturbations of 0—140 kc/s at plasma frequencies up to 800 Mc/s.

Test of the constancy of the velocity of electromagnetic radiation in high vacuum, P. Beckmann and P. Mandics, *Radio Science J. Res. NBS/USNC–URSI* **69D,** *No. 4,* 623–628 (*Apr. 1965*), *$1.00.*
It is pointed out that Einstein's postulate of the constant velocity of light is verified only indirectly by elementary-particle experiments leaning more or less heavily on present electromagnetic theory, the latter being verified only for low velocities. Direct experiments can be explained by the ballistic theory of light if transparent media, such as gases, reradiate as a secondary source. A direct experiment with coherent light reflected from a moving mirror was performed in vacuum better than 10^{-6} torr. Its result is consistent with the constant velocity of light.

Signal degeneration in laser beams propagated through a turbulent atmosphere, P. Beckmann, *Radio Science J. Res. NBS/USNC–URSI* **69D,** *No. 4,* 629–640 (*Apr. 1965*), *$1.00.*
The statistical distributions of the angle of arrival, the spot location, the cross section, the amplitude, the carrier phase, and the modulation phase of a laser beam traversing an anisotropically turbulent atmosphere are derived in terms of the space correlation function of the atmospheric index of refraction and the windspeed. The limitations imposed by the turbulent atmosphere and the loss of coherence on the depth and bandwidth of the modulation, on the length of the path and on the aperture of the receiving apparatus are analyzed. Experiments to obtain numerical parameters and to check functional dependencies are proposed.

Consolidated Supplement to Building Materials and Structures Report 144 (Supersedes Supplements 1 and 2 of BMS Report 144). Sound insulation of wall, floor, and door constructions, R. D. Berendt and G. E. Winzer, *NBS Mono. 77* (*Nov. 30, 1964*), *40 cents.*
The data obtained at the National Bureau of Standards on the sound insulating properties of building structures are summarized. The results of the two previous Supplements to BMS Report 144 (1955) are included, together with later results obtained through January 1964. Single figure ratings, STC and INR, for airborne sound transmission and impact sound transmission, respectively, as well as the octave frequency band spectra of impact noise, are included as additional information. A brief description of the sound-measuring techniques is given.

Investigation of the hydraulics of horizontal drains in plumbing systems, R. S. Wyly, *NBS Mono. 86* (*Dec. 18, 1964*), *35 cents.*
Results are reported from an investigation of the hydraulics of flow in experimental apparatus simulating nominally horizontal simple and branching drains of plumbing systems. The data are correlated with limited findings in an earlier, unpublished NBS study the results of which have been utilized in current plumbing codes. The need for further research is pointed out, particularly in relation to hydraulic performance of drain systems as affected by steep slopes, drain storage volume, energy losses at stack bases, attenuation of water depths and discharge rates in long drains, and large drain diameters.
Analysis yielded equations useful in estimating hydraulic capacities for surge flow or for surge flow superimposed on steady flow over a range of conditions. Capacity estimates for the large drains are substantially greater than formerly assumed. The experimental findings suggest that through careful design it may be possible to reduce the number of conventional vents extending above plumbing fixtures in small systems such as those in one- and two-family houses. The results, of interest to writers of plumbing codes and handbooks, have important applications in computation of optimum plumbing loads on building drains and building sewers, in terms of actual plumbing fixtures.

Ellipsometry in the measurement of surfaces and thin films Symposium Proceedings Washington 1963, *ed.* E. Passaglia, R. R. Stromberg, and J. Kruger, *NBS Misc. Publ. 256* (*Sept. 15, 1964*), *$2.25.*
A Symposium on the Ellipsometer and its Use in the Measurement of Surfaces was held at the National Bureau of Standards in September 1963. This volume contains 19 of the papers included in the program, together with any discussions which followed oral presentation. Topics covered include historical review, theory, computational techniques, measurement techniques, and the use of ellipsometry in measuring metal surface oxide films and organic films.

Standard Reference Materials: Metallographic characterization of an NBS spectrometric low-alloy steel standard, R. E. Michaelis, H. Yakowitz, and G. A. Moore, *NBS Misc. Publ. 260–3* (*Oct. 22, 1964*), *20 cents.*
The *spectrometric standard steel* designated NBS Low-Alloy Steel 461 was investigated by means of *electron probe microanalysis* and *quantitative metallographic techniques* employing a digital computer. Electron probe microanalysis showed the steel to be *homogeneous* in nickel and iron at two to four microns of spatial resolution. The average of all determinations agreed with the certified values for these elements. Inclusions in the steel were identified, classified as to size and shape, and counted. Mean free path data on the inclusions were calculated. The ASTM ferrite grain size number was deduced as 13.5 for the steel in the unetched condition. From the mean free paths in ferrite and pearlite, it was found that the steel is structurally homogeneous at a five micron level. It is concluded that the homogeneity level corresponds closely to the grain size of the material. It is further concluded that NBS–461 steel is sufficiently homogeneous that any present microanalytical technique can be carried out with little chance of inaccuracy due to inhomogeneity.

Legibility of alphanumeric characters and other symbols, I. A permuted title index and bibliography, D. Y. Cornog, F. C. Rose, and J. L. Walkowicz, *NBS Misc. Publ. 262–1* (*Dec. 15, 1964*), *60 cents.*
This permuted title index and bibliography to the literature on the legibility of alphanumeric characters and other symbols includes 325 references. Due to the confusion and overlap of terminology in the legibility literature, this report uses the term "legibility" to include "legibility," "readability," "perceptibility," "visibility" and any other closely related concepts. "Other symbols" include such items as the arrows and other coded symbols used to present information on radar displays. The psychological literature on perception has been included only when it was closely involved with the specific problems of alphanumeric characters and other meaningful symbols. Studies concerned with environmental variables, i.e. illumination and symbol-background contrast, and the legibility of dials and scales have received little attention. An author index is included.

Aluminum nails, *CS263–64* (*Nov. 1, 1964*), *10 cents.*
This Commercial Standard covers the types, sizes, material, and principal dimensions of aluminum wire nails commonly used in the building industry. The finish, the approximate number of nails per pound, and tolerances for the principal dimensions are included. Provision is also made for the labeling or identification of nails complying with the standard. The standard does not cover specific applications or special purpose nails.

The electrical properties of aluminum for cryogenic electromagnets, R. J. Corruccini, *NBS Tech. Note 218* (*Aug. 30, 1964*), *30 cents.*
The published data for the ideal resistivity and the magnetoresistivity of aluminum have been correlated. It is shown that both properties can be calculated for the limited ranges of temperature and purity that are of importance for aluminum cryogenic electromagnets from the residual resistivity ratio alone. Empirical functions are given for these properties, and sample calculations are given of the figure of merit for a particular aluminum solenoid relative to the same solenoid using water-cooled copper.

Radio path length stability of ground-to-ground microwave links, M. C. Thompson, Jr., and H. B. Janes, *NBS Tech. Note 219 (Nov. 15, 1964), 45 cents.*
The Lower Atmosphere Physics Section of the National Bureau of Standards, Troposphere and Space Telecommunications Division, conducted a series of eight field experiments in 1958 and 1959 to study the variation in the apparent path length of ground-to-ground microwave links (i.e., the variations in phase of 9400 Mc/s signals) and the corresponding variations in radio refractive index and other atmospheric parameters measured at the path terminals. This report summarizes the results obtained on paths in Colorado and Florida. It also includes an analysis of long-term variations in the apparent path length and associated variables recorded during each experiment, and a power spectrum analysis of short-term variations in apparent path length and refractivity.

Some modifications in methods of calibration of universal ratio sets, D. Ramaley, *NBS Tech. Note 220 (Aug. 30, 1964), 25 cents.*
Universal Ratio Sets can be calibrated by a number of different methods. The well established methods are very briefly outlined and emphasis is placed on some more recent developments. The choice of methods will depend upon available laboratory equipment and other considerations.

Bibliography on the measurement of bulk resistivity of semiconductor materials for electron devices, J. C. French, *NBS Tech. Note 232 (Oct. 21, 1964), 60 cents.*
In support of a study of accurate measurements of the bulk resistivity of semiconductor materials such as germanium and silicon which are used in electron devices, a literature search has led to the development of a rather large collection of references. The file cards making up the bibliography are reproduced in this Technical Note for the assistance of others who are concerned with the improvement and standardization of these measurements.

Survey of magnetic thin film materials, G. W. Reimherr, *NBS Tech. Note 247 (Sept. 25, 1964), 40 cents.*
This survey lists the materials reportedly made as a magnetic thin film, along with some of their properties and potential applications. Research activity using the less-frequently mentioned magnetic film materials is noted. About 200 references are cited.

Research on crystal growth and characterization at the National Bureau of Standards January to June 1964, ed., H. F. McMurdie, *NBS Tech. Note 251 (Oct. 19, 1964), 45 cents.*
The National Bureau of Standards with partial support from the Advanced Research Projects Agency of the Department of Defense is continuing a wide program of studies involving crystalline materials. These include investigation of methods and theory of growth, study of detection and effects of defects, determination of physical properties, refinement of chemical analysis, and determination of stability relations and atomic structure. The types of materials range from organic compounds, through metals, and inorganic salts to refractory oxides. This Technical Note, the fourth in the series, summarizes the progress of these various projects from January to June 1964, and lists the related publications and participating scientists.

Procedures for precise determination of thermal radiation properties November 1962 to October 1963, J. C. Richmond, D. P. DeWitt, and W. D. Hayes, Jr., *NBS Tech. Note 252 (Nov. 20, 1964), 40 cents.*
The preliminary design of an intergrating-sphere reflectometer, utilizing a helium-neon continuous-wave gas laser as the source, for measuring the reflectance of specimens at high temperature, was completed. Development work on an ellipsoidal mirror reflectometer for measuring spectral reflectance in the wavelength range of 2 to 15 microns of specimens at room temperature was continued. The study of equations relating spectral emissivity of metals to other properties was continued. Platinum-13% rhodium and oxidized Inconel working standards of normal spectral emittance were calibrated over the wavelength range of 1 to 15 microns at temperatures of 800, 1100 and 1300°K. Several modifications of the normal spectral emittance equipment were made to permit operation in the 15–35 micron range.

Disclosures on various subjects; A plumbing vent manifold, a micro-adjuster, a glass joint or stopcock, and a miniature puller, ed., D. Robbins, *NBS Tech. Note 253 (Nov. 30, 1964), 10 cents.*

This Note presents four devices embodying interesting and unusual solutions to problems prevalent in their respective arts. These devices, developed at the National Bureau of Standards and the U.S. Weather Bureau, comprise a vent manifold for a plumbing system; a micro-adjuster providing purely rectilinear motion; a miniature gear, flange and bearing puller, and a glass joint or stopcock preventing capillary action.

On the formulation and numerical evaluation of a set of two-phase flow equations modeling the cooldown process, S. Jarvis, Jr. *NBS Tech. Note 301 (Jan. 1965), 55 cents.*
A model of transient two-phase flow in a pipe is constructed in Eulerian coordinates assuming a single velocity but independent temperatures in the two phases. Experiments on the numerical integration of the system for cooldown problem by both Lax and Courant-Isaacson-Rees methods indicate that a very fine spatial difference net must be used to compensate for the numerical diffusion essential to computational stability if a second surge is to be realized.

National standard reference data system. Plan of operation, E. L. Brady and M. B. Wallenstein, *NSRDS-NBS1 (Dec. 30, 1964), 15 cents.*
In June 1963 the National Bureau of Standards was assigned the responsibility by the President's Office of Science and Technology of administering a government-wide program to promote and coordinate systematic data compilation and evaluation activities in all fields of the physical sciences. This government-wide program has been called the National Standard Reference Data System. The present report describes the background of this program and the mode of approach adopted by the management of the National Bureau of Standards in fulfilling its responsibility.

Weights and measures—a challenge to industry, M. W. Jensen, *Proc. 50th Mid-Year Meeting Chemical Specialties Manufacturers Assoc., Chicago, Ill., May 18–20, 1964, pp. 24–26 (Chem. Specialties Mfg. Assoc. Inc., New York, N.Y.).*
The responsibility for regulatory control over commercial weights and measures in the United States is left principally to the individual States and their political subdivisions. The National Bureau of Standards provides the States with calibration of the reference standards and various technical services pertaining to a weights and measures program. An important vehicle employed by the Bureau in this area is the National Conference on Weights and Measures, which provides a national forum for discussion and a mechanism for developing model laws and regulations.

Computer interpretation of English text and picture patterns, R. A. Kirsch, *IEEE Trans. Electron. Computers* **EC–13,** *No. 4, 363–376 (Aug. 1964).*
This paper considers a class of information sources consisting of text and pictures. The text is English language text appearing in scientific and technical documents. The picture sources are the largely schematic pictures that occur in the same class of documents. However, the discussion is broadened slightly to include other picture sources. For a tiny fragment of English, the paper shows how the syntactic structure of text may be described, and then goes on to suggest that a similar analysis may be performed on the class of pictures under study. The description of these two kinds of information sources with a single class of descriptive techniques is suggested as an alternative to the synthetic approach in which artificial languages are specified and then learned and used. The major reason discussed here for doing syntactical analysis of such sources is that several informa-

tion processing operations, amounting to the interpretation of the information sources looked upon as languages, can be done by the technique of syntax direction which uses the results of syntactic analysis to mediate subsequent processes for manipulating the information tokens. The paper concludes with an illustration of an algorithm for matching the sentences given by a simple grammar against the class of simple pictures which these sentences purport to describe.

Methods of calibration of airglow photometers at Fritz Peak Observatory, L. L. Smith and R. B. Alexander, *IQSY Instruction Manual No. 5: Airglow, pt. II, pp. 25–36* (*IQSY Secretariat, London, England, 1963*).
The problems of establishing low-intensity standard sources for calibrating airglow photometers are discussed; particular attention is paid to a radioactivated phosphor source which has desirable characteristics as a field standard. Attention is called to the necessity of adequate control of the transmission of any interference filters and the spectral response of any photomultipliers used in such photometers.

Ozonation of asphalt flux, P. G. Campbell and J. R. Wright, *I. & E. C. Prod. Res. and Devel.* **3,** *186–194* (*Sept. 1964*).
The effects of ozone on the oxidation of asphalt flux were compared to those of air and of oxygen. Oxidative changes were measured by infrared spectroscopy, increases in softening point, and elemental analysis.
In the oxidation of one flux of Southeastern U.S.A. origin, ozone enrichment of air reduced the time required to reach a given softening point to one-half that needed for air alone. Ozone-enriched oxygen reduced this time to one-sixth that needed for air. Reaction temperatures did not exceed 158 °C, approximately one-half those used in commercial air-oxidation; gas flow rates were about one-fourth the commercial rate. Coating-grade asphalts produced under these mild conditions were more stable to photooxidation than was a commercial asphalt from the same flux. Similar results were obtained with a California-Coastal asphalt flux.
Ozonation of a ferric chloride-catalyzed flux of California Coastal origin produced different results in that no oxidative changes could be detected in the residual hardened asphalt; the rate of hardening, however, was increased over that of other oxidants. Possible reactions explaining the role of $FeCl_3$ are presented.

On the validity of the Einstein-Smoluchowski theory light scattering, R. Zwanzig, *J. Am. Chem. Soc.* **86,** *3489–3493* (*Mar. 30, 1964*).
The molecular basis of the Einstein-Smoluchowski macroscopic theory of light scattering is investigated, using a generalization of Frohlich's theory of dielectrics. The macroscopic and molecular theories differ by an experimentally negligible quantity, associated with the electric field dependence of the dielectric constant. A slight depolarization, not accounted for by the macroscopic theory, is associated with the same quantity. Because of the method of derivation, the results obtained here are valid only in the limit of long wavelength and low frequency.

Pulsed and CW sinusoidal voltage and current measurements, M. C. Selby, *Proc. URSI XIVth General Assembly, Tokyo, Japan, Sept. 1963,* **XIII,** *92–100* (*1964*).
A Triannual progress review on the art of measuring single frequency and wideband voltages and currents in the USA is presented for the URSI. This is the first report on these quantities in the series of URSI, Commission I reports and covers the approximate period of 1960–1962. Present day significant applications, parameters and ranges of pulsed voltages and currents are briefly pointed out. Only the relatively more important publications are indicated and the more outstanding contributions commented on at some length.

Thermodynamic data compilation and review at the National Bureau of Standards, G. T. Armstrong, *Svensk Kem. Tidskr.* **76,** *No. 8, 419–427* (*1964*).
Three examples of activities at the National Bureau of Standards involving compilation and critical review of thermodynamic data are described in some detail: (1) Selected values of chemical thermodynamic properties, (2) phase diagrams for ceramists, (3) thermodynamic properties of a selected group of light elements. The type of literature search, the scope of substances covered, the types of data gathered, the method of review and the manner of publication are described. A brief description is given of plans for the new Standard Reference Data Program at the National Bureau of Standards.

Propagation of a reflected shock wave in a transverse magnetic field, Y. Boublil and K. B. Earnshaw, *Phys. Fluids* **7,** *No. 6, 876–881* (*June 1964*).
Shock waves are reflected from a wall in the presence of a transverse magnetic field. The gas is highly ionized and therefore the lines of force can be considered "frozen in." In such a case the magnetic field is compressed and the Rankine-Hugoniot relations, including magnetic pressure and magnetic energy as given by de Hoffmann and Teller, are used. The magnetic probes show an increase of the magnetic field behind the reflected shock, and the velocity of the reflected shock waves (measured from streak camera photographs) increases with increasing fields. For a constant incident velocity, the dependence of the reflected shock velocity on the magnetic field is given by a linear function: $U_r^2 = a + bB^2$ where a and b are constant in a first approximation. This law has been verified by experimental results.

Refractivities of the rare earth oxides, E. M. Levin (*Proc. Third Rare Earth Research Conf., Apr. 2–24, 1963*), *Book, Rare Earth Research, Chapter on Magnetic and Optical Studies, pp. 339–350* (*Gordon and Breach, Science Publ., Inc., New York, N.Y., May 1964*).
Index of refraction and density data obtained for a number of rare earth borates (ABO_3) and aluminates and gallates ($A_3B_5O_{12}$) permitted the calculation of the specific refractivities (by the Gladstone and Dale formula) of the rare earth sesquioxides. This was done using the additive rule between the products of the specific refractivities and the weight fractions of the constituent oxides. The specific refractivity values decreased with decreasing ionic radius of the cation, ranging from 0.148 for La_2O_3 to 0.107 for Dy_2O_3 to 0.090 for Lu_2O_3, and include the lowest values ever reported for oxides. Specific refractivities and molar refractivities (Lorentz-Lorentz formula) were calculated also from data on crystal fragments of the cubic rare earth oxides, obtained from two sources. Specific refractivities decreased from a value of 0.120 for Dy_2O_3 to 0.099 for Lu_2O_3, and were 10 to 13% higher than those calculated from the binary oxide compounds. Molar refractivities (Lorentz-Lorentz) of the pure oxides varied from 22.5 for Dy_2O_3 to 20.2 for Lu_2O_3 and were in good agreement with reported data.

Analysis of a differential phase shifter, D. A. Ellerbruch, *IEEE Trans. Microwave Theory Tech.* **MTT–12,** *No. 4, 453–459* (*July 1964*).
This paper presents the theory and analysis of a ganged pair of "line stretcher" microwave phase shifters. The error analysis shows that some of the errors inherent in a single phase shifter of this type can be reduced through the use of a differential system; however, the magnitudes of other errors may more than offset the reduction. Graphical data are included to facilitate the rapid determination of the limit of error for any specified angle measurement.

Comparison calibration of inductive voltage dividers, R. V. Lisle and T. L. Zapf, *ISA Trans.* **3,** *No. 3, 238–242* (*July 1964*).
Calibrated inductive voltage dividers serve as excellent standards of voltage ratio for use in the comparison calibration of other a-c voltage dividers. Differences in phase angles in the dividers can be accommodated by the production of a voltage in the detector circuit in quadrature with the reference voltage. The paper discusses the comparison circuit, the handling of stray impedances, guarding, measurement procedures, quadrature voltage production, and errors. The comparison method described can be used in standardizing laboratories for the calibration of inductive voltage dividers and other voltage ratio equipment.

Heater lead problem in calorimetry, D. C. Ginnings and E. D. West, *Rev. Sci. Instr.* **35,** *No. 8, 965–967 (Aug. 1964).*
A study has been made of possible calorimetric errors resulting from the use of potential leads at the mid points of current lead segments between a calorimeter and its surrounding shield. With simple assumptions believed justified in most calorimetry, there is derived a mathematical solution for this error in the case where the calorimeter and shield are at different temperatures and there are different thermal contacts between the current lead and the calorimeter and shield. It is concluded that when accuracies of better than 0.1% are desired, careful consideration should be given to heater lead design.

Aspects of the National Bureau of Standards instrumentation literature reference file, J. F. Mayo-Wells (*ISA 19th Annual Conf. and Exhibit, New York, N.Y., Oct. 12–15, 1964*), *ISA Preprint 20.6–5–64 (1964).*
The Instrumentation Literature Reference File and the associated Peek-a-Boo retrieval system of the National Bureau of Standards Instrumentation Division are briefly described. Some capabilities of multi-aspect indexing which extend beyond those of classical indexing are discussed, as are advantages of the so-called inverted file. For instrumentation information and related questions, the NBS Instrumentation File activity is seen as a means of access to the Bureau as a whole, which may in itself be regarded as a measurements information center of particular interest to other standards laboratories. Various NBS publications series are described.

Versatile Stark waveguide for microwave spectroscopy, D. R. Lide, Jr., *Rev. Sci. Instr.* **35,** *No. 9, 1226 (Sept. 1964).*
A simple waveguide design for Stark-modulation microwave spectrometers is described. The guide provides a homogeneous Stark field which is perpendicular to the microwave electric field. The design has been used successfully in spectrometers operating at high frequencies, high temperatures, and for other special purposes.

Behavior of coaxial cable connectors for pulses with nanosecond risetimes, R. B. Schwartz and A. C. B. Richardson, *Nuclear Instr. Methods* **29,** 83–88 (*North-Holland Publ. Co., Amsterdam, The Netherlands, 1964*).
Reflections and risetime distortion caused by connector mismatches were measured for several common cable-connector combinations, using a fast pulser and sampling oscilloscope (system risetime=0.4 nsec). It was found that excellent connectors are available for 125Ω (RG 63/U) cable, as well as for 50Ω cables. In addition, details are given for the construction of a connector which may be used with 185Ω (RG 114/U) cable. Measurements are also reported for 125Ω attenuators and a 125Ω pulse inverting transformer.

Theory of boil-off calorimetry, R. B. Jacobs, *Rev. Sci. Instr.* **35,** *No. 7, 828–832 (July 1964).*
The usual formulation used to compute heat flow in boil-off calorimetry ignores the sensible heating of the vapor in the calorimeter. A formulation which includes this heating is derived; a single temperature measurement (of the vapor leaving the calorimeter) permits this effect to be computed. As the required temperature measurement has not been given for reported experiments, the vapor heating effect cannot be computed directly for those cases. Therefore, an expression for the computation of this temperature is derived theoretically and applied to reported experiments. It is shown that, even in optimally designed calorimeters, the sensible heating of the vapor can be appreciable, and that the use of the usual formulation can introduce significant error in the computed heat flow. Finally, it is indicated how this error can explain, at least partially, the Heat Paradox which has been observed in insulation and Dewar evaluation tests.

"Thumbtack" accelerometer for the 1.5–150 kc range, P. Hertelendy and P. Reynard, *Rev. Sci. Instr.* **35,** *No. 10, 1305–1306 (Oct. 1964).*
A special purpose mechanical vibration detector using a piezoelectric sensing element is described. Also, one application, a method of calibration, and some limitations of the device are discussed. Its chief merits are (1) low impedance, (2) a nearly point contact, and (3) low transverse-to-longitudinal sensitivity.

Microwave spectroscopy, D. R. Lide, Jr., *Annual Rev. of Phy. Chem.* **15,** *225–250 (1964).*
This article is a critical review of research in microwave spectroscopy of gasses during the past several years. The major topics covered are accurate structure determinations, structures of new or unusual molecules, internal rotation, vibrational information, high temperature spectroscopy, and instrumentation. A bibliography of the most important publications is included.

The application of Archimedes' principle to determination of the apparent volume of leather, J. R. Kanagy, *J. Am. Leather Chem. Assoc.* **LIX,** *No. 11, 636–649 (Nov. 1964).*
Studies were made of the volume changes occurring when acetone-dehydrated hide, chrome-retanned leather, vegetable-tanned strap leather, and chrome-retanned packing leathers were immersed in water, hydrocarbon solvent, 6*M* lithium bromide, and 8*M* urea. None of these samples showed any volume changes in hydrocarbon solvent. All of the samples swelled considerably in water. All except vegetable-tanned strap leather showed shrinkage in 6*M* lithium bromide, and all showed some swelling in 8*M* urea.
Determinations of volume were made on specimens of hide and leather by immersing them in water after treatment with paraffin oil or dibutyl phthalate to fill the pores. These values were compared to values obtained for volumes by immersion in hydrocarbon solvent and by measurement of the dimensions of the specimens. The buoyancy methods were found to be quick, simple, and accurate procedures for determining volumes. Determinations in hydrocarbon solvent were found to average consistently approximately 0.8% higher than those obtained by filling the pores and immersing in water.

Spectral tristimulus values for the CIE (u, v, w) uniform spacing system, I. Nimeroff, *J. Opt. Soc. Am. Letter to Editor* **54,** *No. 11, 1365–1367 (Nov. 1964).*
The CIE uniform chromaticity space, u, v, w, developed by MacAdam and adopted in 1959, is known only by its chromaticity transformations. The spacing should be known by its spectral tristimulus values as well if it is to be of greatest use in colorimetry. The set of trisimulus values, $\bar{u}_\lambda$, $\bar{v}_\lambda$, $\bar{w}_\lambda$, is found to have two bimodal functions, $\bar{u}_\lambda$ and $\bar{w}_\lambda$. As the CIE recommends, since 1963, the use of a 10° observer system as well as the 1931, 2° system, spectral tristimulus values are given for both systems. Also reported are the chromaticity coordinates of several standard sources, the locus of Planckian radiators, and the spectrum locus.

Change in the heat capacity of boron trioxide during the glass transformation, S. S. Chang and A. B. Bestul, *J. Phys. Chem.* **68,** *3082 (1964).*
A previous compilation showed that for B_2O_3 the change in heat capacity during the glass transformation, Δc_p, is only about one fifth of the "universal" value which applies to most glass-forming substances. A computational error has been found in the value for B_2O_3 in the above-mentioned compilation. The correct value of Δc_p for B_2O_3 is 2.65 cal. deg.$^{-1}$ per "bead", which agrees very well with Wunderlich's "universal" Δc_p value of 2.7 ± 0.5 cal. deg.$^{-1}$. Thus B_2O_3 in fact behaves like other glass-forming substances in this respect, rather than being exceptional.

Electrochemical calorimetry III. Thermal effects of nickel-cadmium batteries, W. H. Metzger, Jr., and J. M. Sherfey, *Electrochem. Technology* **2,** *No. 9–10, 285–289 (Sept.–Oct. 1964).*
This paper reports some interesting sidelights obtained while making calorimetric measurements during various charges discharge cycles of nickel-cadmium cells proposed as satellite power sources by the National Aeronautics and Space Administration (NASA). Typical curves of heat changes as a function of time during operation are shown and discussed. The heat of reaction of oxygen with the constituents of the cell was measured and close agreement was obtained with the literature value for the heat of formation of cadmium oxide.

Electrochemical calorimetry IV. Measurement of the Peltier heat and voltage attending the passage of current across a liquid junction, A. Brenner and S. L. Gray, *J. Electrochem. Soc.* **111**, *No. 11, 1225–1230 (Nov. 1964).*
The experiments involved the measurement of the temperature change resulting from the passage of current across the interface of two electrolytes. Measurements were made at various distances from the junction so as to yield a temperature profile of the effect. The total heat effect was calculated from the integrated area under the curve of temperature profile. The coefficient obtained by dividing the total heat effect in joules by the current in coulombs was reported as a voltage equivalent.
The following values were obtained for three systems of electrolytes and are probably correct to within about 7 mv:

0.04 *M* hydrochloric acid and 0.4 *M* hydrochloric acid, 30 mv.
0.90 *M* hydrochloric acid and 3.0 *M* potassium chloride, 80 mv.
1.15 *M* hydrochloric acid and 1.21 *M* lithium chloride, 80 mv.

A hypothesis was advanced to relate the voltage equivalent of the heat effects to the diffusion liquid junction potentials and to the Peltier effect.

The National Bureau of Standards tritiated water standards, W. B. Mann, *J. Appl. Rad. and Isotopes* **15**, *628, Pergamon Press Ltd. (1964).*
This letter notes the very close agreement obtained by Euratom and the National Bureau of Standards in their calibration, by gas counting, of the National Bureau of Standards tritiated water standard.

Microwave and High-Frequency Calibration Services of the National Bureau of Standards, W. E. Larson, *IEEE Trans. Microwave Theory Tech.* **MTT-12**, *No. 4, 480–482 (July 1964).*
This is the second of a series on Microwave and High Frequency Calibration Services available at the National Bureau of Standards Boulder Laboratories, Boulder, Colorado. The quantities, attenuation, and field strength are described.

Diffusion in a polymer with lamellar morphology, polyethylene, R. K. Eby, *J. Appl. Phys.* **35**, *No. 9, 2720–2724 (Sept. 1964).*
Data for the diffusion of ethane in polyethylene are presented together with the results of optical microscopy and of large- and small-angle x-ray diffraction for the same samples. The orientation of the lamella boundaries with respect to the concentration gradient of the diffusing molecules is important in determining the diffusion rate. In unoriented, as-crystallized polymers, the diffusion constant varies inversely with the lamella thickness. The results support the concept of lamella boundary diffusion. Lamella perfection is also important. In both oriented and unoriented polymers, the solubility constant apparently varies inversely with the lamella thickness, suggesting absorption in the lamella boundaries.

Determination of the propagation constant for ultrasonic waves in melting and molten polyethylene, R. K. Eby, *J. Acoust. Soc. Am.* **36**, *No. 8, 1485–1487 (Aug. 1964).*
An extension of McSkimin's technique to polymer melts and soft amorphous polymers is reported. For 12 Mc longitudinal waves, the modulus and internal friction are presented for the melting, supercooling, and annealing or recrystallization of polyethylene. Maxima of internal friction are observed in the solid at −52°, +60°, and between 100° and 130°C. The last, which is associated with the presence of crystals, decreases sharply near the melting temperature and is not present in the supercooled melt. In the melt, the internal friction exhibits a low, nearly constant value between 140° and 290°C. In this range the ratio of the thermal coefficient of velocity change to the thermal coefficient of volume expansion is −2.6. Above 300°C, there is a decrease of modulus and increase of internal friction believed to be associated with thermal degradation of the polymer.

Lasers for length measurement, A. G. McNish, *Science* **146**, *No. 3541, 177–182 (Oct. 1964).*
CW lasers will find extensive use in length measurement because of the high coherence and intensity of the light they produce.

Nonspattering solder flux, W. R. Bjorklund, *Rev. Sci. Instr.* **35**, *No. 10, 1369–1370 (Oct. 1964).*
This article gives uses, methods of preparation and advantages of a polyethylene glycol soldering flux.

Simple arc devices for spectral excitation in controlled atmospheres, M. Margoshes and B. F. Scribner, *Appl. Spectry.* **18**, *No. 5, 154–155 (1964).*
A gas-sheathed arc is described for the excitation of spectra of solid materials in an atmosphere of any desired composition without the disadvantages associated with the chambers usually employed for this purpose. The atmosphere is controlled by enclosing the electrodes and the excitation zone in a tubular flow of gas which effectively excludes air. The sample is held in an anode cap electrode which can be changed rapidly between exposures. The arc may be ignited within a few seconds after the flow of gas is started. The tubular flow of gas also stabilizes the arc to a marked degree.

Making precision measurements of zener diode voltages, W. G. Eicke, Jr., *IEEE Trans. Commun. Elec.* **83**, *No. 74, 433–438 (Sept. 1964).*
The problems of making precise measurements of zener diode voltages are reviewed and discussed. Power supplies for the zener diode, measurement of the diode current, grounding of the circuit, shielding, mounting of the diode, and temperature control of the diode are discussed as they affect the measurement of the diode voltage. Equations are given that relate variations in diode voltage to variations in supply voltage and other parameters that affect the diode voltage. Three general classifications of methods for measuring diode voltages are defined. Specific techniques using equipment available in standards laboratories are described and equations for calculating the zener voltage and variation of zener voltage with variations in circuit parameters are given.

Ethylene-propylene copolymers: crystallinity, infrared and creep studies, F. J. Linnig, E. J. Parks, and L. A. Wood, *J. Appl. Polymer Sci.* **8**, *2645–2651 (1964).*
Density, infrared, and creep studies have been made of ethylene-propylene copolymers containing up to about 50 mole % propylene and their homopolymers. The degree of crystallinity (volume fraction of polyethylene crystals), as measured by density and X-ray studies, decreases with increased propylene content. This change is also reflected in the intensity of the 13.7 μ band in the infrared spectra of the polymers. The measured amount of unsaturation (0.1–0.2%) in the copolymers is too small to account for the presence of several infrared bands which are often attributed to unsaturation. An unsaturation of 0.90% was obtained for a terpolymer where the third component was unsaturated. Indentation-creep studies showed the creep to be nearly proportional to the logarithm of time with a slope of 10% creep per decade for 0.1 to 10 minutes. Compliance-temperature graphs were found to be quite similar to those for the styrene-butadiene rubber SBR 1500.

The accurate measurement of voltage ratios of inductive voltage dividers, *Acta IMEKO, pp. 317–331 (1964).* Several methods have been developed at the National Bureau of Standards for the very accurate measurement of audio frequency voltage ratios associated with inductive voltage dividers. Uncertainties in voltage ratio of less than 2×10^{-7} have been obtained in measurements with transformer-type capacitance bridges. The attainment of such accuracy has provided a firm base for further investigations on inductive voltage dividers. An inherent major error arises from the interaction between distributed shunt impedances and leakage impedances in the windings. In specific designs of inductive voltage dividers the relative magnitudes of such errors are calculable and are characteristic of the design. A divider may be completely characterized by the designation of the

characteristic relative errors combined with an absolute measurement. A method involving complementary measurements has been developed to yield an absolute measurement of the in-phase and quadrature components of the voltage ratio characteristic. Single-decade inductive voltage dividers have been constructed with ratio magnitude characteristics and residual errors less than 5×10^{-8}. This recent work has verified the accuracy of measurements made by other methods.

Sampling and statistical design, W. J. Youden (*Proc. Symp. Environmental Measurements, Cincinnati, Ohio, Sept. 4, 1964), Public Health Service No. 999–AP–15, pp. 35–39 (July 1964).*
A sampling scheme specifies the type of sample as well as the number and location of the samples. The placement of the samples depends on the region of interest. The type of sample depends on the accuracy or cost of the analytical work. Composite samples may be used to conserve analytical effort. Alternatively, if the analytical errors are large, each sample should be large enough to permit multiple determinations. In any event the sampling scheme should be well adapted to statistical evaluation. For example, in order to detect trends in time or distance it is well to arrange for pairs of samples as follows:

. . . . . etc.

The paired dots represent samples taken at nearly the same time, or place, and the separation of the pairs corresponds to intervals in time or location. The ability to demonstrate heterogeneity in the region (temporal, spatial, or both) depends upon the agreement of adjacent samples. The pairs are not necessarily arranged in a straight line. Other arrangements will be discussed in detail.

The needs of the statistical engineering programs of the National Bureau of Standards, C. Eisenhart, *Proc. 9th Conf. Design of Experiments in Army Research Development and Testing, Directorate of Research and Development, U.S. Army Missile Command, Redstone Arsenal, Ala., Oct. 23–25, 1963, ARO–D Report 64–2 (1964).*
The Statistical Engineering Laboratory of the Applied Mathematics Division is the largest of the three statistical engineering groups of the National Bureau of Standards. The staffing needs and recruitment difficulties of the Statistical Engineering Laboratory are, it is believed, symptomatic of the problems faced by many statistical advisory and consulting groups in Government laboratories. It is pointed out that these recruitment difficulties stem in large part from the strong emphasis on theory and comparative neglect of applications in many undergraduate and postgraduate courses in mathematical statistics in the U.S.A., and from the absence in American colleges and universities of undergraduate programs leading to a bachelor's degree in Statistics. The present recruitment problems of statistical engineering programs in Government laboratories are much as would be those of the corresponding physics programs if the only available physicists were MA's and PhD's in Theoretical Physics.

Studies on the tungsten-rhenium thermocouple to 2000 °C, D. B. Thomas, *Proc. 18th Annual ISA Conf. and Exhibit, Sept. 9–12, 1963, Chicago, Ill., Preprint 57.3.63, pp. 57.3.63–1—57.3.63–9 (1963).*
Various lots of tungsten and rhenium wire were obtained from leading American manufacturers. Eleven tungsten-rhenium thermocouples were fabricated from these wire lots and tested at approximately 100 degree intervals up to 2000 °C. Two polynomial equations were derived to represent the average emf of the test thermocouples. Tables of temperatures versus emf are presented in 5 degree C intervals from 0 to 2000 °C and in 10 °F intervals from 32 to 3640 °F. Spectrochemical analyses of the tungsten and rhenium elements used in this study are listed. A graphic comparison is made between the NBS emf values and values by other investigators.

Modulus of rupture of glass in relation to fracture pattern, M. J. Kerper and T. G. Scuderi, *Am. Ceramic Soc. Bull.* **43,** *No. 9, 622–625 (Sept. 7, 1964).*
Glass which is broken in flexure shows a fracture face which normally consists in part of a smooth area which includes the fracture origin. The area of this smooth portion or "mirror" bears a relationship to the magnitude of the stress causing rupture. This relationship has been studied for eight different glasses tested under a variety of conditions. It was observed that the conditions of the glass surface, the test temperature, difference in exposure time to test temperature, and the rate of loading, all had an effect on the strength of glass but did not affect the relationship between modulus of rupture and the mirror size. The composition did, however, affect this relationship. This relationship is generally expressed as a power function where the modulus of rupture times the radius of the mirror to the one-half power is equal to a constant. This expression is not, however, valid for the full range of the data.

Effect of particle shape and size distribution in a reinforced polymer, R. L. Bowen, *J. Am. Dental Assoc.* **69,** *481–495 (Oct. 1964).*
Vinylsilane-treated silica-glass powders, bonded together with a self-curing monomer system, gave composites that could be used to restore anterior teeth. Spherical reinforcement particles required six to eight percent less resin (by volume) as a binder than did irregular-shaped particles. Intermittent or gap grading in the size distribution (three parts of fine combined with seven parts of coarse particles, medium sizes being omitted) eliminated an additional six to eight volume percent of the resin binder. Such a bimodal size distribution of spherical particles required only 13 percent resin (24 volume percent); this composite had a relatively low coefficient of thermal expansion and a high modulus of elasticity. The feasibility of using such composites (with reduced resin content) for dental restorations was supported, but the use of smaller particles was indicated.
The shear strength of human dentin was measured, using a punch test on transverse sections of tooth specimens. The average shear strength was about 14,000 pounds per square inch.

Free-field correction for condenser microphones, W. Koidan and D. S. Siegel, *J. Acoust. Soc. Am.* **36,** *No. 11, 2233–2234 (Nov. 1964).*
Differences in the free-field corrections of one-inch condenser microphones, caused by their different acoustic driving-point impedances, were found to be of sufficient magnitude to warrant a cautious approach to the determination of the free-field response level from measurements of the pressure response level and the addition of a "standard" free-field correction.

A magnetic fixed point for thermometry below 1 °K, J. C. Eisenstein, R. P. Hudson, and B. W. Mangum, *Appl. Phys. Letters 5, No. 11, 231 (Dec. 1, 1964).*
It is suggested that a peak in the magnetic susceptibility of $CeCl_3$ at 0.345 °K would be useful as a thermometric fixed point.

Some activities of the cooperative dental research between the Federal Government and the American Dental Association at the National Bureau of Standards, G. C. Paffenbarger, *Ann. Dentistry* **XIII,** *No. 4, 111–126 (Dec. 1964).*
Some aspects of the cooperative dental research between the Federal Government and the American Dental Association conducted at the National Bureau of Standards include (1) the necessary research and testing to formulate specifications for dental materials, (2) the establishment of a List of Certified Dental Materials by the Association, (3) the development of diagnostic instruments, (4) the production of motion pictures depicting how the research findings may be applied in practice, (5) the determination of physical and chemical properties of dental materials and the hard tooth tissues, (6) the development of new, and improvements in old, materials, and (7) establishment of the validity of some laboratory findings. Examples in each category are presented.

Studies of the thicknesses of adsorbed glass finished by ellipsometry, D. J. Tutas, R. R. Stromberg, and E. Passaglia, *SPE Trans.* **4,** *No. 4, 1–7 (Oct. 1964).*

The thickness of the adsorbed layer of two glass finishes, vinyl *tris*(2-methoxyethoxy)silane and gamma aminopropyltriethoxysilane, was measured by ellipsometry. The vinyl silane was adsorbed on glass from solutions in water and in methyl ethyl ketone. The adsorption from water resulted in a film initially at least 50 Å thick, which increased in thickness with time. Adsorption from methyl ethyl ketone solution resulted in a film of about 10 Å. The amino silane was adsorbed on glass and on chrome from solutions in water. Adsorption on glass resulted in a film at least 60 Å in thickness, which remained constant over a period of about 5 hours. Adsorption on chrome resulted in a film about 10 Å in thickness. From the results it appears that a polymer, rather than the small molecules of glass finish, are adsorbed from the water solution on glass and that small unpolymerized "finish" molecules are adsorbed from the methyl ethyl ketone solution.

Influence of radiant energy sources on bitumen oxidation, K. G. Martin, *J. Appl. Chem.* **14,** *No. 11, 514 (1964).*
Using the steady change in infrared absorption of the carbonyl functional groups of asphalt with increase of radiant energy flux, the oxidation rates of four air-blown asphalts of coating grade have been obtained for the three sources of radiation, carbon arc, xenon arc, and sunlight. Differences in the pattern of oxidation for the much used carbon arc compared to both xenon-arc and solar irradiation were found, whereas the latter two sources induced nearly identical behaviour in the asphalts. Continuous measurement of the intensity of the solar radiation by pyroheliometry has indicated that the asphalt oxidation rates are directly proportional to intensity, sensitive to very low intensities and independent of diurnal changes. Potassium ferrioxalate dosimetry has shown that the intensity of the xenon-arc irradiation as used in a weatherometer simulated that of summer sunshine extremely well, whereas the carbon-arc irradiation as used in the ASTM method of evaluating weatherometer durability of asphalts had a fivefold greater intensity. This increased intensity changed the pattern of rate of asphalt oxidation rather than simply accelerating the steady-state oxidation rates.

Which measure of precision? The evaluation of the precision of analytical methods involving linear calibration curves, F. J. Linnig and J. Mandel, *Anal. Chem.* **36,** *No. 13, 25A–32A (Dec. 1964).*
Three sources of error can affect the precision of an analytical procedure involving calibration lines: (1) variability among replicates, (2) scatter about the calibration line, and (3) uncertainty of the calibration line. In many cases, the first of these is small in comparison with the other two; yet, it is often used as *the* measure of the precision of the analytical method. A detailed analysis is given of the three sources of error, and methods of calculation are presented for the segregation of these errors on the basis of a calibration experiment.

Other NBS Publications

Journal of Research 69A (Phys. and Chem.), No. 2 (Mar.–Apr. 1965), 70 cents.
Radiolysis of $N^{15}N^{14}O$. R. Gorden, Jr., and P. Ausloos.
Oscillator strengths for lines of Ni I. C. H. Corliss.
More wavelengths from thorium lamps. W. F. Meggers and R. W. Stanley. (See above abstracts).
Phase equilibria in the system vanadium oxide–niobium oxide. J. L. Waring and R. S. Roth.
Thermodynamics of the ternary system: water-glycine-potassium chloride at 25 °C from vapor pressure measurements. V. E. Bower and R. A. Robinson.
Heat of formation of aluminum fluoride by direct combination of the elements. E. S. Domalski and G. T. Armstrong.
Relative enthalpy of polytetrafluoroethylene from 0 to 440 °C. T. B. Douglas and A. W. Harman.
Anionic polymerization of isoprene at low concentrations of polyisoprenyllithium. L. J. Fetters.
One particle transitions and correlation in quantum mechanics. A. R. Ruffa.
Disaccommodation of magnetic spectra of two manganese zinc ferrites. A. L. Rasmussen.
Splitting of a set of equivalent sites in centrosymmetric space groups into subsets under homogeneous stress. J. B. Wachtman, Jr., and H. S. Peiser. (See above abstracts.)

Radio Sci. J. Res. NBS/USNC–URSI 69D, No. 2 (Feb. 1965), $1.00.
Electromagnetic wave penetration of reentry plasma sheaths. M. P. Bachynski.
On the use of refractive index diagrams for source-excited anisotropic regions. L. B. Felsen.
Surface waves along a perfectly conducting plane covered with semi-infinite magneto-plasma. S. Adachi and Y. Mushiake.
On the point of emergence of a microwave beam entering a linearly graded plasma. A. L. Cullen.
Self and mutual admittances of waveguides radiating into plasma layers. J. Galejs. (See above abstracts.)
Effect of electron collisions on the formulas of magneto-ionic theory. K. G. Budden.
Momentum transfer collisions in oxygen for thermal electrons. M. H. Mentzoni.
Experimental studies of perturbations in ionospheric plasma. L. H. Heisler.
Electromagnetic scattering by gyrotropic cylinders with axial magnetic fields. W. C. Y. Lee, L. Peters, Jr., and C. H. Walter.
Radar cross sections of plasma bodies at the plasma frequency. L. Peters, Jr.
Electroacoustic waves excited by a space vehicle in ionized atmosphere and its effect on radar return. K.-M. Chen. (See above abstracts.)
Discussion on basic equations with source terms in compressive plasmas. K.-M. Chen.
Scattering of electromagnetic and electroacoustic waves by a cylindrical object in a compressible plasma. J. R. Wait.
Multiphase periodic very-low-frequency emissions. N. Brice.
Radio studies of the high-latitude ionosphere during the solar eclipse of 20 July 1963. R. D. Hunsucker.
VLF and LF fields propagating near and into a rough sea. R. M. Lerner and J. Max.
Insulated and loaded loop antenna immersed in a conducting medium. R. H. Williams. (See above abstracts.)
Capacitance of biconical antennas in magneto-ionic media; elliptic cone capacitance. V. P. Pyati and H. Weil.
Calculations of the bistatic scattering cross section of a sphere with an impedance boundary condition. J. R. Wait and C. M. Jackson.
Concept of differential reflectivity as applied to the reflection of beam-limited radiation by a convex body. A. Erteza, J. A. Doran, and D. H. Lenhert.

Radio Sci. J. Res. NBS/USNC–URSI 69D, No. 3 (Mar. 1965), $1.00.
Propagation in nonuniform gyrotropic media. S. H. Gross and L. B. Felsen.
Geometrical optics for gyrotropic bodies. W. C. Y. Lee, L. Peters, Jr., and C. H. Walter.
Attenuation of hydromagnetic waves in the ionosphere. S. I. Akasofu.
Self distortion of radio signals in the *D* region. L. R. Megill.
Atmospheric gravity waves: a new toy for the wave theorist. C. O. Hines.
Electromagnetic fluctuations in an equilibrium plasma. R. E. Burgess.
A generalized hydromagnetic wave in an inhomogeneous, cylindrical plasma. C. K. McLane and T. Tsukishima.
Angular dependence of the refractive index in the ionosphere. G. A. Deschamps.
Electrodynamics of moving anisotropic media: the first-order theory. C. T. Tai.
Study of the phenomenon of whistler echoes. T. Laaspere, W. C. Johnson, and J. F. Walkup.
Multiple-frequency investigations of radio wave absorption during the dawn-breakup phase of auroras. R. Parthasarathy, and F. T. Berkey.
Sferic excitation of a two-layer conducting medium. M. B. Kraichman.

Currents, charges, and near fields of cylindrical antennas. R. W. P. King and T. T. Wu.

A note on the radiation conductance of an axial slot on a cylinder. C. M. Knop and C. T. Swift.

Analytical formulas for radio paths in spherically stratified ionospheres. E. Woyk (Chvojkova).

Radio Sci. J. Res. NBS/USNC–URSI 69D, No. 4 (Apr. 1965), $1.00.

Waves in Plasma Papers

Dispersion of waves in a cold magneto-plasma from hydromagnetic to whistler frequencies. H. G. Booker and R. B. Dyce.

Study on the guiding mechanism of whistler radio waves. S. Adachi.

Electromagnetic waves along an infinitely long and thin conducting wire in a magneto-ionic medium. Y. Mushiake. (See above abstracts.)

Use of the phase-integral method to determine the reflection properties of a stratified ionosphere. C. Altman.

E-mode propagation in a plane-stratified plasma. P. Hirsch and J. Shmoys.

Radiation from an infinite axial slot on a circular cylinder clad with magnetoplasma. P. de Marchin and G. Tyras.

Index of refraction surfaces for plasma waves. T. Yeh and M. H. Cohen.

Impedance of a short dipole in a compressible plasma. K. G. Balmain.

Waves circulating around a rigid cylindrical obstacle in a compressible plasma. J. R. Wait.

Wave propagation in a two component warm plasma. S. R. Seshadri.

Harmonic currents excited by an electromagnetic wave in a plasma. L. Wetzel and T. W. Tang.

Excitation of acoustic waves in plasmas. W. A. Saxton. (See above abstracts.)

Wave interaction in oxygen magneto plasmas. K. V. Narasinga Rao.

Regular Contributions

Test of the constancy of the velocity of electromagnetic radiation in high vacuum. P. Beckmann and P. Mandics. (See above abstracts).

Signal degeneration in laser beams propagated through a turbulent atmosphere. P. Beckmann. (See above abstracts).

High frequency backscatter from the earth measured at 1000 km altitude. R. C. Chia, A. K. Fung, and R. K. Moore.

Observation of NPG VLF transmissions at Tracy, California during path equinox. G. B. Carpenter and A. L. Whitson.

Small magnetic toroid antenna imbedded in a highly conducting half space. G. R. Swain.

Radio Sci. J. Res. NBS/USNC–URSI 69D, No. 5 (May 1965), $1.00.

Preface to fourth of "Waves in Plasma" papers. J. R. Wait.

On electromagnetic radiation from a magnetic dipole with arbitrary orientation embedded in a lossless magneto-ionic medium. H. Motz.

A systematic study of the radiation patterns of a dipole in magnetoplasma based on a classification of the associated dispersion surfaces. R. Mittra and G. L. Duff.

Propagation of vertically polarized electromagnetic waves in a horizontally stratified magnetoplasma. R. Burman and R. N. Gould.

A note concerning the reflection of waves in inhomogeneous layers with asymmetric profiles. R. Burman.

On the terrestrial propagation of ELF and VLF waves in the presence of a radial magnetic field. J. Galejs.

Electron density profiles in cylindrical plasmas from microwave refraction data. B. A. Aničin.

Study of the waves supported by a warm plasma slab. P. R. Caron.

Transmission and reflection of electromagnetic waves by a hot plasma. E. C. Taylor.

Radiation from electrons in a magnetoplasma. H. B. Liemohn.

Radiation from a uniformly moving charge in an anisotropic, two component plasma. S. R. Seshadri and H. S. Tuan.

Microwave spectral tables line strengths of asymmetric rotors, P. F. Wacker and M. R. Pratto, NBS Mono. 70, Vol. II (Dec. 15, 1964), $3.00.

On the statistical theory of electromagnetic waves in a fluctuating medium (II). Mathematical basis of the analogies to quantum field theory, K. Furutsu, NBS Mono. 79 (Dec. 7, 1964), 35 cents.

A complete mode sum for LF, VLF, ELF terrestrial radio wave fields, J. R. Johler and L. A. Berry, NBS Mono. 78 (Oct. 1, 1964), 20 cents.

A study of lunar surface radio communication, L. E. Vogler, NBS Mono. 85 (Sept. 14, 1964), 70 cents.

Standard Reference Materials: Preparation of NBS copper-base spectrochemical standards, R. E. Michaelis, L. L. Wyman, and R. Flitsch, NBS Misc. Publ. 260–2 (Oct. 15, 1964), 35 cents.

Quarterly radio noise data June, July, August, 1963, W. Q. Crichlow, R. T. Disney, and M. A. Jenkins, NBS Tech. Note 18–19 (Aug. 21, 1964), 50 cents.

Quarterly radio noise data September, October, November 1963, W. Q. Crichlow, R. T. Disney, and M. A. Jenkins, NBS Tech. Note 18–20 (Oct. 23, 1964), 50 cents.

Calculation of sunrise and sunset times at ionospheric heights along a great circle path, A. H. Brady and D. D. Crombie, NBS Tech. Note 209 (Nov. 8, 1964), 20 cents.

Demagnetizing factors for oblate spheroids used in ferrimagnetic resonance measurements, L. B. Schmidt, W. E. Case, and R. D. Harrington, NBS Tech. Note 221 (Sept. 4, 1964), 20 cents.

Concerning the theory of radiation from a slotted conducting plane in a plasma environment, J. R. Wait, NBS Tech. Note 223 (Sept. 28, 1964), 20 cents.

An atlas of VLF emission spectra observed with the "Hiss recorder," J. A. Koch and V. C. Edens, NBS Tech. Note 226 (Nov. 13, 1964), 40 cents.

VHF ionospheric scatter system loss measurements European-Mediterranean area, V. H. Goerke and O. D. Remmler, NBS Tech. Note 230 (Dec. 25, 1964), 40 cents.

A program for plotting circles of constant overpressure around targeted points, M. L. Joel and D. D. Lottridge, NBS Tech. Note 249 (Oct. 28, 1964), 40 cents.

A nomogram for computing $\frac{a+jb}{c+jd}$ and a nomogram for computing $\left|\frac{a+jb}{c+jd}\right|$, H. S. Bowman, NBS Tech. Note 250 (Oct. 2, 1964), 15 cents.

On the pictorial structure of Chinese characters, B. K. Rankin III, W. A. Sillars, and R. W. Hsu, NBS Tech. Note 254 (Jan. 4, 1965), 30 cents.

Characteristics of the earth-ionosphere waveguide for VLF radio waves, J. R. Wait and K. P. Spies, NBS Tech. Note 300 (Dec. 30, 1964), 50 cents.

Interpretation of potentiometric titrations of weak acids in methanol-water solvents, K. C. Ong, R. A. Robinson, and R. G. Bates, Anal. Chem. **36,** 1971–1972 (Sept. 1964).

Fluctuations in ionospheric absorption events at conjugate stations, J. K. Hargreaves and H. J. A. Chivers, Nature **203,** No. 4948, 963–964 (Aug. 29, 1964).

RF and microwave power measurements, G. F. Engen, Proc. URSI XIVth General Assembly, Tokyo, Japan, Sept. 1963, XIII, 77–80 (1964).

LF–VLF frequency and time services of the National Bureau of Standards, D. H. Andrews (Proc. 19th Annual ISA Conf. and Exhibit, New York, N.Y., Oct. 12–15, 1964), ISA Preprint 21. 3–2–64 (1964).

Fresnel zone diffraction effects at 50 Gc/sec. determined from measured aperture field data, R. C. Baird, Program and Digest 1963 IEEE Prof. Group Ant. and Prop. Symp.

Space Telecommunications, July 9–11, 1963, Boulder, Colo., pp. 171–173 (1963).

Electronic energy bands in strontium titanate, A. H. Kahn and A. J. Leyendecker, Phys. Rev. **135,** No. 5A, 1321–1325 (Aug. 31, 1964).

On the implication of diurnal, seasonal and geographical variations in composition of high atmosphere from *F*-region measurements, J. W. Wright (Proc. NATO Advanced Study Institute, Sheikampen, Norway, Apr. 17–26, 1963), Book, Electron Density Distribution in the Ionosphere and Exosphere, pp. 186–198 (North Holland Publ. Co., Amsterdam, The Netherlands, 1964).

Ionospheric winds: motions into night and sporadic *E* correlations, N. W. Rosenberg, H. D. Edwards, and J. W. Wright (Proc. 4th Intern. Space Science Symp., Warsaw, June 4–10, 1963), Book, Space Research, ed., P. Muller, IV, 171–181 (North Holland Publ. Co., Amsterdam, The Netherlands, 1964).

Oblique incidence pulse measurement at 100 kc, R. H. Dougherty, AGARDograph **74,** Propagation of Radio Waves at Frequencies below 300 KC, p. 133–148 (Pergamon Press Inc., New York, N.Y., 1963).

Nonresonant absorption and collision diameters in the foreign-gas broadening of symmetric top molecules, G. Birnbaum and A. A. Maryott, J. Chem. Phys. **41,** No. 1, 154–157 (July 1, 1964).

Electromagnetic cross sections for electron and nuclear research, H. W. Koch, Nucl. Instr. Methods **28,** 199–204 (1964).

Exclusion of parity unfavored transitions in forward scattering collisions, U. Fano. Phys. Rev. **135,** No. 3B, B863–B864 (Aug. 10, 1964).

Microscopic-astrophysics and the development of astrophysical-laboratories, R. N. Thomas, Bull. Centre Intern. d'Astrophysique del'Observatoire de Nice, No. 1, pp. 7–16 (Nice, France, 1964).

Alouette ionic, magnetic-field and plasma studies, W. Calvert, H. Rishbeth, and T. E. VanZandt, IG Bull. No. 83, 16–19 (May 1964); Trans. AGU **45,** No. 2, 398–401 (June 1964).

Propagation of radio waves past a coast line with a gradual change of surface impedance, J. R. Wait and K. P. Spies, IEEE Trans. Ant. Prop. **AP–12,** No. 5, 570–575 (Sept. 1964).

On the propagation of longwave-length terrestrial radio waves—two theoretical techniques, J. R. Johler and L. A. Berry, AGARDograph **74,** Propagation of Radio Waves below 300 KC, pp. 101–129 (Pergamon Press Inc., New York, N.Y., 1963).

Experiments on self-ionizing shock waves in a magnetic field, Y. Nakagawa and K. B. Earnshaw, Book, Comptes Rendus de la VI^{e} Conference Internationale sur les Phenomenes D'Ionisation dans les Gaz, ed. P. Hubert and E. Cremieu-Alcan, IV, 303–309 (S.E.R.M.A., Paris, France, 1963).

Microwave propagation in an overdense bounded magneto-plasma, B. Wieder, Phys. Fluids **7,** 964–972 (July 1964).

Ionosonde studies of some chemical releases in the ionosphere, J. W. Wright (Proc. NATO Advanced Study Institute, Sheikampen, Norway, Apr. 17–26, 1963), Book, Electron Density Distribution in the Ionosphere and Exosphere, pp. 116–137 (North Holland Publ. Co., Amsterdam, The Netherlands, 1964).

Standard nuclear instrument modules, L. Costrell, U.S. Atomic Energy Commission TID Report 20893, 12 pages (July 1964).

Charge-transfer absorption spectra of NO in Kr and CH_3OH solutions, E. E. Ferguson and H. P. Broida, J. Chem. Phys. **40,** No. 12, 3715–3716 (June 15, 1964).

Ionospheric storms, S. Matsushita, Proc. URSI XIVth General Assembly, Tokyo, Japan, Sept. 1963, **XIII,** 169–180 (1964).

Symplectic modulary groups, M. Newman and J. R. Smart, Acta Arithmetica **IX,** 83–89 (1964).

Standards and measurement of attenuation, impedance and phase shift, R. W. Beatty, Proc. URSI XIVth General Assembly, Toyko, Japan, Sept. 1963, **XIII,** 80–92 (1964).

Vapour pressure, G. T. Armstrong, Encyclopaedic Dictionary of Physics **7,** 586–587 (Pergamon Press Inc., New York, N.Y., 1962).

Exterior corrosion of cast-iron pipe, M. Romanoff, J. Am. Water Works Assoc. **56,** No. 9, 1129–1143 (Sept. 1964).

The energy loss of electrons in solids, A. M. Rauth and J. A. Simpson, Radiation Res. **22,** No. 4, 643–661 (Aug. 1964).

Coherence theories of tropospheric radio propagation, J. R. Wait, IEEE Trans. Ant. Prop. **AP–12,** No. 5, 649–651 (Sept. 1964).

Solar activity, J. V. Lincoln, IQSY Instruction Manual. No. 2, Report of sudden ionospheric disturbances, Suppl., pp. 1–11 (IQSY Secretariat, London, England, 1963).

Vibration-rotation bands of deuterium cyanide and hydrogen cyanide, A. G. Maki, E. K. Plyler, and R. Thibault, J. Opt. Soc. Am. **54,** No. 7, 869–876 (July 1964).

IQSY Instruction Manual. No. 1. World days, A. H. Shapley, 32 pages, IQSY Secretariat, London, England (July 1963).

Influence of the refractive index profile in VHF reflection from a tropospheric layer, J. R. Wait and C. M. Jackson, IEEE Trans. Ant. Prop. **AP–12,** No. 4, 512–513 (July 1964).

Photometric observations of the airglow during the IQSY, F. E. Roach, IQSY Instruction Manual. No. 5: Airglow, pt. I, 1–24 (IQSY Secretariat, London, England, 1963).

Correlation matrix for radio waves in the troposphere, E. C. Barrows (Proc. Symp. Electromagnetic Theory and Antennas, Copenhagen, 1962), Monograph, Electromagnetic Theory and Antennas 2, Sec. C, 743–746 (Macmillan and Co., Ltd., London, England, 1963).

Frequency and time broadcast services of the National Bureau of Standards, A. H. Morgan, Proc. ISA 17th Annual Automation Conf. and Exhibit, New York, N.Y., Oct. 15–18, 1962, pt. I, Paper 1.1.62, 9 pages (1962).

Frostbite: signs, prevention, and treatment, J. R. Meyer-Arendt, Trail and Timberline, p. 3 (Jan. 1964).

Formation of an electron depleted region in the ionosphere by chemical releases, D. Golomb, N. W. Rosenberg, J. W. Wright, and R. A. Barnes (Proc. 4th Intern. Space Science Symp., Warsaw, June 4–10, 1963), Book, Space Research, ed., P. Muller, **IV,** 389–398 (North Holland Publ. Co., Amsterdam, The Netherlands, 1964).

The ionosphere, A. H. Shapley, U.S. Information Agency Voice of America Forum Series on Space Science, Lecture No. 7, 6 pages (1963).

Infrared spectroscopy of weak charge-transfer complexes, E. E. Ferguson, J. Chim. Phys. **61,** 257–262 (1964).

Franck-Condon factors for the ionization of CO, NO, and O_2, M. E. Wacks, J. Chem. Phys. **41,** No. 4, 930–936 (Aug. 1964).

Alkaline earth cation distributions in various borates, S. Block and G. J. Piermarini, Phys. and Chem. of Glasses **5,** No. 5, 138–144 (Oct. 1964).

Growth spirals on $NiBr_2$ platelets, E. N. Sickafus and D. R. Winder, J. Appl. Phys. **35,** No. 8, 2541–2545 (Aug. 1964).

On the twilight sodium emission—1: Observations from a southern hemisphere station, M. Gadsden, Ann. Geophys. **20,** No. 3, 261–272 (1964).

Infrared spectrum of CF_2, D. E. Milligan, D. E. Mann, and M. E. Jacox, J. Chem. Phys. **41,** No. 5, 1199–1203 (Sept. 1, 1964).

Proton-transfer reactions between H_3+ and saturated hydrocarbons, P. Ausloos and S. G. Lias, J. Chem. Phys. **40,** No. 12, 3599–3605 (June 15, 1964).

Resinography with 8–A X-rays, S. B. Newman, Symp. on Resinographic Methods, Special Tech. Publ. No. 348, ASTM (1963).

Microwave spectrum of the SO radical, F. X. Powell and D. R. Lide, Jr., J. Chem. Phys. **41,** No. 5, 1413–1419 (Sept. 1964).

Resonances of a spherical void in a compressible isotropic plasma, J. R. Wait, J. Geophys. Res. **69,** No. 19, 4189–4191 (Oct. 1, 1964).

The structure of the triclinic form of sodium tetrametaphosphate tetrahydrate, H. M. Ondik, Acta Cryst. **17,** No. 9, 1139–1145 (Sept. 1964).

Experimental transition probabilities for six oxygen multiplets, J. E. Solarski and W. L. Wiese, Phys. Rev. **135,** No. 5A, A1236–A1241 Aug. 31, (1964).

Evaluating computer systems analysis and design work in the Federal Government, W. H. Gammon, Book, Ideas for Management, Systems and Procedures 1964, 319–322 (1964)

Some remarks on microgrammars, W. C. Watt, Proc. Wash. Linguistics Club 2, No. 1, 13–17 (Oct. 26, 1964).

Radiation from sources immersed in compressible plasma media, J. R. Wait, Can. J. Phys. **42,** 1760–1780 (Sept. 1964).

Conductance of copper *m*-benedisulfonate hexahydrate in *N*-methylpropionamide from 20 to 40°, T. B. Hoover, J. Phys. Chem. **68,** No. 10, 3003–3008 (Oct. 1964).

Polarized electrons and positrons by tagging technique, H. Olsen and L. C. Maximon, Phys. Rev. Letters **13,** No. 3, 112–114 (July 20, 1964).

Theory of whisker growth and evaporation, J. A. Simmons, R. L. Parker, and R. E. Howard, J. Appl. Phys. **35,** No. 7, 2271–2272 (July 1964).

Mass spectrometric study of the production of methylamine from azomethane, M. E. Wacks, J. Phys. Chem. **68,** No. 9, 2725–2726 (Sept. 1964).

Infrared spectrum and structure of gaseous Al_2O, M. J. Linevsky, D. White, and D. E. Mann, J. Chem. Phys. **41,** No. 2, 542–545 (July 15, 1964).

High resolution infrared spectra of $C_2{}^{12}H_2$, $C^{12}C^{13}H_2$ and $C_2{}^{13}H_2$, W. J. Lafferty and R. J. Thibault, J. Mol. Spectry. **14,** No. 1, 79–96 (Sept. 1964).

Gaussian correlation functions: Two-electron systems, W. A. Lester, Jr., J. Chem. Phys. **41,** No. 5, 1407–1413 (Sept. 1, 1964).

Use of the index of refraction as a means for study of plasma configurations, E. G. Johnson, Phys. Fluids **7,** 1551–1552 (Sept. 1964).

Application of the theory of absorbing Markov chains to the statistical thermodynamics of polymer chains in a lattice, J. Mazur, J. Chem. Phys. **41,** No. 8, 2256–2266 (Oct. 15, 1964).

A combinatorial problem and a simple decoding method for cyclic codes, M. Nesenbergs, IEEE Trans. Inform. Theory **IT-10,** 250–252 (July 1964).

Observed line shapes of collective excitations in Al, Be, and Ge, N. Swanson, J. Opt. Soc. Am. **54,** No. 9, 1130–1133 (Sept. 1964).

Flash-photolysis spectroscopy of matrices, L. J. Schoen and D.E. Mann, J. Chem. Phys. **41,** No. 5, 1514 (Sept. 1964).

Rotation-vibration interaction and other corrections to the spin doublet separation in $^2\Pi$ diatomic molecules, T. C. James, J. Chem. Phys. **41,** No. 3, 631–641 (Aug. 1, 1964).

Effect of electrical fields in the gamma radiolysis of propane, P. Ausloos and R. Gorden, Jr., J. Chem. Phys. **41,** No. 5, 1278–1284 (Sept. 1, 1964).

Mass spectrometric investigation of the yttrium chlorine surface reaction, J. D. McKinely, J. Chem. Phys. **49,** No. 9, 2914–2817 (Nov. 1, 1964).

Angular momentum distribution and emission spectrum of OH ($^2\Sigma^+$) in the photodissociation of H_2O, T. Carrington, J. Chem. Phys. **41,** No. 7, 2012–2018 (Oct. 1, 1964).

Kinetics of the acid-catalyzed hydrolysis of acetal in dimethyl sulfoxide-water solvents at 15, 25, and 35°, R. K. Wolford, J. Phys. Chem. **68,** No. 11, 3392–3398 (1964).

Morphology of thermally evaporated zinc cleavage surfaces, A. W. Ruff, Jr., J. Chem. Phys. **41,** No. 5, 1204–1213 (Sept. 1, 1964).

Simple arc devices for spectral excitation in controlled atmospheres, M. Margoshes and B. F. Scribner, Appl. Spectry. **18,** No. 5, 154–155 (1964).

Collision-induced microwave absorption in compressed gases. III. CO_2-foreign-gas mixtures, A. A. Maryott and S. J. Kryder, J. Chem. Phys. **41,** No. 6, 1580–1582 (Sept. 1964).

Statistical surface thermodynamics of simple liquid mixtures, C. A. Eckert and J. M. Prausnitz, A.I. Ch. E. J. **10,** No. 5, 677–683 (Sept. 1964).

The National Bureau of Standards, E. L. Graminski, Capital Chemist **14,** No. 9, 2778–2781 (Dec. 1964).

Correlation factors for impurity diffusion—Bcc, diamond, and Fcc structures, J. R. Manning, Phys. Rev. **136,** No. 6A, A1758–A1766 (Dec. 14, 1964).

Thermal decomposition of some alkyl halides by a shock-tube method, W. Tsang, J. Chem. Phys. **41,** No. 8, 2487–2494 (Oct. 15, 1964).

Relaxation of a Lorentz gas with repulsive r^{-s} force law, H. Oser, K. E. Shuler, and G. H. Weiss, J. Chem. Phys. **41,** No. 9, 2661–2666 (Nov. 1, 1964).

Plastics and the dental market, G. M. Brauer, Plastics World **12,** 12 (Oct. 1964).

NMR studies of asymmetric ethanic rotators: 1,2-disubstituted propanes, H. Finegold, J. Chem. Phys. **41,** No. 6, 1808–1818 (Sept. 15, 1964).

Triplet—state energy transfer from acetone to aliphatic aldehydes in the gas phase, R. E. Rebbert and P. Ausloos, J. Am. Chem. Soc. **86,** 4803–4807 (1964).

Impact parameter treatment of vibrational excitation, F. H. Mies, J. Chem. Phys. **41,** No. 3, 903–904 (Aug. 1, 1964).

The inverse multiplier for abelian group difference sets, E. C. Johnsen, Can. J. Math. **16,** 787–796 (Sept. 4, 1964).

Gas-phase photoylsis of methyl radicals with added organic compounds, R. D. Doepker and P. Ausloos, J. Chem. Phys. **41,** No. 6, 1865–1871 (Sept. 5, 1964).

18-cm spectrum of OH, H. E. Radford, Phys. Rev. Letter **13,** No. 17, 534–535 (Oct. 26, 1964).

Low temperature magnetic transitions in lanthanon trichlorides, Physics Letters **12,** No. 1, p. 5 (Sept. 1, 1964).

An investigation of plasma boundaries with electromagnetic surface waves, H. W. Wassink and A. J. Estin, J. Appl. Phys. **35,** 2795–2800 (Oct. 1964).

Mass-spectrometric study of the reactions of O atoms with NO and NO_2, F. S. Klein and J. T. Herron, J. Chem. Phys. **41,** No. 5, 1285–1290 (Sept. 1, 1964).

Growth of oxalic acid single crystals from solution: solvent effect on crystal habit, J. L. Torgensen and J. Strassburger, Science **146,** No. 3640, 53–55 (Oct. 2, 1964).

Infrared studies of the photolysis of HN_3 in inert and reactive matrices. The infrared spectrum of NH, D. E. Milligan and M. E. Jacox, J. Chem. Phys. **49,** No. 9, 2838–2841 (Nov. 1, 1964).

The solubility of water vapor in molten alumina, J. J. Diamond and A. L. Dragoo (Proc. Conf. Arthur D. Little, Inc., Cambridge, Mass., Oct. 4–5, 1962), Book, Thermal Imaging Techniques, ed., P. E. Glaser and R. F. Walker, ch. 17, pp. 225–228 (Penum Press Inc., New York, N.Y., 1964).

Contributions to the theory of shell corrections, U. Fano and J. E. Turner, ch. 4, 49–67, Nuclear Sci. Series Report No. 39, Natl. Acad. Sci.–Natl. Res. Council Publ. 1133 (1964).

Error bounds for asymptotic expansions, with an application to cylinder functions of large argument, F. W. J. Olver, Book, Asymptotic Solutions of Differential Equations and their Applications, ed., C. H. Wilcox, pp. 163–183 (John Wiley & Sons, Inc., New York, N.Y., 1964).

Spectral study of active nitrogen flames exhibiting CN "tail" bands, R. L. Brown and H. P. Broida, J. Chem. Phys. **41,** No. 7, 2053–2060 (Oct. 1, 1964).

Note on the partition functions, N. Newman, Am. Math. Mo. **71,** No. 9 (Nov. 1964).

Electrode potentials in fused systems. VIII. Oxidation kinetics of silver in sodium chloride, K. H. Stern and W. E. Reid, Jr., J. Phys. Chem. **68,** No. 12, 3757–3764 (Dec. 1964).

Automatic optical design, O. N. Stavroudis, Book, Advances in Computers **5,** 227–252 (Academic Press Inc., New York, N.Y., 1964).

Infrared spectrum of HCO, D. E. Milligan and M. E. Jacox, J. Chem. Phys. **41,** No. 10, 3032–3036 (Nov. 1964).

A magnetic fixed point for thermometry below 1°K, J. C. Eisenstein, R. P. Hudson, and B. W. Mangum, Appl. Phys. Letters **5,** No. 11, 231 (Dec. 1, 1964).

Continuum description of a high temperature plasma, L. S. Klein and J. L. Jackson, Proc. VI Intern. Conf. Ionization Processes in Gases, Paris, France, 1963, II, No. 11, 215–216 (June 1964.)

Gas thermometer, L. A. Guildner, Encyclopaedic Dictionary of Physics, pp. 405–406 (Pergamon Press, New York, N.Y., 1961).

Configurations $4f^26s$ and $4f^26p$ in doubly ionized Pr, N. Spector, J. Opt. Soc. Am. **54,** No. 11, 1359–1362 (Nov. 1964).

Electron scattering without atomic or nuclear excitation, J. W. Motz, H. Olsen, and H. W. Koch, Rev. Mod. Phys. **36,** No. 4, 881–928 (Oct. 1964).

K-ionization cross sections for relativistic electrons, J. W. Motz and R. C. Placious, Phys. Rev. **136,** No. 3A, A662–A665 (Nov. 2, 1964).

Tables of energy losses and ranges of electrons and positrons, M. J. Berger and S. M. Seltzer, Natl. Aeronaut. Space Admin. NASA SP–3012, 1–127 (1964).

Tables of energy losses and ranges of heavy charged particles, W. H. Barkas and M. J. Berger, Natl. Aeronaut. Space Admin. NASA SP–3013, 1–131 (1964).

Photochemical changes in thin-layer chromatograms of polycyclic, aromatic hydrocarbons, M. N. Iniscoe, Anal. Chem. **36,** No. 13, 2505–2506 (Dec. 1964).

Photoelimination of ethylene from 2-pentanone, P. Ausloos and R. E. Rebbert, J. Am. Chem. Soc. **86,** No. 20, 4512 (Oct. 20, 1964).

Second dissociation constant of deuteriophosphoric acid in deuterium oxide from 5 to 50°. Standardization of *p*D scale, R. Gary, R. G. Bates, and R. A. Robinson, J. Phys. Chem. **68,** No. 12, 3806–3809 (Dec. 1964).

Application of the theory of absorbing Markov chains to the statistical thermodynamics of polymer chains in a lattice, J. Mazur, J. Chem. Phys. **41,** No. 8, 2256–2266 (Oct. 15, 1964).

The Statistical Analysis of Experimental Data, J. Mandel, Book, 410 pages (Interscience Publ., Inc., New York, N.Y., 1964).

Proton and fluorine NMR spectra of HBF_2, T. C. Farrar and T. D. Coyle, J. Chem. Phys. **41,** No. 9, 2612–2613 (Nov. 1, 1964).

APS division of electron physics the first 20 years, L. Marton, Phys. Today, pp. 44–50 (Oct. 1964).

Liouville representation of quantum mechanics with application to relaxation, U. Fano (Proc. Lectures on the Many-Body Problems, 5th Intern. School of Physics, Ravello, Italy, Apr. 17– May 4, 1963), Book, Lectures on The Many-Body Problems **2,** 1–294 (Academic Press Inc., New York, N.Y., 1964).

Our measurement system and its future, R. D. Huntoon, Res./Develop. **16,** No. 1, 16–21 (Jan. 1965).

Fracture processes in polymeric solids, I. Wolock and S. B. Newman, Book, Fracture Processes in Polymeric Solids. Phenomena and Theory, ed. B. Rosen, Ch. IIC, pp. 235–290 (Interscience Publ. Inc., New York, N.Y., Jan. 1965).

**Publications for which a price is indicated are available by purchase from the Superintendent of Documents, U.S. Government Printing Office, Washington, D.C., 20402 (foreign postage, one-fourth additional). Reprints from outside journals and the NBS Journal of Research may often be obtained directly from the authors.*

UNIVERSITY MICROFILMS INC
EDITORIAL DEPARTMENT
313 NORTH FIRST ST
ANN ARBOR MICH
S/P-C JUNE

UNITED STATES
GOVERNMENT PRINTING OFFICE
DIVISION OF PUBLIC DOCUMENTS
WASHINGTON, D.C. 20402

OFFICIAL BUSINESS

POSTAGE AND FEES PAID
U.S. DEPARTMENT OF COMMERCE

JOURNAL OF RESEARCH of the National Bureau of Standards — Vol. 69C, No. 2 — April–June 1965
C. Engineering and Instrumentation

Contents

	Page
Temperatures of thermocouple reference junctions in an ice bath. Frank R. Caldwell.	95
Superimposed birefractory plates. L. H. Adams and R. M. Waxler.	103
A self-calibrating instrument for measuring conductance at radio frequencies. Leslie E. Huntley.	115
Exact inductance equations for rectangular conductors with applications to more complicated geometries. Cletus Hoer and Carl Love.	127
Common volume of two intersecting cylinders. J. H. Hubbell.	139
Steady-state heat conduction in an exposed exterior column of rectangular cross section. B. A. Peavy.	145
Publications of the National Bureau of Standards.	153

Library of Congress Catalog Card Number: 62–3900

For sale by the Superintendent of Documents, U.S. Government Printing Office, Washington, D.C., 20402. Price 75 cents (single copy). Subscription price: $2.25 a year; 50 cents additional for foreign mailing.
UNITED STATES GOVERNMENT PRINTING OFFICE, WASHINGTON : 1965